UNIVERSITA' DEGLI STUDI DI NAPOLI FEDERICO II

DIPARTIMENTO DI INGEGNERIA CHIMICA

Dottorato di Ricerca in Ingegneria Chimica
(XXII Ciclo)

CATALYTIC BIOMASS GASIFICATION PROCESS IN FLUIDIZED BED REACTOR

Scientific committee:

Prof. Gennaro Russo

Ing. Riccardo Chirone

Prof. Pier Ugo Foscolo

Dott. Luciana Lisi

Candidate:

Bruno Piriou

ANNO ACCADEMICO 2008-2009

ABSTRACT

This thesis focuses on the development of a new catalytic system for conversion of tar produced during biomass gasification in a fluidized bed gasifier in order to overcome the typical drawbacks (low activity, coke deactivation) of conventional catalysts.

The innovative catalytic system is a γ-alumina-supported lanthanum-cobalt perovskite (20 wt %) promoted with small amounts of rhodium (0.1 to 1wt%) which was proposed for the high reforming activity of the noble metal and the good oxygen availability of perovskite, respectively. In addition, the large dispersion of rhodium into the $LaCoO_3$ matrix inhibits its possible sintering at high temperatures, typical of biomass gasification (800-900°C).

In order to investigate the catalytic properties by modifying both the catalyst formulation and the operative parameters, an experimental plant at a laboratory scale, which allows the contact between catalyst and a real mixture of biomass devolatilization products, has been set up. It consists of two connected fixed bed micro-reactors, heated independently in two different electric furnaces and it is equipped with an analysis system for detection and characterization of all gaseous and liquid products. This set up allowed an easy and economic catalytic screening, since it did not involve the multiplicity of phenomena (fluidodynamics, segregation and mass transfer) occurring in a real scale fluidized bed gasifier and allowed the use of much smaller amounts of catalytic material.

The activity in biomass tar conversion of the novel catalytic formulation has been compared, in pyrolysis conditions, to that of conventional catalysts (olivine, dolomite, Ni/Al_2O_3). It was found that the novel catalyst was able to completely convert tar and light hydrocarbons contained in the biomass devolatilization products, but also to significantly increase the syngas yield due to prevailing of reforming properties in contrast with more conventional catalysts mainly providing cracking activity. Moreover, the catalyst had a limited sensitivity to coke deactivation.

These findings were supported by the study of redox properties of the active phases deposited on the alumina support by TPR analysis. The study of catalytic activity and redox properties also led to define the best catalytic formulation. The best performances were obtained with catalysts containing both rhodium and perovskite due to the synergic effect of the two phases coupling the highest reforming activity with the lowest coke deposition. In addition, the deposition of the perovskite layer prevents the encapsulation of rhodium into the alumina matrix which led to the formation of a less active rhodium aluminate.

A very efficient tar conversion activity was maintained also for a rhodium content as low as 0.1 wt% thus strongly limiting the amount of the expensive precious metal. Likewise, the operation temperature can be lowered to 600°C keeping the same performances observed at high temperatures.

The set-up of a stainless steel fluidized bed gasifier at pilot-scale (140 mm ID) was also performed. The efficiency of the mixing between biomass, volatiles and catalyst, which is difficult due to the low density of biomass with respect to the catalytic bed particles and to the formation of endogenous volatiles bubbles, was improved by the use of a conical gas distributor at the bottom of the fluidizing column. Sampling of the elutriated solid and unconverted tars was performed isokinetically. Gaseous, liquid products and elutriated solid fines were characterized by suitable analytical systems.

An experimental campaign of air/steam gasification, to enhance the production of an hydrogen-rich syngas, using conventional catalyst (olivine, dolomite, Ni/Al_2O_3) was carried out in the fluidized bed gasifier.

INDEX

I-INTRODUCTION

Renewable energy is of growing importance in satisfying environmental concerns over fossil fuel usage. In this framework, biomass, including both plants (trees and agricultural crops) and waste materials (agricultural and forestry wastes), represents an abundantly available and renewable energy resource (Bridgwater, 2003). Moreover, biomass is a practically non exhaustive energy resource and has a CO_2-neutral effect on environment (CO_2 rejected during the conversion processes is the same as CO_2 absorbed by the plant during its life, and so-on), contributing significantly towards the objectives of the Kyoto Agreement in reducing the green house gases emissions and the problems related to climate change (Shen et al., 2007). Consequently, biomass is considered the renewable energy source with the highest potential to contribute to the energy needs of modern society for both the developed and developing economies world-wide (Foscolo et al., 2007). It is presently estimated to contribute ~10-14% of world's energy supply (Cui and Grace, 2007).

On the other hand, biomass is characterised by a low energy density, so that many practical applications require that it should be first transformed into gaseous, liquid or solid derived-fuels. Biomass fuels and residues can be converted to energy via thermo-chemical, biological and physical processes. In particular, there are three main thermo-chemical processes available for converting biomass to a more useful energy form: combustion, gasification and pyrolysis. Among the thermo-chemical conversion technologies, biomass gasification has attracted the highest interest as it offers higher efficiencies compared to combustion and pyrolysis, but it is still at a relatively early stage of development (Bridgwater, 2003). In particular, converting biomass into a hydrogen-rich gas is a possible more efficient way of biomass utilization (Ni et al., 2006). Moreover, biomass gasification processes can be easily down scaled and allow a good control of the product distribution.

However, there are inefficiencies in the non-catalytic biomass gasification technology, which at present make biomass gasification economically unviable. The presence of condensable organic compounds and methane in the product gas renders the gas unsuitable for specific applications. Elimination of the condensable organic compounds and methane by a suitable technology, such as the use of a catalyst able to further convert these products, will enhance the economic viability of biomass gasification (Sutton et al., 2001).

I-1 Biomass

The definition of biomass is the total mass of living organisms, bacteria and plankton, advanced vegetal, mammals and human beings. All the matter produced by biological organisms can be considered biomass, even for energetic applications. The term biomass also includes a wide range of materials, from plastic bags to agricultural wastes (Goring, 1971; Abächerli, 1996; Sales et al., 2004).

Biomass for energetic use can be classified as follows:

- Waste (industrial, civil)
- Landfill gas
- Agricultural crops
- Wooden biomass
- Alcohol fuels (grapefruit, sugar cane, beetroot,…)

Woody or ligno-cellulosic biomass is accepted as one of the best feedstock for energetic production, for reasons of availability, costs and relative homogeneity. The heating value of those fuels range from 8 $MJ \cdot kg^{-1}$ for a green wood to 20 $MJ \cdot kg^{-1}$ for a dry plant matter (for comparison, the heating values of natural gas and of coal are 36 $MJ \cdot kg^{-1}$ and 27 $MJ \cdot kg^{-1}$, respectively) (Ni et al., 2006).

Wood is made of three organic polymers, celulose (40-50 wt%), hemi-celulose (20-25 wt%) and lignin (20-25 wt%), containing in some extent volatiles and mineral matter or ash (1-15 wt%), as reported in Figure 1. The volatile part represents the fluid contained inside the wood cells and is made of water and resins, also called “extractives”, such as triglycerides, fatty acids, resin acids, steryl esters and sterols (Kallioinen et al., 2003).

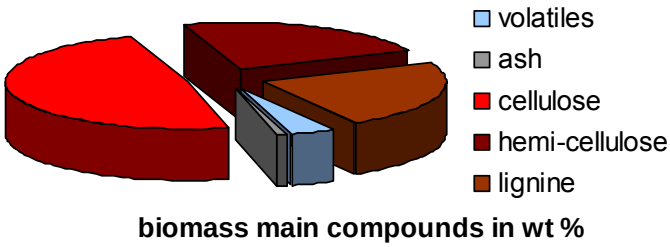

Hemicellulose

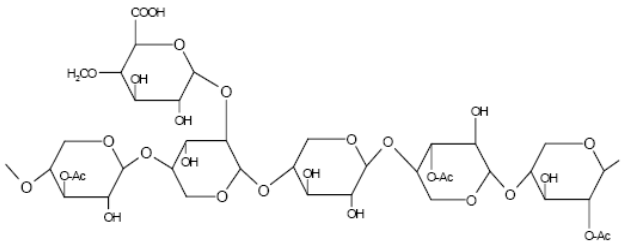

Cellulose

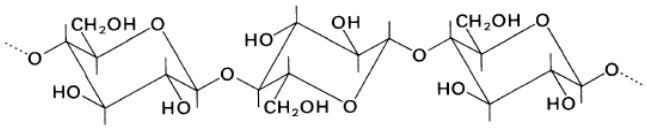

Lignine

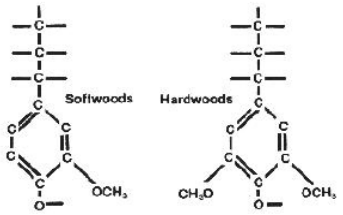

Figure 1. Woody biomass composition. Above: proportion of components in wt %. Under: representation of constitutive organics.

Figure 2 reports the elemental composition of different biomass fuels and shows that the organic part of different biomass fuels is roughly the same, but their ash content (minerals) can be very different. The high oxygen-content in biomass lowers the energetic yields of the final product. The mean hydrogen content of biomass is about 6 wt% with respect to 25 wt% in methane which is the 70% of still largely available natural gas. Hopefully, this low hydrogen yield is counter-balanced by the overall process costs and the control of emissions.

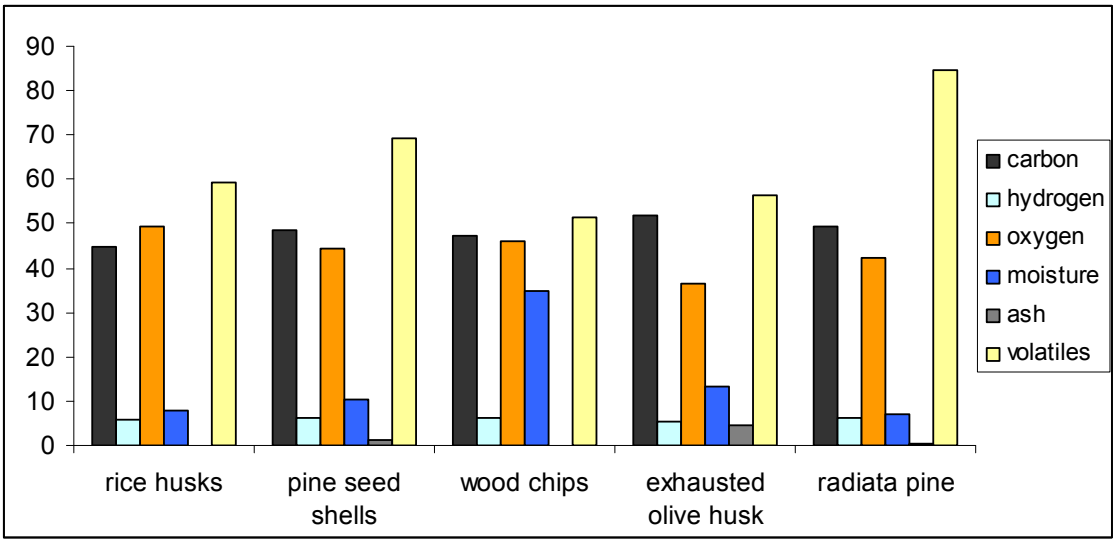

Figure 2. Composition (wt%) of some typical biomasses.

I-2 Biomass conversion technologies

Biomass can be converted to more valuable compounds by extraction of its fundamental constituents under gaseous, liquid and/or solid form. The aim is to increase both the versatility of the material, in particular for transport and storage, and the energy density of the fuel.

The multi component character of woody materials makes the study of its thermal degradation a complex research topic. On microscopic scale, wood cells are composed of so-called microfibrils, which are cellulose molecules 'coated' with hemicellulose. Lignin acts as a seal between and sometimes within the amorphous regions of the microfibrils. These wood fractions show different thermal behaviour. Three zones may therefore be distinguished in weight loss curves of wood.

Among the organic compounds contained in wood, holocellulose (cellulose plus hemicellulose) is the most reactive part due to its bidimensional structure. In particular, hemicellulose decomposes at temperature in the range of 225–325°C, whereas cellulose at 305–375°C. Due to a 3D polymerisation, lignin is the most stable component and its thermal decomposition leads to the heaviest (and most difficult to treat) part of the products (Raveendran et al., 1996). Lignin gradually decomposes over the temperature range of 250–500°C (Prins et al., 2006). Figure 3 reports the decomposition temperature ranges of lignin, hemi-cellulose and cellulose.

More generally, during the heating of a biomass fuel, the structure decomposes by breaking the least stable bonds, i.e. the methylene and oxygen bridges between the aromatic building blocks.

This phenomenon results in the formation of radical components, which are to some extent volatile under the operating conditions. These radicals are very reactive and can undergo secondary reactions, like cracking and carbon deposition (soot), both inside and outside the particle. Stabilization of a radical, primarily via hydrogen addition, leads to a volatile component (Demirbas, 2002).

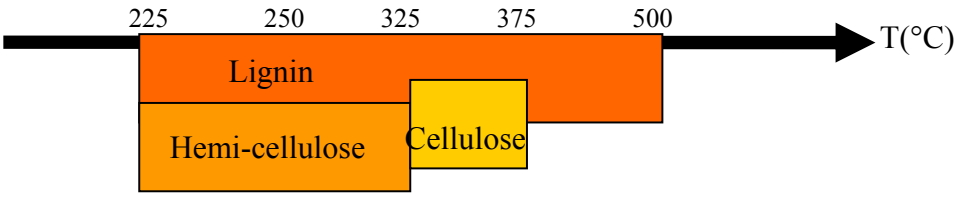

Figure 3. Decomposition temperature ranges.

The amount of water present in the fuel is an important parameter, since it modifies the thermal conductivity of the raw material, dilutes the products containing energy and makes much more complex fuel-processing like transport, feeding, etc, thus strongly influencing the efficiency of the technologies that are used for biomass conversion (Demirbas, 2001).

Another feature faced in energetic extraction is represented by the biomass mineral additives. The mineral matter does not vary so much qualitatively from one biomass type to another. Generally the main elemental constituents of biomass minerals are Si, Ca, K, Na and Mg, with smaller amounts of S, P, Fe, Mn and Al. These constituents occur as oxides, silicates, carbonates, sulphates, chlorides and phosphates (Ganesh, 1990). The mineral part of biomass can not be converted. Since its concentration can be very different from one type to another, the thermal behaviour of solid fuel is difficult to predict. Many studies indicate that small amount of inorganic material is sufficient to alter the biomass decomposition efficiency to a large extent (Shafizadez, 1968; Gray, 1984; Essig et al., 1989; Ganesh, 1990; Obernberger et al., 2006; Vamvuka et al., 2006; Glarborg, 2007). Alkali metals contained in ash have a low fusion temperature and the vapours generated at more than 750°C are very corrosive and difficult to separate from the desired products (Bartels et al., 2008).

The biomass conversion processes, industrially scaled or not (yet), can be mainly divided into biochemical and thermochemical processes (Goyal, 2008), as schematically reported in Figure 4.

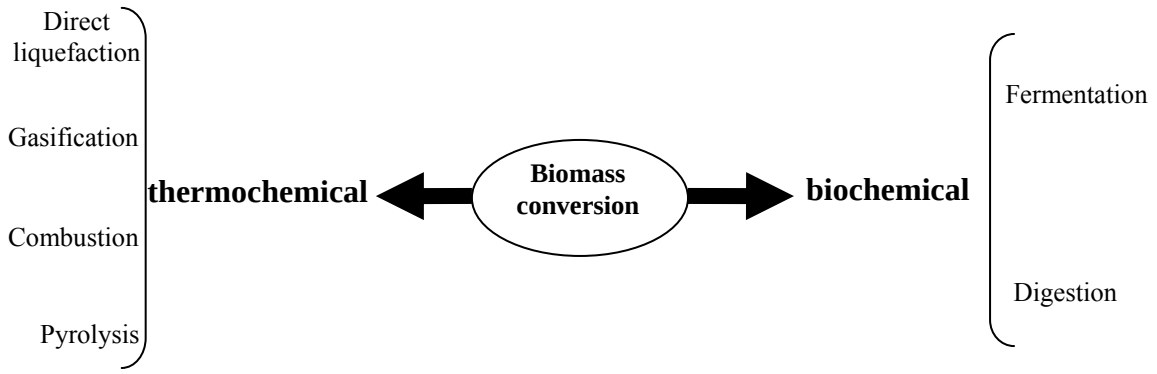

Figure 4. Classification of biomass conversion processes.

Biochemical processes are essentially microbic digestion and fermentation of holocellulose. High moisture (20 to 50 wt%) herbaceous plants (vegetables, sugar cane, sugar beet, corn, sorghum, cotton), marine crops and manure are most suitable for biological digestion (Demirbas, 2001). Digestion is made by specific anaerobic micro-organisms able to decompose the sugar-like cellulose and hemicellulose into a CO_2 and CH_4 mixture called biogas. Fermentation converts holocellulose into ethanol. In these processes, lignin is not converted, which is a serious limitation for energetic production (Saxena et al., 2008).

Thermochemical decompositions, such as direct liquefaction, combustion, pyrolysis and gasification, can be utilised for all biomass materials, but low moisture (10-20 wt%) herbaceous (small grain field residues) and woody (woody industry wastes and standing vegetation not suitable for lumber) are the most suitable.

In direct liquefaction, biomass is heated to 250–325°C in water under a pressure of 5–20 MPa in the absence of air. Solvent or catalyst can be added in the process. The main disadvantage of biomass liquefaction is the difficulty to achieve the operative conditions (Ni et al., 2006).

Combustion is the most common biomass conversion technique. It consists in the direct burning of biomass to convert the chemical energy into heat, mechanical power or electricity using equipment such as stoves, furnaces, boilers or steam turbines. Combustion processes are still largely used in developing countries for heat generation or cogeneration, even if the thermal efficiency is low (10–30%) and pollutant emissions are important (NO_x are produced if air is used) (Bridgwater, 2002).

Pyrolysis and gasification are the most studied conversion processes for advanced applications. The overall efficiency of conversion of biomass to energy using gasification and pyrolysis is estimated as 75-80%.

Pyrolysis is a thermal decomposition occurring in the absence of oxygen. It is also the common first step of combustion and gasification processes where it is followed by total or partial oxidation of the primary products. Pyrolysis of biomass is commonly used for biomass conversion to liquids called pyrolysis oil (biocrude) then refined for use in engines or chemicals production. In this liquid form, the material is much easier to transport, especially when harvesting is made in difficult to access areas. In details, pyrolysis products are solid char, oils (biocrude) and permanent gases (CO_2, CO, H_2, H_2O, CH_4, C_2H_4). The relative yields depends mostly on the rate of heating, the final temperature and the gas residence time (see Table 1) (FAO, 1994). Thus, these parameters can be tailored in order to produce more char, oil or gas. Low process temperature (< 500°C), low heating rate and long vapour residence times (>> 2 sec) favour the production of charcoal. Moderate temperature (500-700°C), high heating rate (300°C·min^{-1}) and short vapour residence time (< 2 sec) are optimum for producing liquids. High temperature (800-1000°C), very high heating rates (>>300°C·min^{-1}) and long residence time (>2 sec) increase the biomass conversion to gas. The latter process is called flash pyrolysis and is adapted to hydrogen production (Bridgwater, 2004). However, the refining costs of biocrude oil (unstable since very oxygenated and with high water content) for application to synthetic fuel production limit the technological issues of the overall process. Moreover, the produced char remains unconverted in the process, then the energy of a non negligible part of the initial feed is lost.

The gasification process represents one of the most economically competitive technologies and one of the best way to optimise the extraction of energy from biomass in terms of conversion-efficiency. Gasification is the conversion of biomass to a gaseous fuel by heating in a gasification medium such as air, oxygen, steam or CO_2 at temperatures >800°C. Unlike combustion where oxidation is substantially complete in one process, gasification converts the intrinsic chemical energy of the carbon in the biomass into a combustible gas (mostly H_2, CO, CO_2, CH_4 and steam) in two stages. The gas obtained from biomass gasification can be standardized for use in gas engines and gas turbines, or used as a chemical feedstock to produce liquid fuels. For these reasons, it is more versatile and easier to use with respect to raw biomass or pyrolysis oils, which are difficult to refine (McKendry, 2002; Foscolo et al., 2007). More details on biomass gasification are reported in the next section.

Table 1. Pyrolysis processes and phase yields. (FAO, 1994)

Technology	Gas residence time	Heating rate	Temperature (°C)	Products
Carbonation	days	very low	400	charcoal
Conventional	5-30min	low	600	oil, gas, char
Fast	0.5-5s	very high	650	bio-oil
Flash-liquid	< 1s	high	< 650	bio-oil
Flash-gas	< 1s	high	< 650	chemicals, gas
Ultra	< 0.5s	very high	1000	chemicals, gas
Vacuum	2-30s	medium	400	bio-oil
Hydro-pyro	< 10s	high	< 500	bio-oil
Methano-pyro	< 10s	high	> 700	chemicals

I-3 Biomass gasification process

When an oxidant gas (air, steam, CO_2, O_2) is flowed on a biomass particle at a sufficiently high temperature (>500°C) with an oxidant/fuel Equivalent Ratio (ER) in the range 0.25<ER<0.5, most of the products are gaseous. More specifically, the gaseous phase (permanent and condensable) can represent up to 80% of the products (Dayton, 2002). Unconverted char (including mineral matter), tars - defined as all organic compounds with higher molecular mass than benzene - and coke, formed from reactive tar, being the remaining products.

Biomass gasification is a multistep process. In practice, the gasification of the biomass particle occurs through a first particle drying step, followed by a pyrolytic step which leads to devolatilization and shrinking of the original particle. The last step being char gasification.

The pyrolysis step occurs gradually from the surface to the centre of a biomass particle, as shown in Figure 5.

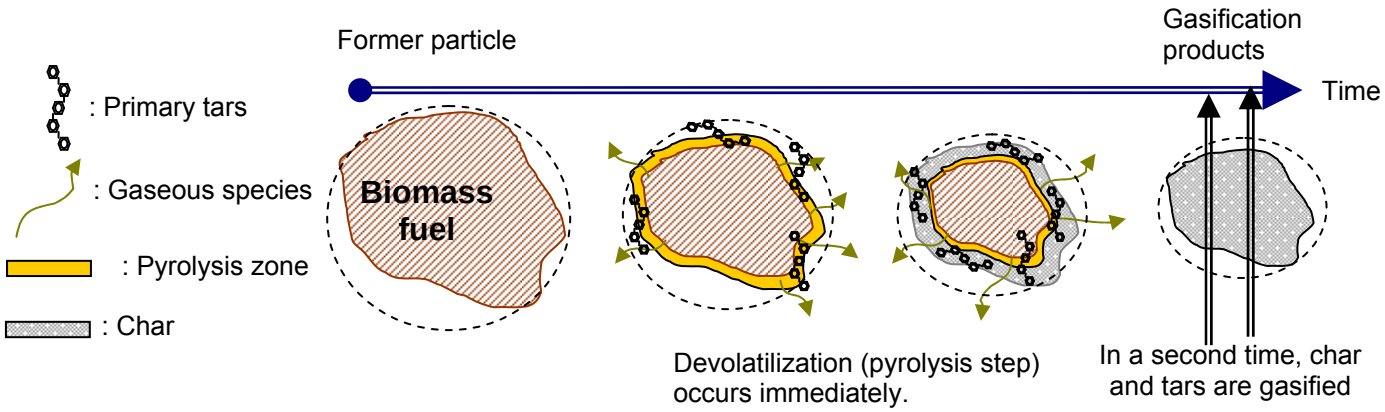

Figure 5. Different stages in the gasification of a biomass particle.

The dissociated and volatile components of the fuel formed during the pyrolysis step are vaporized at temperatures as low as 600°C. Those primary vapours are made of gaseous permanent species and larger condensable molecules (acetol and acetic acid) called primary tars. Their formation can not be avoided (Morf et al., 2002). In gasification conditions, secondary reactions involving primary tars initiates at 700-850°C, producing secondary compounds (phenolics and other monoaromatics). At higher temperatures, tertiary conversion to polyaromatic hydrocarbons (PAHs) starts and the soot formation is observed simultaneously (Morf et al., 2002). All these reactions (cracking, partial oxidation, (re)polymerisation, and condensation reactions) take place in the gas phase between permanent gases and tar vaporized species. They can react even inside the biomass particle unless it has a diameter < 1mm. The surface of the char formed by devolatilization of the original particle catalyzes those reactions (see § I-5.2). This tar formation pathway can be visualised as reported in Figure 6.

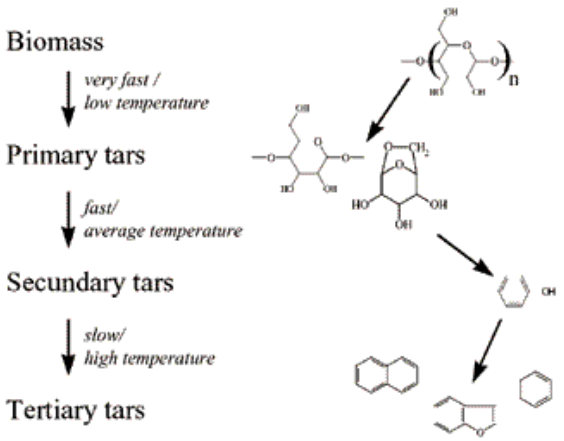

Figure 6. Biomass-tar reactions (Morf et al., 2002)

Char (fixed carbon and ash) are the pyrolysis by-products that are not vaporized.

In the last step, the char is gasified through reactions with oxygen, steam or hydrogen (but air is commonly used to reduce costs and security hazards). Some of the unburned char may be combusted to release the heat needed for the endothermic pyrolysis reactions.

Generally pyrolysis proceeds much more rapidly than gasification, and the latter is thus the rate-controlling step.

The reactions taking place in the gasification step can be summarized as reported below (Bangala et al., 1997).

Partial oxidation	$C + 1/2O_2 \rightarrow CO$	$\Delta H = -268 MJ/kg\ mol$
Complete oxidation	$C + O_2 \rightarrow CO_2$	$\Delta H = -406 MJ/kg\ mol$
Water gas reaction	$C + H_2O \leftrightarrow CO + H_2$	$\Delta H = +118 MJ/kg\ mol$

The heats of reactions for the three processes show that the greatest energy release is derived from the complete oxidation of carbon to carbon dioxide i.e. combustion, while the partial oxidation of carbon to carbon monoxide accounts for only about 65% of the energy released during complete oxidation. Unlike combustion that produces only a hot gas product, carbon monoxide, hydrogen and steam can undergo further reactions during gasification as follows:

Water gas shift reaction	$CO + H_2O \leftrightarrow CO_2 + H_2$	$\Delta H = -42 MJ/kg\ mol$
Methane formation	$CO + 3H_2 \leftrightarrow CH_4 + H_2O$	$\Delta H = -88 MJ/kg\ mol$

The double arrows indicate that the reactions are in equilibrium and can proceed in either direction, depending on the operating conditions. As for pyrolysis, proportions of each product largely depends on parameters like fuel nature, temperature, heating rate, residence time inside the conversion system. If the heating rate is high enough (hundreds of °C per second) to provoke immediate devolatilization of the solid fuel and if the temperature is high enough (> 750°C) to avoid condensation reactions, gas phase is mainly produced. It is constituted of H_2, CO, CH_4, CO_2, $H_2O_{(vap)}$ and light hydrocarbons like C_2H_4. It can be further processed towards hydrogen-rich gas by methane and light hydrocarbons reforming, as well as by water gas shift reaction. Gasification coupled with water-gas shift is the most widely practised process route for biomass-to-hydrogen

technologies (Shafizadez, 1968). Thermal, steam and partial oxidation gasification technologies are under development around the world.

A number of studies have focused on gasifier configuration, screening the impact of temperature, carrier gas used, biomass composition, feeding and particle size, as well as the modification of the overall efficiency using catalysis (Corella et al., 1999; Rapagnà et al., 2000; Chaudhari et al., 2001; Matsumura and Minowa, 2004; Hu et al., 2006).

Three product gas qualities can be produced from gasification by varying the gasifying agent, the method of operation and the process operating conditions. The main gasifying agent is usually air but oxygen/steam gasification and hydrogenation are also used.

The three types of product gas have different calorific values (Morf et al., 2002):

Low Calorific Value	4-6 MJ/Nm^3	Using air and steam/air
Medium Calorific Value	12-18 MJ/Nm^3	Using oxygen and steam
High Calorific Value	40 MJ/Nm^3	Using hydrogen

Low calorific value gas is used directly in combustion or as an engine fuel, while medium/high calorific value gases can be utilized as feedstock for subsequent conversion into basic chemicals, principally methane and methanol.

As the use of oxygen for gasification is expensive, air is normally used for processes up to about 50 MW_{th}. The disadvantage is that the nitrogen introduced with air dilutes the product gas, giving a gas with a net calorific value of 4-6 MJ/Nm^3 (compared with natural gas at 36 MJ/Nm^3). Gasification with oxygen and with steam gives a gas with a net calorific value of 10-15 MJ/Nm^3 and 13-20 MJ/Nm^3, respectively.

It can be seen that while a range of product gas qualities can be produced, economic factors are a primary consideration. In contrast to steam and oxygen gasification, the process with air is particularly suitable for operation at small-to-medium scale due to its simplicity and lack of dependence on complex industrial infrastructures and utilities. Unlike the reaction with air/oxygen, the reaction of carbon with steam (the water gas reaction) is endothermic, requiring heat to be transferred at temperatures around 700°C, which is difficult to achieve. Gasifiers self-sufficient in heat are termed auto-thermal whereas if they require heat they are named allothermal; auto-thermal processes are the most common (McKendry, 2002).

The main challenge of biomass gasification is the conversion of tar produced.

The tarry compounds are highly undesirable since they condense in the cold parts of the plants, plugging the tubes and provoking agglomeration. Tars are highly carcinogenic and represent an important amount of unconverted energy (Abu-El-Rub et al., 2004). The knowledge of the tar formation phenomena is of interest in gasification applications to control secondary and tertiary reactions of the products. Then the production of condensable species (Simell et al., 1997; Simell et al., 1999; Pengmei et al., 2003) can be limited. The possible abatement/conversion of tar will be discussed later.

I-3.1 Biomass gasifiers

Gasification technology can be operated either as a simple, low technology system based on a fixed bed gasifier, or as a more sophisticated one using fluidized bed technology. The properties of the biomass feedstock (moisture content, particle size and ash content) and its preparation (drying, fractionation and leaching) are key design parameters when selecting the gasifier system (McKendry, 2002). In particular, woody biomass fuels have very low heat conduction properties, mainly due to the water content (5 to 50% in mass), which makes difficult the heat transfer to the solid fuel and lowers the conversion efficiency. Above 30 wt%, the gasification of the fuel is impossible. Therefore, a drying step is generally necessary. As far as the particle size is concerned, larger particles can form bridges which prevent the feed moving down, while smaller particles tend to clog the available air voidage, leading to a high pressure drop. Feed particle sizes in the range 20-80 mm are typical. Finally, alkali metals contained in ash start melt roughly at 800°C, provoking agglomeration of fuel particles as well, thus, lowering the contact with the gasifying agent. Ash can be partially extracted from the former biomass material, performing a preliminary treatment which increases, in turn, the cost of the final product (Arvelakis et al., 2002). Gasifiers are of two main types, fixed and fluidized bed.

I-3.1.1 Fixed bed biomass gasifiers

The fixed bed gasifiers have been traditionally used for gasification at operating temperatures around 1000°C. Depending on the direction of the gas flow, the fixed bed gasifiers are classified as updraft (Figure 7a), downdraft (Figure 7b) or cross-flow (McKendry, 2002).

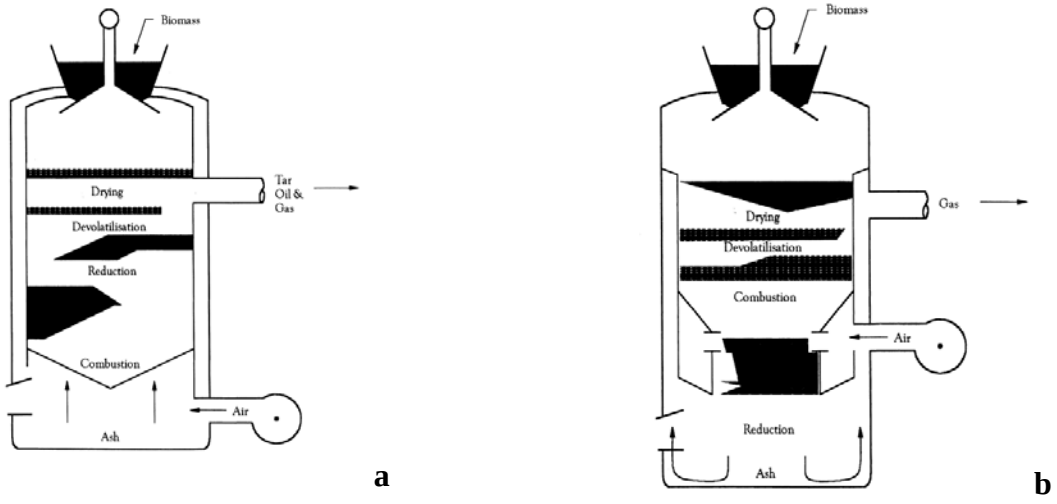

Figure 7. a) Updraft gasifier; **b)** Downdraft gasifier (McKendry, 2002).

In the updraft gasifier the feed is introduced at the top and the gas at the bottom of the unit; in the downdraft the feed and the gas move in the same direction; finally, in a cross-flow gasifier the feed moves downwards while the gas is introduced from the side, the gases being withdrawn from the opposite side of the unit at the same level.

In general fixed bed gasifiers have the advantage of a simple design but the disadvantage of producing a low calorific value gas with a high tar content. The product gas composition is typically 40-50% N_2, 15-20% H_2, 10-15% CO, 10-15% CO_2 and 3-5% CH_4, with a net calorific value of 4-6 MJ/Nm^3.

Improvements of gas quality have been proposed by operating a two-stage (two-reactor) process. Pyrolysis of the biomass takes place in the first stage using an external heating at 600°C. The gases formed in the first zone are then reacted with steam to crack the tars. In the second zone the gases react with the char from the first stage to produce the final product gas.

I-3.1.2 Fluidized bed biomass gasifiers

Fluidized bed technologies are very promising in biomass gasification. Fluidized bed gasification has been used extensively for coal gasification for many years, its advantage over fixed bed gasifiers being the uniform temperature distribution achieved in the gasification zone. The uniformity of temperature is achieved using a bed of fine material into which gas is introduced, fluidizing the bed material and ensuring intimate mixing of the hot bed material, the hot gas and the biomass feed. The system has also a good fuel flexibility and support low operating temperature. Thanks to a high heat transfer rate, the introduced biomass fuel is heated very quickly (more than

100°C·s^{-1}). Two main types of fluidized bed gasifiers are in use: low-velocity bubbling fluidized bed (Figure 8a) and high-velocity circulating fluidized bed (Figure 8b).

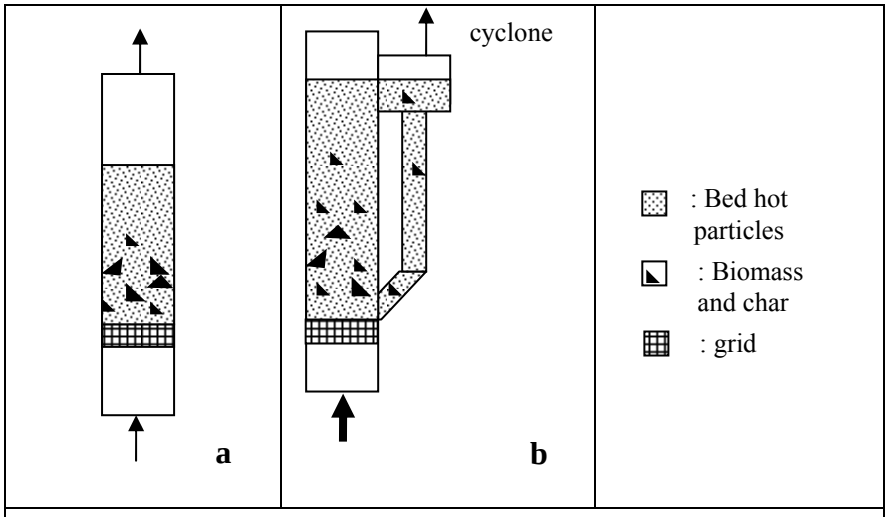

Figure 8. a) Bubbling fluidized bed; **b)** Circulating fluidized bed.

A third type of fluidized bed is currently being developed, termed a fast, internally circulating gasifier, which combines the design features of the other two types.

The bubbling fluidized bed gasifier consists of a vessel with a grate at the bottom through which the gas is introduced. The moving bed of fine material into which the prepared biomass feed is introduced is above the grate. Bubbling fluidized bed technology provides a good gas and solid mixing, uniform temperatures and high reaction rates; in comparison with fixed bed gasification, it results in greater tolerance to particle size range and safer operation due to good temperature control. In addition, tar cracking and reforming catalysts can be added to the bed inventory. However there are drawbacks, in particular: i) the tendency of the biomass and volatiles emitted from the biomass to segregate to the surface of the bed as a result of both the low density of biomass with respect to the bed particles, which constitute the major component of the bed inventory, and the production of volatiles bubbles, which could promote the biomass and volatiles segregation on the top of the bed; ii) the tendency of the fine carbon particles produced in the reaction process due to comminution phenomena to be elutriated by the product gas, thereby increasing the solid load in the cyclone and the filter (Foscolo et al., 2007).

In the circulating fluidized bed the material is circulated between the reaction vessel and a cyclone separator, where the ash is removed and the bed material and char returned to the reaction vessel. In the application of fluidization technology to reaction processes involving heterogeneous systems, circulation of the bed inventory has often been considered beneficial, resulting in

improvements in gas solid contact and reactor throughput. Fast circulating fluidized bed reactors have proved to be very efficient in cases where rapid reaction kinetics are involved, especially with regard to gas phase reactions.

The experimental evidence, however, shows that the heterogeneous gasification reactions and the cracking and reforming processes of the organic vapours, which all follow the fast biomass devolatilization step, are relatively slow processes, and that the residence time of these vapours at the high temperature of the gasifier contributes positively to the quality of the fuel gas. For these reasons a bubbling fluidized bed reactor would appear to offer clear advantages in cases where the yield of a clean, gaseous energy vector is of overriding priority (Foscolo et al., 2007).

The fluidization characteristics of biomass materials are very important for fluidized bed reactor design and modelling. Biomass fuels cannot be easily fluidized due to their peculiar shapes, sizes, densities, moisture content and compressibility (Cui and Grace, 2007). For proper fluidization and processing in the reactor, a second solid, usually an inert material like silica sand, alumina, calcite, etc., is used to facilitate fluidization of biomass. It also acts as a heat transfer medium in the reactor. In other words, many of the applications involve biomass particle co-fluidized with much denser and more regular particles, such as sand or catalysts. Although considerable progress has been made in utilizing biomass in bubbling and circulating fluidized bed reactors, the characterization of the multi-phase flow aspects is actually under study. Flow is complex given the heterogeneous nature of the particles, turbulence of fluidizing fluid, complex geometry, simultaneous heat and mass transfer and rapid gas release during devolatilization. Rao and Bheemarasetti (2001) proposed a study of the influence of size, density and fuel/bed particle ratio on the minimum fluidization velocity of the mixture. Rasul (1998) worked on biomass fluidizability at room temperature using light bed materials compared to sand (FCC and Pumice stone) in the aim to increase fluidization capability of bagasse.

Interaction and mixing of the species then become major issues (Cui and Grace, 2007), especially for bubbling fluidized beds. In the case of a binary system of particles (biomass and bed material) used in a bubbling fluidized bed, large differences in size and density between biomass and bed particles lead to a non-uniform distribution of biomass particles within the bed. In fact, one kind of particle (biomass) tends to migrate towards the upper region of the bed, and the other (bed particles) towards the lower section of the bed. This would correspond to a bad mixing (segregation) of biomass particles in a bubbling fluidized bed. If the vertical mixing between biomass and bed particles is low and the biomass particles tend to float in the upper regions of the bubbling fluidized bed gasifier, volatiles are released into the freeboard. Thus, the energy requirements for water evaporation and heating of fluidizing stream inside the bed may not be

fulfilled, resulting in difficulties to maintain a sufficiently high gasification temperature. The gas product yield would be reduced as a result of the lower heating rates involved (Shen et al., 2007).

Moreover, the production of volatiles during the devolatilization phase could promote the biomass segregation on the top of the bed. Fiorentino et al. (1997a and 1997b) and Bruni et al. (2002) highlighted the conditions under which interaction between the gas-emitting particle and the emulsion phase results into the formation of an endogenous volatile bubble that eventually rises to the bed surface. The uprising of endogenous bubbles can induce faster self-segregation of the fuel particle to the top of the bed according to either single bubble segregation (SBS) or multiple bubble segregation (MBS) patterns. The former occurs when the first generated volatile bubble is able alone to lift the fuel particle to the top of the bed. The MBS pattern occurs when particle segregation results from stepwise motion associated with generation of multiple volatile bubbles to promote endogenous bubbles.

In a bubbling fluidized bed, a possible solution to avoid or at least limit the biomass segregation phenomena is to use a bed material having a density similar to that of the biomass fuel and of the corresponding char. Biagini et al. (2005) studied the properties (densities, shape factors, etc.) of different biomass derivative chars obtained at high heating rates in a sand fluidized bed.

Moreover, to increase the mixing between hot particles surface and solid fuel it is possible to adopt some ad hoc configuration of the reactor with the goal of improving particle circulation into the reactor.

In this framework Foscolo et al. (2007) recently proposed a novel reactor design for application to fluidized bed biomass gasification with air. It is based on the principle of interconnected fluidized beds. The reactor vessel is divided in two distinct fluidization chambers, separated by a baffle plate, which communicate by means of an opening at the base and a common freeboard. The two chambers are operated at different gas velocities. The more dense bed will move downwards, while the other, which contains a greater fraction of bubbles, will move upwards. The light biomass particles are fed to the more dense bed, where their tendency to segregate by migration towards the surface is counteracted by the circulation process in the opposite direction. Solid circulation, that takes place around these two zones, is capable of maintaining the buoyant biomass particles immersed in the bed throughout the whole heterogeneous reaction process. Gaseous streams leaving the low and the high density beds mix together in a joint freeboard before leaving the reactor. Circulation of the solids through the two beds, delivering a better distribution of the relatively light biomass fuel, assists the rapid heating of the fuel particles by providing a uniform, high temperature environment throughout the whole thermo-chemical conversion process; fine carbon particle elutriation is also reduced. These factors all favour the yield and quality (low tar content) of the product gas.

Pfeifer et al. (2004) proposed the coupling of a stationary and a fast fluidized bed for biomass steam gasification. The two reactors are interconnected as far as the bed inventory is concerned and with the separation of the fuel gas (the gasification product) from the flue gas (the combustion product). Gasification takes place in the bubbling fluidized bed, utilizing thermal energy provided by the granular solids (sand, olivine, etc.). These in turn, together with some char formed as a by-product of the biomass devolatilization process, are circulated to the bottom of the fast fluidization column, where they are contacted with air, and some additional fuel, to produce the necessary heat by means of combustion reaction. The "double-zone" design avoids contamination of fuel gas by the nitrogen contained in the air, thus delivering a gaseous fuel of medium-high calorific value, without the need for pure oxygen as the gasification agent. The process is of necessity a somewhat complex one: two different gas output streams have to be dealt with, each with its corresponding treatment device; and careful control of pressure in both reactor zones is crucial for delivering the correct bed circulation and for avoiding gas contamination; in addition, carbon conversion of the biomass is reduced as a result of the consumption of charcoal in the combustion zone (Foscolo et al., 2007).

Finally, one of the major operational difficulties experienced with fluidized bed gasifiers is the risk of agglomeration of the bed material due to the ash content of the biomass. Of particular importance is the alkali metal content of the biomass. To avoid agglomeration, the bed temperature can be lowered but this results in an increased loss of char with the ash removed. Natarajan et al. (1998) have shown the necessity to control the temperature of the gasification process with different biomass fuels, using an ASTM standard ash fusion test in fluidized bed (see Table 2).

Table 2. Initial agglomeration temperatures in fluidized bed gasification (Natarajan et al., 1998).

	Initial agglomeration temperature (°C)	
	Bed material = quartz	Bed material = lime (CaO)
Rice husks	>1020	>1020
Sugar cane bagasse	>1020	>1020
Cane trash	834	-
Olive flesh	880	-

I-4 Gas conditioning

Conditioning and upgrading the biomass gasification products are necessary whatever the end use of the gas produced (gas turbine, fuel cells, methanol or Fischer-Tropsch synthesis). As already mentioned, one of the main problems is the formation of tars which can condense in the exit pipelines and filters in addition to other troubles related to specific applications. As a consequence, biomass gasification products require substantial conditioning including tar conversion not only for tar removal but also to achieve the optimal gas composition.

Morf et al. (2002) attempted to classify in three classes tarry compounds produced in biomass gasification as reported in Table 3. Several compounds appear in the second and in one of the other two classes as well, demonstrating the evolutionary development and the somewhat arbitrary boundaries for the three tar classes. They mostly begin to condense at temperatures < 450 °C. Tars are very reactive compounds, and the kinetics of their reactions are not well known for gasification.

Gas conditioning generally involves a multi-step approach depending on the end use of the product gas. Milne and Evans (1998) tabulated the tar tolerance limit for various end use devices, suggested by different researchers. If the end use requires cooling to near room temperature, physical removal techniques, like wet scrubbing and filtration, are employed. Nevertheless, these methods do not eliminate tar but just transfer it from the gas phase to a condensed phase thus not solving the environmental problems related to tar accumulation.

If the end use requires that products remain at high temperature, tar can be eliminated by hot gas cleaning methods (thermal cracking at 900–1100°C and catalytic cracking at 600–900 °C (Bangala et al., 1997)) converting it into desired gas components thus keeping its chemical energy and avoiding additional treatment of the waste stream. The catalytic cracking methods also have the advantage to allow a suitable adjustment of gas product composition achieved also through steam addition (Dayton, 2002).

Table 3. Classification of biomass gasification tars (Morf et al., 2002).

tar compound class	compound type	compound name
Primary tars	Acids	acetic acid propionic acid butyric acid
	Ketones	acetol
	Phenols	phenol 2,3-dimethylphenol 2,4/2,5-dimethylphenol 2,6-dimethylphenol 3,4-dimethylphenol 3,5-dimethylphenol
	Guaiacols	guaiacol 4-methylguaiacol
	Furans	furfural furfural alcohol 5-methylfurfural
Secondary tars	Phenols	phenols o-cresol p-cresol m-cresol
	Monoaromatic hydrocarbons	p/m-xylene o-xylene
Secondary/Tertiary tars	Monoaromatic hydrocarbons	benzene ethylbenzene a-methylstyrene 3&2-methylstyrene 4-methylstyrene 3-ethyltoluene 4-ethyltoluene 2-ethyltoluene
	Miscellaneous hydrocarbons	2,3-benzofuran dibenzofuran biphenyl indene
	Methyl derivatives of aromatics	2-methylnaphthalene 1-methylnaphthalene toluene
	PAH: 2 ring	acetylnaphtylene acetylnaphtene fluorene naphtalene
	3-ring	phenanthrene antracene fluoanthene pyrene
	4-ring	benz(a)anthracene chrysene benz(e)acephenanthtrylene benzo(k)fluoranthene
	5-ring	benzo(a)pyrene perylene dibenzo(ah)anthracene indenol(1,2,3-cd)pyrene
	6-ring	benzo(g,h,i)perylene

I-5 Use of catalysts in biomass gasification

The use of a catalyst in biomass gasification has two main goals: i) enhancement of gas formation by converting tars; ii) promotion of the reforming reactions of hydrocarbons (including methane) contained in the gas phase.

Moreover, the catalyst has to demonstrate particular properties such as an acceptable life time in the considered operative conditions, such as coking resistance, easy regeneration and moderate cost.

In order to solve the problem of tar formation in biomass gasification two approaches exist both based on the use of a catalyst: primary methods (the catalyst is inside the gasifier) and secondary methods (the catalyst acts downstream). Both primary and secondary techniques show a quite good tar reduction capability but, for economic reasons, a single process is generally preferred.

Three groups of catalyst materials have been applied in biomass gasification systems: alkali metals, natural non-metallic oxides, and supported metallic oxides (Sutton et. al., 2001). Alkali salts are mixed directly with the biomass as it is fed into the gasifier. The non-metallic and supported metallic oxide catalysts are usually located in a separate fixed bed reactor, downstream from the gasifier, to reduce the tar content of the gasification product gas and are therefore, referred to as secondary catalysts. Although the non-metallic catalysts are sometimes used as bed material in fluidized bed gasifiers to affect tar formation, single catalytic reactors can be used with any gasification technology and controlled to maximize the versatility of the hot gas conditioning process. The literature associated with the above described classes of catalysts is reviewed in the next sections.

I-5.1 Alkali metals catalysts

Although they cannot be strictly considered catalysts, alkali metals can lead to positive catalytic effects on pyrolysis process. A better effect has been attributed to K_2CO_3 with respect to Na_2CO_3 (for olive husk pyrolysis). The performance of Na_2CO_3 also appears to be a little bit stronger than that of $CaCO_3$ (Caglar and Demirbas, 2002). It is well known from several fundamental studies of cellulose and biomass pyrolysis that alkali metals enhance char formation reactions during thermo-chemical conversion (Antal and Varhegyi, 1995; Raveendran, 1995; Raveendran et al., 1996). Poorer carbon conversion, increased ash content, and the fact that the

added alkali metals are difficult to recover make alkali metals unattractive gasification catalysts for commercial use.

I-5.2 Natural non-metallic oxides catalysts

The most widely studied non-metallic catalysts for the conversion of tar from biomass gasification are dolomites (calcium magnesium carbonates). Their general formula is $Ca(Mg,Fe)(CO_3)_2$ and the amounts of magnesium and iron can vary, modifying the catalytic activity. The dolomite is generally calcined before use, giving calcium, magnesium carbonates and iron oxides. The latter was shown to have particular activity in tar conversion in the form Fe_2O_3 (Uddin et al., 2008). These naturally occurring catalysts are relatively inexpensive and disposable so it is possible to use them as primary catalysts (in bed) as well as in secondary, downstream reactors. Corella et al. (1999) showed that the use of dolomite as secondary catalyst could led to tar conversion as high as 95%. Nevertheless, many investigators have reported a decrease in the mechanical strength of the calcined dolomite over time, which is a problem when used as primary catalyst in a fluidized bed reactor since it leads to catalyst attrition (Baker et al., 1987; Simell et al., 1995).

An interesting alternative to calcined dolomite is olivine, a magnesium and iron aluminosilicate of general formula $(Mg,Fe)_2SiO_4$. Rapagnà et al. (2000) found the tar reforming activity of olivine comparable to that of calcined dolomite. Olivine, however, is a much stronger material and has a good attrition resistance in fluidized bed reactors; for this reason, it is an attractive material for use as an in-bed tar reforming catalyst in fluidized bed gasifiers.

Studies have also been performed using char as catalyst for biomass tar decomposition. The activity of char is essentially due to its very high surface area. It has been shown that char resulting from biomass devolatilization was more efficient than the ones obtained from coal (Sutton et al., 2001). The main advantage of such catalyst is that it is already present inside the gasifier, but it also continuously gasified, thus a separate feeding is required.

I-5.3 Supported metallic oxides catalysts

I-5.3.1 Commercial synthetic reforming catalysts

The success of reforming biomass gasification tars with supported Ni-based catalysts has also been extensively demonstrated.

A wide variety of Ni-based steam reforming catalysts are commercially available because of their application in the petrochemical industry for naphtha reforming and methane reforming to make syngas. Nickel-based catalysts have also proven to be very effective for hot conditioning of biomass gasification product gases. They have high activity for tar destruction, for methane reforming in the gasification product, and for water-gas shift to adjust the H_2/CO ratio of the product gas. Nevertheless, sulphur, chlorine and alkali metals, that may be present in gasification product gases, act as Ni-catalyst poisons. In addition, Ni promotes coke formation which reversibly deactivates the catalyst (Juutilainen et al., 2006). However, even if coke can be removed by regenerating the catalyst, repeated high temperature processing of nickel catalysts can lead to sintering, phase transformations, and volatilization of the metal. Because of this sensibility, nickel catalysts are generally used in secondary bed reactors for hot gas cleaning (Baker et al., 1987; Hepola and Simell, 1997a and 1997b).

Several studies have been devoted to the modification of Ni reforming catalysts. Improving of gas yields were obtained with Ni/Al catalysts (Garcia et al., 2000). Impregnation of olivine with Ni was also attempted (Courson et al., 2000) as well as the addition of different promoters as Cr, La_2O_3 and MgO inhibiting NiC and coke formation and providing a better mechanical resistance to the support, respectively. Generally, the addition of basic oxides to the support and promotion with Co or Cr increase H_2 yield and catalyst lifetime (Garcia et al., 2000). Some of the problems (coke formation, sintering) related to the use of Ni based catalysts have be successfully reduced by dispersing Ni in a perovskite matrix. Rapagnà et al. (2002) identified $LaNi_{0.3}Fe_{0.7}O_3$ as the best bi-metallic perovskite composition to obtain a good activity at the temperature and concentration conditions typically encountered in the conditioning process of the hot gas produced by fluidized bed steam gasification of biomass materials.

I-5.3.2 Other synthetic catalysts

Among transition metal oxides, Cr_2O_3 appears to have a stronger catalytic role in hydrogen production (and gas yield in general) from biomass pyrolysis (Chen et al., 2003), whereas CuO appears to have a negative influence in the process (Simell et al., 1992). The catalytic capability of

the iron oxides FeO, Fe_2O_4, and Fe_3O_4 have also been studied in previous studies. The results, however, indicate that they do not possess any catalytic capacity for enhancing gas production. On the other hand, the iron in metallic state (and Fe_2O_3) showed high catalytic activity as far as carbon-breaking ability was concerned. In fact, the intrinsic capability of iron was shown to be comparable to that of the calcined dolomite which at present is the most commonly used catalyst for tar breakdown in gasification applications (Nordgreen et al., 2006).

Juutilainen et al. (2006) studied the effect of zirconia/alumina catalyst in the selective oxidation of tar and ammonia in biomass gasification. They used toluene as tar model compound. The presence of both zirconia and alumina in the catalyst promoted toluene and ammonia conversions at low temperatures: zirconia enhanced the oxidation activity, while alumina improved the oxidation selectivity. The presence of H_2S had little effect on the activity of alumina-doped zirconia.

Supported noble metal-based catalysts are the main components of catalysts for controlling emissions of exhaust gases from internal combustion engines. When used in biomass gasification systems, they demonstrate very high tar conversion efficiency and no coking tendency. These materials are usually preferred as active phase, since they generally allow one to operate at lower temperature and higher space velocity than other types of catalysts. However, noble metals are expensive, sensitive to poisons (sulphur) and sometimes demonstrate a poor thermal stability (sintering phenomena). Nevertheless, their very high activity explains the multiple studies made in order to stabilize small amounts of these elements with ceramic oxides containing or not transition metals, thus, limiting the poisoning and sintering phenomena.

CeO_2 supported Rh catalyst efficiently converted cellulose to gas products even at 550°C with very few coke formation (Asadullah et al., 2001 and 2002). Rh was selected among different noble metals (Rh, Ru, Pt, Pd and Ni) providing the best results (Asadullah et al., 2001, Tomishige et al., 2004). Sintering of cerium oxide was avoided by deposition on SiO_2. The authors also compared the catalyst performances in a single (primary) and dual (secondary) reactor configuration (Tomishige et al., 2004). They found a good gasification activity of the $Rh/CeO_2/SiO_2$ catalyst in the single bed reactor for a low ash content biomass (cedar wood), whereas a rapid deactivation was observed for biomass with a high ash content (rice straw) suggesting the use of a dual bed configuration in that case. On the other hand, coke formation is highly suppressed in the single bed reactor due to the good oxidation activity provided by ceria. In contrast to Ni, Rh-ceria based catalysts also show a high resistance to carbon deposition and sulphur poisoning likely due to the oxidation of adsorbed sulphur to SO_2 in oxidizing atmosphere or to the reduction to H_2S in a reducing atmosphere (Tomishige et al., 2004; Strohm et al., 2006).

I-5.4 Catalysts from other processes

In addition to these catalysts other materials should be mentioned which can be potentially applied in biomass gasification processes.

I-5.4.1 Modified FCC catalysts

In the last decade, several studies have been carried out in order to investigate the properties of transition (Ni, Cu, Co, Cr, Mn) and noble metal (Pt, Pd, Rh) exchanged or impregnated zeolite catalysts in partial and deep oxidation of hydrocarbons. The results have shown that the catalytic behaviour depends on the reducibility and acidity of the catalysts and on the oxygen carrier capacities (Antunes et al., 2001). In fact, transition metal cations improve the zeolite activity for hydrocarbon conversion by increasing both the zeolite acidity (by cation hydrolysis) and oxygen chemisorption (Antunes et al., 2001). However, most of the literature has been devoted to coking occurring during hydrocarbon reactions which proceed in an oxygen-free environment. This remains the main cause of catalyst deactivation during the transformation of organic reactants.

The catalytic cracking performances of the hierarchical zeolite catalyst (both micro- and macro-porous) and the microporous ZSM-5 have been tested (in a fixed bed reactor) for catalytic cracking of 1,3,5-triisopropylbenzene (TIPB, denoted as isopropylbenzene, m-diisopropylbenzene and p-diisopropylbenzene, respectively) at 623 K. The microporous ZSM-5 has 10-ring pores with diameter no larger than 0.56 nm, while TIPB has a dynamic diameter of 0.94 nm and cannot diffuse through the inner pores of ZSM-5. Therefore, catalytic reaction can only occur on the external surface of ZSM-5 crystals. However, the hierarchical zeolite catalyst showed an initially high catalytic activity corresponding to 98% conversion (Lei et al., 2006). Nevertheless, the moisture concentration of the biomass feed makes impossible the use of such catalyst as in-bed catalyst.

Although vanadium and nickel are known to be active in hydrocarbons oxidation (Ferreira et al., 2004), they can not be deposited on zeolite compounds, since they causes their destruction by a mechanism of acid attack or solid-solid transformation.

Antunes et al. (2001) developed a copper modified zeolite Y (dealuminated then stable at high temperatures, even with steam) which showed good yields in toluene conversion as well as for soot abatement. Their CuNaHY catalysts was found to decompose toluene in water and carbon dioxide, and to modify the coke formation, promoting the deposition of oxygenated compounds at low temperature (< 250°C) (Antunes et al., 2001).

I-5.4.2 Soot oxidation catalysts

The following compounds are applied to soot removal in diesel engine applications but could be applied to biomass decomposition since formation of soot particles has been observed in biomass pyrolysis (Uner et al., 2005). Catalytic decomposition of soot is considered to be an oxygen donor mechanism, rather than an electronic mechanism. The catalytic effect is due to the fact that carbon adsorbs metal-bound oxygen atoms (–MO) faster than molecular-bound oxygen (Stanmore et al., 2001).

Cerium and noble metals (generally Pt) are commonly used for the control of diesel soot emissions. Alkali and alkaline earth metals are especially effective in reforming with H_2O and CO_2 but have low melting points, then deactivates at temperatures <500°C. Some recent studies highlight the activity of mixed oxides ($CoCr_2O_4$) or noble metal supported catalysts in soot and more specifically aromatics oxidation as well as NO_X abatement (Fino et al., 2006; Lei et al., 2006). Uner et al. (2005) developed a CoO_x-PbO_x catalyst promoted with 0.5 wt% of Pt able to decrease the soot oxidation temperature down to 378°C in a gas stream of 8% O_2 in nitrogen. The stabilisation of alkali metals in mixed oxides ($La_{0.8}Cr_{0.9}Li_{0.1}O_3$) structures provided good results in soot oxidation as well, even at 400°C (Russo et al., 2005). The use of catalysts inspired from these applications could be considered for in-bed biomass gasification process.

In Table 4 a summary of the different catalysts commonly used to limit tar formation is reported (Abu-El-Rub et al., 2004).

Table 4. Summary of tar-destruction catalysts (Abu-El-Rub et al., 2004).

catalyst	advantages	disadvantages
calcined rocks	inexpensive and abundant attain high tar conversion ~95% conversion with dolomite often used as guard beds for expensive catalysts most popular for tar elimination	fragile materials and quickly eroded from fluidized beds
olivine	inexpensive high attrition resistance	lower catalytic activity than dolomite
clay minerals	inexpensive and abundant fewer disposal problems	lower catalytic activity than dolomite most natural clays do not support the high temperatures (800–850 °C) needed for tar elimination (lose pore structure)
iron ores	inexpensive abundant	rapidly deactivated in the absence of hydrogen lower catalytic activity than dolomite
char	inexpensive natural production inside the gasifier high tar conversion comparable to dolomite	consumption because of gasification reactions
FCC	relatively inexpensive but not cheaper than the above more known about it from experience with FCC units	rapid deactivation by coke lower catalytic activity than dolomite
alkali-metal-based	natural production in the gasifier reduce ash-handling problems	particle agglomeration at high temperatures lower catalytic activity than dolomite
activated alumina	high tar conversion comparable to that of dolomite	rapid deactivation by coke
transition-metal-based	able to attain complete tar elimination at ~900 °C increase the yield of CO_2 and H_2 Ni-based catalysts are 8–10 times more active than dolomite	rapid deactivation because of sulfur and high tar content in the feed relatively expensive

I.6 Aim of the PhD thesis

On the basis of the data collected in the literature, it emerges that a gas with suitable composition and purity could be in principle obtained from biomass gasification process carrying out the reaction in a catalytic fluidized bed using a catalyst with high efficiency in biomass tar conversion. This requires the development of either a catalytic system and an adequate reactor configuration which favors the contact between biomass and catalyst particles.

Therefore, one of the main objective of the present PhD thesis is the development of a novel catalyst to convert products from biomass decomposition to a H_2-rich syngas. The properties required to the catalyst are: good reforming and oxidation activity, chemical, thermal and mechanical resistance, low sensitivity to coke deposition and a long lifetime. The research activity will involve the choice of both suitable active phase and support for the catalyst, and the development of an ad-hoc plant for catalytic screening providing qualitative and quantitative information on the catalyst performances under different operative conditions (reaction temperature, contact time). The experimental data obtained will be used to optimize the catalyst formulation taking into account both efficiency and costs of the material.

The second objective is the development of a pilot fluidized bed gasifier with a suitable configuration to limit the segregation of biomass during biomass gasification operation by the design of an ad-hoc conical gas distributor. An experimental campaign using conventional catalysts will be carried out in order to set up the pilot scale fluidized bed gasifier.

The detail of the performed research activity of this PhD is schematically reported below:

1. Development of a protocol for characterization of the thermal behaviour of different biomass.
2. Development of catalysts with defined properties able to convert biomass tar into syngas.
    - Catalyst synthesis.
    - Catalyst characterization.
3. Development of a lab scale test ring, equipped with a dual fixed bed reactor, for catalytic screening.
    - Development of an analysis protocol for gas, condensable tar and solid.
    - Catalytic screening campaign involving comparison of the chosen catalyst with conventional catalysts, study of the synthesis parameters on activity and evaluation of activity range of the chosen material.
4. Development of a pilot plant fluidized bed gasifier with a suitable configuration for biomass air/steam gasification, to enhance the production of an hydrogen-rich syngas.

- Development of an analysis protocol for gas, condensable tar and solid.
- Catalytic campaign involving conventional catalysts as bed material.

The present thesis will start with a description of the experimental materials (biomass and catalysts) and experimental plants, exposed in the section II. The section III will present the results of materials characterization (III-1), followed by the catalytic activity tests performed in the lab scale test plant (III-2) and in the pilot scale fluidized bed gasifier (III-3). The conclusions of the work will be presented in the part IV. The last part of the thesis (Annexes) will focus on studies of a possible catalytic support with a density as close as possible to that typical of the biomass (Annex A) and of mixing efficiency occurring inside the pilot scale gasifier (Annex B).

II-EXPERIMENTAL SECTION

In the present section the synthesis of the catalysts, the different techniques used to characterize the materials (both biomass and catalysts) as well as the experimental plants for catalytic tests and the test procedures employed in this study will be described in details.

II-1 Materials

II-1.1 Biomass materials and characterization

Maple wood chips and commercial spruce wood pellets were used as fuels. Commercial pellets were used in the pilot scale gasifier because of their availability and low price and maple wood chips were used in the lab scale dual fixed bed plant.

They have been characterized chemically and as concerns their energetic content with the following analysis techniques and experimental apparatus.

The determination of carbon, hydrogen and nitrogen content of the fuels (oxygen was calculated by difference) has been performed using a CHN 2000 LECO analyser. For these experiments, about 20 mg of homogenised sample (by grinding) were introduced in the apparatus. The C, H, N content was obtained by burning the sample at 950°C and measuring the gaseous concentrations using a TCD for N_2 (previously obtained from catalytic NO_x reduction) and two separated NDIR cells for C and H. The others elements (under the forms of SO_x), possibly interfering, were removed before measurements.

The moisture, the volatile, the fixed carbon and the ash content of the biomass materials have been determined using a TGA 701 LECO thermo gravimetric analyzer.

The analysis of the ash composition was determined by ICP-MS using a Agilent 7500CE instrument after dissolving 200 mg of material in 9 ml of a H_2O_2/HNO_3 (2:7) solution kept at 180°C, according to the US-EPA 3051 method.

The determination of the low heating value of the two biomass fuels has been performed using a Parr 6200 Calorimeter. About 1 g of material, grinded in the sizes 3-4 mm, 1 mm and <125

μm was dried in a stove at 120°C and then introduced in the calorimeter bomb. After having filled the tank with pure O_2, a tungsten filament ignited the fuel combustion. The apparatus measured the increase in temperature of two litres of distilled water, which surrounded the tank, to calculate the heating value.

The study of the thermal behaviour of wood chips and the characterization of the species emitted during heating of the fuel has been performed using a Perkin Elmer TGA7 thermo-balance connected to a gas cell of a FTIR spectrometer (Perkin Elmer Spectrum GX) for the analysis of released products. Both FTIR cell and transfer line were heated at 200°C in order to avoid tar condensation. During the experiment, about 25 mg of maple wood chips (125-212 μm) were heated under a constant nitrogen (99.998%) flow rate of 25 $ml \cdot min^{-1}$. The sample was firstly heated up to 100°C at $2°C \cdot min^{-1}$ and this temperature was kept for about 15min in order to completely remove water; then the sample was heated up to 800°C at $5°C \cdot min^{-1}$. When the sample reached a stable weight, in order to burn the fixed carbon after total devolatilization of the sample, kept at 800°C, oxygen (2%vol.) was added to the gas stream. During the heating ramp single scan FTIR spectra were collected each 12 s with 4 cm^{-1} resolution. Thus, an IR spectra of the gaseous products of biomass devolatilization could be registered every degree during the ramp up to 800°C. Tests at heating rates of 1 and $50°C \cdot min^{-1}$ and with different particle sizes (1 mm and 3-4 mm) have also been performed. The TG/FTIR experiment has been repeated several times obtaining the same weight loss and the same profiles of released species.

II-1.2 Catalysts preparation and characterization

One of the aims of this work was the development of a catalyst active in biomass tar conversion to a H_2-rich syngas.

The study of literature led to the conclusion that the active elements should provide good reforming properties to convert tars and light hydrocarbons produced by the biomass into syngas, but also a high oxidation activity to avoid coke formation on the catalyst surface causing catalysts deactivation. In this work, a Rh-$LaCoO_3$ supported on γ-alumina catalyst has been proposed for tar conversion due to the reforming and oxidation properties of noble metal and perovskite respectively, which can potentially improve hydrocarbon conversion and avoid coke formation. In particular, the incorporation of a noble metal in a perovskite matrix represents an interesting solution since perovskite oxide could provide at the same time i) a high thermal resistance related to the stability of the structure, ii) elevate dispersion of the noble metal thus preventing sintering

phenomena (Cimino et al., 2006), which can take place at the typical temperatures of biomass gasification processes (up to 900°C) and allowing the reduction of the metal content reducing catalyst costs, iii) good oxidation properties due to the high oxygen mobility in the perovskite structure. Among noble metals, rhodium is a good candidate due to the high reforming activity and also to the high resistance to sulphur poisoning (Truex, 1999).

The activity and the chemical stability of the Rh-perovskite structure in the partial oxidation of methane has been recently demonstrated by our research team (Cimino et al., 2005 and 2006) and it can be reasonably be supposed that this catalytic behaviour can be extended to more complex systems.

Rhodium promoted $LaCoO_3$ perovskite supported on γ -alumina has been synthesized by wet impregnation. A γ-Al_2O_3 Puralox SCF140-L3 (SASOL) with a superficial area of 140 $m^2 \cdot g^{-1}$ and stabilized by 3wt% of lanthanum oxide to inhibit the γ to α transition of alumina has been used as support. Stoichiometric amounts of cobalt $Co(NO_3)_2 \cdot 6H_2O$ (FLUKA, ≥99%) and lanthanum nitrates $La(NO_3)_3 \cdot xH_2O$ (ALDRICH, >99.9%) were dissolved in water together with the corresponding amount of Puralox in order to obtain a perovskite load of 20wt% corresponding to the theoretical monolayer coverage of the γ-Al_2O_3. Few drops of nitric acid (ALDRICH, 65%) were added to the mixture, which was heated and stirred until complete drying. The remaining powder was then dried for 2 hours at 120°C, and calcined under 150 $ml \cdot min^{-1}$ air flow in an electric furnace (HAEREUS) at $10°C \cdot min^{-1}$ up to 800 or 900°C for 3 hours. The Al_2O_3 deposited with $LaCoO_3$ was consecutively impregnated with a $Rh(NO_3)_3 \cdot xH_2O$ (Riedel-de-Haën) solution using an amount of rhodium corresponding to 0.1, 0.5 and 1 wt% depending on the desired noble metal load, then drying and calcination were repeated following the same procedure as described previously. Catalysts containing 20 wt% $LaCoO_3$ or 1 wt% Rh only were also prepared for comparison with the bi-functional samples.

In the following, the catalysts will be referred to, according to the following notation: T/p/xRh, where T is the calcination temperature, p is $LaCoO_3$ perovskite, Rh indicates the presence of the noble metal and x is the Rh amount in wt%. Table 5 reports this nomenclature as well as the reactor (catalytic screening plant or fluidized bed gasifier), where the different catalysts have been employed. For example: 900/p/1Rh is a catalyst containing both perovskite and 1wt% of rhodium calcined at 900°C.

The performances of this catalyst in biomass tar conversion has been compared with that of conventional materials studied in literature for biomass gasification: natural dolomite and olivine as well as a Ni/γAl_2O_3 catalyst synthesized in our laboratory.

The dolomite was pre-calcined under air for 3 hours at 800°C before use in order to decompose the carbonate, while olivine was used as received. The general chemical formulas of these two natural catalysts are also reported in Table 5.

The nickel catalyst supported on γ-alumina with a nickel content of 5.5 wt% has been synthesized by wet impregnation of γ-alumina particles. Nickel nitrate was dissolved in water and added to a suitable amount of γ-alumina powder (PURALOX SCCA-150/200, SASOL) with a surface area of 160 $m^2 \cdot g^{-1}$). The suspension was dried under vacuum at 60°C. The impregnated powder was calcined for 3 h in air flow at 800°C. As reported in Table 5, this catalyst will be noted Ni/Al_2O_3 in the following.

Table 5. List of catalysts used for activity tests in the lab scale dual fixed bed reactor and in the fluidized bed gasifier.

Notation	Composition and calcination temperature (°C)	Reactor used
Olivine	$(Mg,Fe)_2SiO_4$	Fluidized bed gasifier
Dolomite	$Ca(Mg,Fe)(CO_3)_2$ (800)	
Ni/Al_2O_3	5.5 wt% $Ni/\gamma\text{-}Al_2O_3$ (800)	
800/p/1Rh	1 wt%Rh-20 wt% $LaCoO_3/\gamma\text{-}Al_2O_3$ (800)	Lab scale dual fixed bed reactor
900/1Rh	1 wt% $Rh/\gamma\text{-}Al_2O_3$ (900)	
900/p	20 wt% $LaCoO_3/\gamma\text{-}Al_2O_3$ (900)	
900/p/1Rh	1 wt%Rh-20 wt% $LaCoO_3/\gamma\text{-}Al_2O_3$ (900)	
800/1Rh	1 wt% $Rh/\gamma\text{-}Al_2O_3$ (800)	
800/p	20 wt% $LaCoO_3/\gamma\text{-}Al_2O_3$ (800)	
800/p/0.1Rh	0.1 wt%Rh-20 wt% $LaCoO_3/\gamma\text{-}Al_2O_3$ (800)	
800/p/0.5Rh	0.5 wt%Rh-20 wt% $LaCoO_3/\gamma\text{-}Al_2O_3$ (800)	

The materials have been characterized using the experimental techniques reported below.

Superficial area measurements were carried out according to the BET method using N_2 at 77K with a QUANTACHROM 1-C analyzer. The samples were dried 2 h at 150°C under vacuum before the measurement.

The metal content of the catalysts was determined by ICP-MS using the Agilent 7500CE described in § II-1.1.

Hydrogen Temperature Programmed Reduction (TPR) analysis allowed the determination of the reducibility of the active phase. Two different apparatus were used for TPR measurements. The first was a Micromeritics 2900 TPD/TPR analyzer equipped with a TCD detector. Water produced during the reduction was condensed in a cold trap kept at -90°C in a bath of isopropanol at freezing point. The calibration was made by reducing different amounts of CuO, which undergoes a complete reduction. The catalyst samples (100 mg) were pretreated in air (100 $ml \cdot min^{-1}$) up to 800°C or 900°C depending on the calcination temperature of the material. The material was kept one hour at this temperature. The reduction of the catalysts was then performed under 25 $ml \cdot min^{-1}$ of diluted hydrogen (2% vol. in Ar) heating 10°C·min^{-1} up to 800 or 900°C. The second instrument consisted of a fixed bed micro-reactor plant equipped with an on line continuous analyzer with a TCD detector for hydrogen measurement (Rosemount NGA2000). 700 mg of catalyst were pretreated in the same conditions as described above, and then reduced with a 2% vol. H_2/Ar mixture (250 $ml \cdot min^{-1}$) at 10°C·min^{-1} up to 800°C.

XRD characterization was also performed on the materials in order to control their crystalline composition. The X-Ray diffraction patterns were obtained with a PW 1100 Philips diffractometer using the Cu-Ka wavelength. Around 50 mg of finely grinded material were used for each analysis.

A Malvern Instruments Mastersizer 2000 granulometer was used for the estimation of the size distribution of the materials for the fluidized bed. Not only the bed inventory size distribution but also those of elutriated fines collected both in the hot ceramic filter and in the cyclone were measured in this way. This apparatus is based on the diffraction properties of the considered material introduced in a solvent (water in this case). Two LASER sources, the first He/Ne with 633 nm wavelength (red) and the second diode laser with 450 nm wavelength (blue), are aligned with a 3D photodiode revelator. Two low angle lateral and one back scattering detectors are also present in the analysis cell. This system allows detection of particles in the range 0.02-2000 μm.

The morphology of materials was investigated with a Philips XL30 SEM equipped with an EDAX instrument for micro-analysis.

The fluidization capability and the attrition rate of the materials used in the fluidized bed gasifier have been studied in pre-existing experimental plants of the IRC, developed by Ammendola et al. (2009) and Scala (2009), respectively.

The study of the fluidization behaviour was performed in a stainless steel cylindrical reactor (diameter = 1" and 400 mm high), heated by a Tersid furnace. Pressure drop was measured by difference before and after bed with two ABB HART series 600T EN transducers. A ceramic filter was placed downstream the reactor to collect elutriated fines (>300 nm). Pressure drops *versus* superficial gas velocity have been measured in experiments carried out at 25°C and 800°C.

To perform attrition tests, a stainless steel bubbling fluidized bed reactor 40 mm ID and 1 m high has been used. A 0.6 m high stainless steel column for gas preheating and mixing was placed under the distributor. Two semi-cylindrical 2.2 kW electric furnaces were used for heating the fluidization column and the preheating section. A two-exit brass head was fitted to the top flange of the fluidization column. By operating this valve it was possible to convey flue gases alternately to two removable filters made of sintered brass. Elutriated fines were collected by means of the two-exit head by letting the flue gas flow alternately through sequences of filters (one was in use while the previous one was replaced) for definite periods of time. In order to prevent hydration of the collected material, each filter was readily put in a drier after being used, where it was cooled down before it was weighed. The difference between the weights of the filters before and after operation, divided by the time interval during which the filter was in operation, gave the average fines elutriation rate relative to that interval. The assumption underlying this procedure was that the residence time of elutriable fines in the reactor could be neglected and that elutriation rate could be assumed equal to the rate of fines generation by attrition at any time. Attrition tests have been carried out using N_2 as fluidizing gas at 800°C and at a superficial gas velocity of 10 $cm \cdot s^{-1}$.

II-2 Apparatus for catalytic screening

The production of a gas with suitable composition and purity from biomass gasification using a catalyst with high tar conversion activity required the development of either a catalytic system and an adequate reactor configuration which favors the contact between biomass, volatiles emitted from biomass and catalyst particles.

During the development of a more active synthetic catalyst, it was unwise to perform a preliminary catalytic screening in real fluidized bed gasification because of the multiplicity of parameters inherent to gasification in fluidized bed at pilot-scale (fluidodynamics, segregation,

mass transfer). Moreover, the operation in fluidized bed gasifier implies the loading of large amounts of catalyst, which is not an economical approach.

In order to carry out a catalytic screening of different catalysts in biomass tar conversion, a dual fixed bed lab-scale plant involving small amounts of catalyst has been developed. The experimental data obtained will be used to optimize the catalyst formulation taking into account both efficiency and costs of the material.

In addition, the developed catalytic screening plant provides qualitative and quantitative information on the catalyst performances under different operative conditions (reaction temperature, contact time).

This screening plant is also an alternative and more complete solution with respect to systems reported in literature using biomass model compounds like benzene or toluene. (Antunes et al., 2001 and Darvell et al., 2003), since it allows to contact the catalyst, kept at a fixed operating temperature, with a real mixture of products coming from the biomass decomposition.

II-2.1 Plant description

The catalytic screening set up consists of two fixed bed quartz micro-reactors (ID=1 cm, length=60 cm) which can be heated independently in two different electric furnaces (Heraeus Thermicon P and Eurotherm Carbolite), as reported in Figure 9a and Figure 9b. The biomass sample was heated up in the first furnace under pure N_2 (99.998%) constant flow rate regulated with a Brooks mass flow controller (SLA 5850). Pyrolysis conditions were chosen to simplify the process, and since the biomass pyrolysis products include all biomass gasification products. The gaseous and condensable products formed during biomass pyrolysis in the first reactor passed through the second reactor containing the catalyst kept at a fixed temperature. Two K thermocouples were used to measure the temperature inside both reactors.

The gaseous and condensable products coming from the second reactor were then sent to a two stage-condenser in order to sample the condensable species representing the unconverted tars. The first stage (one pear-shaped flask of 75ml) was at room temperature for heavier tars, the second one (three Erlenmeyer flasks of 50 ml each) at -10°C for lighter ones, according to the CEN/TS 15439 (2006) procedure for sampling and analysis of tars. The gas stream was consecutively sent to a micro GC, used for analysis of permanent gases, not condensed in the cold trap.

To avoid condensation of tarry compounds, the line between the first and second reactor, as well as between the line between the second reactor and the tar condensation train, was heated with

an electrical tape, so that the temperature was kept between 300°C and 400°C (not higher to avoid thermal cracking).

a

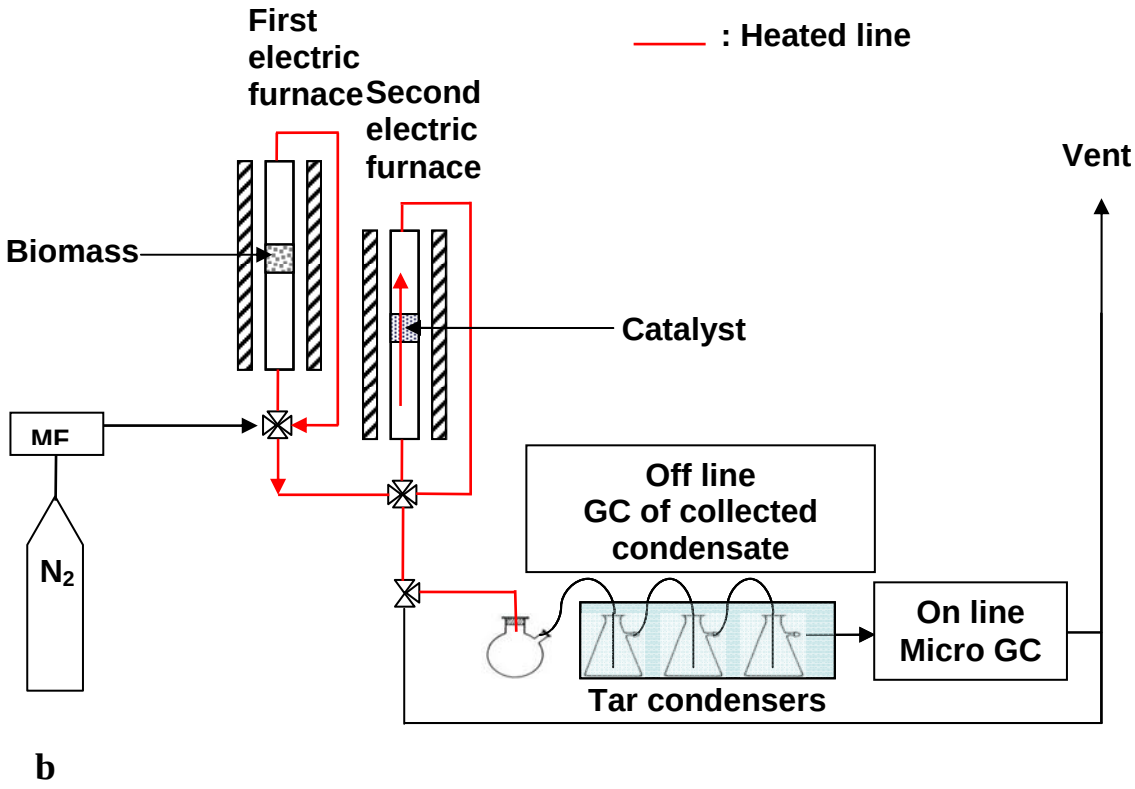

b

Figure 9. a) Dual fixed bed catalytic screening plant; **b)** scheme of the dual fixed bed catalytic screening plant.

II-2.2 Test procedure

In each experiment, 500 mg of wood chip in the size range 800-900 μm (chosen to avoid fluidization of particles and to limit thermal transfer resistance inside the particles) were introduced in the first reactor and dried in situ at 100°C under nitrogen flow (12Nl·h^{-1}) for 30 minutes before starting the test. The first furnace was programmed to heat up the material at 5°C·min^{-1} up to 800°C, temperature at which all volatiles were released. For catalytic measurements, the gaseous and vaporized products produced in the first reactor were passed through an identical quartz reactor, loaded with the catalytic or inert material (in the size range 200-400 μm) kept at fixed temperature.

The effect of different catalyst amounts, catalyst temperatures and N_2 flow rates, as reported in Table 6, has been investigated.

Table 6. Operative conditions.

Catalyst amount (mg)	250, 500, 1000
Second reactor temperature (°C)	500, 550, 600, 650, 700
N_2 flow rate (Nl·h^{-1})	12, 24, 48, 60

The products then passed through the condensation train of glassware at low temperature (described in § II-2.1), obtaining a gas cleaned from the condensable products, that could be further analysed. This stream of permanent gas was consecutively sent to a micro gas chromatograph (Agilent 3000A), able to sample the gas every 3 minutes. It was equipped with four different independent channels (with the respective four columns: OV-1, Alumina, PLOT-U and MS5A) as reported in Table 7. Helium was generally used as carrier gas for the analysis of O_2, CO, CO_2, CH_4 and C_2–C_6 light hydrocarbons for all channels. Hydrogen concentration could not be monitorized due to its value of thermoconducibility close to the one of helium. Consequently, after a modification, argon was sent as carrier gas for the MS5A column in order to also measure the H_2 profiles. The micro GC acquisition was started and stopped manually at the beginning and at the end of the temperature ramp of the first reactor.

Table 7. Micro GC module configuration (sampling line at 70°C).

module	column	lenght (m)	stationery phase thickness (μm)
A	OV-1	8	1.2
B	Alumina	14	5
C	PLOT-U	8	3
D	MS5A	10	12

Then the sampling train was weighted before and after each experiment for the quantitative evaluation of the condensable tar yield in the products. The qualitative analysis of condensed tars, after diluting with isopropanol, was performed off line in a gas chromatograph following the CEN/TS 15439 (2006) procedure for sampling and analysis of tars. In particular, an Agilent 7890A gas chromatograph equipped with an HP 35 PhenylEthylMethyl Siloxane (length: 30 m, diameter: 0.25 mm, stationary phase thickness: 0.25 mm) and a FID detector as well as a mass spectrometer 5975C-VLMSD was used. After injection of the tarry solution, the GC column was kept at 50°C for 5 minutes, then heated up to 200°C at 5°C·min^{-1}, then to 270°C at 10°C·min^{-1} and to 310°C at 5°C·min^{-1}. The column was finally kept at 310°C for 15 minutes.

At the end of each experiment the amount of coke deposited on the secondary bed catalyst was determined by oxidation of the material after cooling down under inert atmosphere. The oxidation was performed following a heating ramp of 5°C·min^{-1} from ambient temperature up to 800°C under O_2/He mixture (0.5%vol.) constant flow rate (17 Nl·h^{-1}). The concentration of released carbon dioxide was measured by the micro-GC. The numerical integration of the signal provided the stoichiometric amount of coke formed during the previous catalytic tar conversion experiment.

As a measure of the catalysts performance, the difference between the yields and type of gas, liquid and solid products with and without catalyst, according to the method reported in Corella et al. (1999) and in Collot et al. (1999), was used. For all experiments the mass balance was closed with a maximum error of ±10%wt.

II-3 Fluidized bed gasifier

The second objective of this PhD activity was the development of a pilot fluidized bed gasifier with a suitable configuration to limit the segregation of biomass and volatiles during gasification

Among the possible fluidized bed gasifiers, a bubbling fluidized bed reactor has been adopted because, as explained in § I-3.1.2, the heterogeneous gasification reactions and the cracking and reforming processes of the organic vapours, which all follow the fast biomass devolatilization step, are relatively slow processes, and the residence time of these vapours at the high temperature of the gasifier contributes positively to the quality of the fuel gas. For these reasons, bubbling fluidized bed technology has been chosen since it offers clear advantages in cases where the yield of a clean, gaseous energy vector is of overriding priority.

In order to limit the segregation of biomass and volatiles an ad-hoc conical gas distributor has been designed.

An experimental campaign using conventional catalysts was then carried out in order to set up the pilot scale fluidized bed gasifier.

II-3.1 Plant description

The fluidized bed gasifier at pilot-scale is formed by two vertical stainless steel tubes having different sizes and connected by means of a conical adapter. The lower tube has an internal diameter of 140 mm and a height of 1010 mm whereas the upper tube is 200 mm ID and 1800 mm high. The gas distributor at the bottom of the fluidizing column has a conical shape and a total volume of around one litre. The use of a conical distributor was found to increase the circulation of the materials inside the bed, thus, limiting the biomass and volatiles segregation phenomenon (see annex B). A view of the reactor is shown in Figure 10 and the scheme of the plant is reported in Figure 11.

The reactor was heated by electrical resistors at different levels: gas distributor, bed of fluidized solid and freeboard. An air pre-heater was also placed before the gas distributor. Three thermocouples (K) were used for the control of temperatures in the gas distributor, the fluidized bed and the freeboard.

The gasification air flow rate was controlled by a mass flow controller (5850S, Brooks). The gas was sent to the pre-heater, where it was preheated up to 600°C, and then to the wind box of the gas distributor, where it was fed through 72 holes (1.5 mm ID), that are arranged in 6 regular rows along the conical surface of the gas distributor.

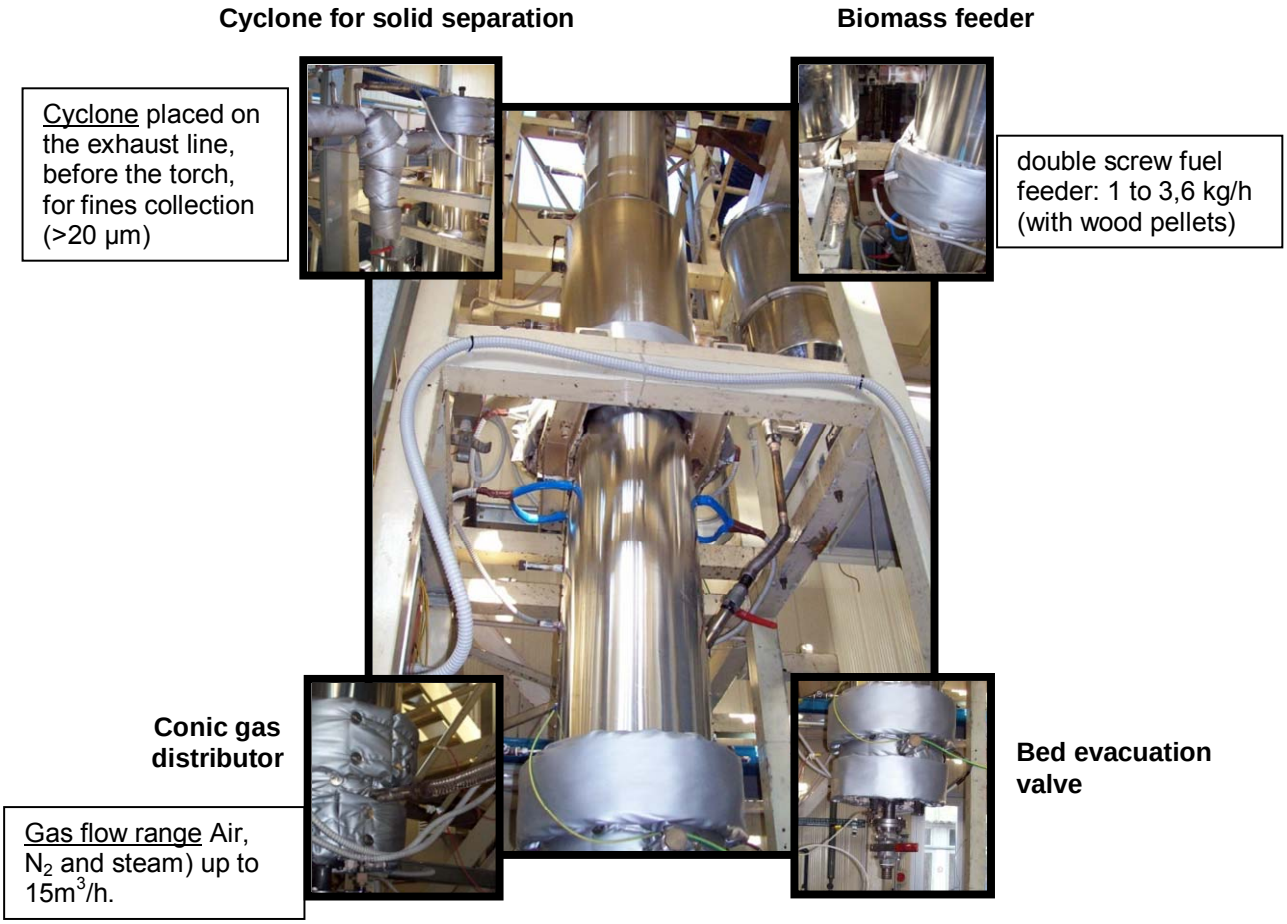

Figure 10. Fluidized bed biomass gasifier.

To perform steam gasification tests, distilled water was also fed by means of a peristaltic pump with adjustable rate (0-1.8 $l \cdot h^{-1}$) to an electric tubular steam generator in order to produce steam at moderate gauge pressure (20 kPa) and temperature up to 400ºC. The steam generator consisted in a 2.54 cm (1") internal diameter stainless steel tube, linked at its extremity to form a "U". The two entrance tubes were fed continuously with water thanks to a peristaltic pump and the base of the "U" was drilled and connected to the gasifier by a flexible tube. The whole system was heated by three resistors of 2 kW each, tightly attached to the tubes, making possible a production of steam up to 1.9 $kg \cdot h^{-1}$. The steam directly entered the wind box of the gas distributor where it was mixed with the preheated air flow.

The fuel was fed under-bed into the reactor, by means of a screw conveyor, 130 mm above the conical distributor. The fuel flow rate was regulated by means of an additional screw feeder, rotating at changeable rate and directly connected to a sealed fuel hopper. An auxiliary nitrogen stream was used for inertizing the fuel feeding devices and was flowed into the gasifier together with the fuel.

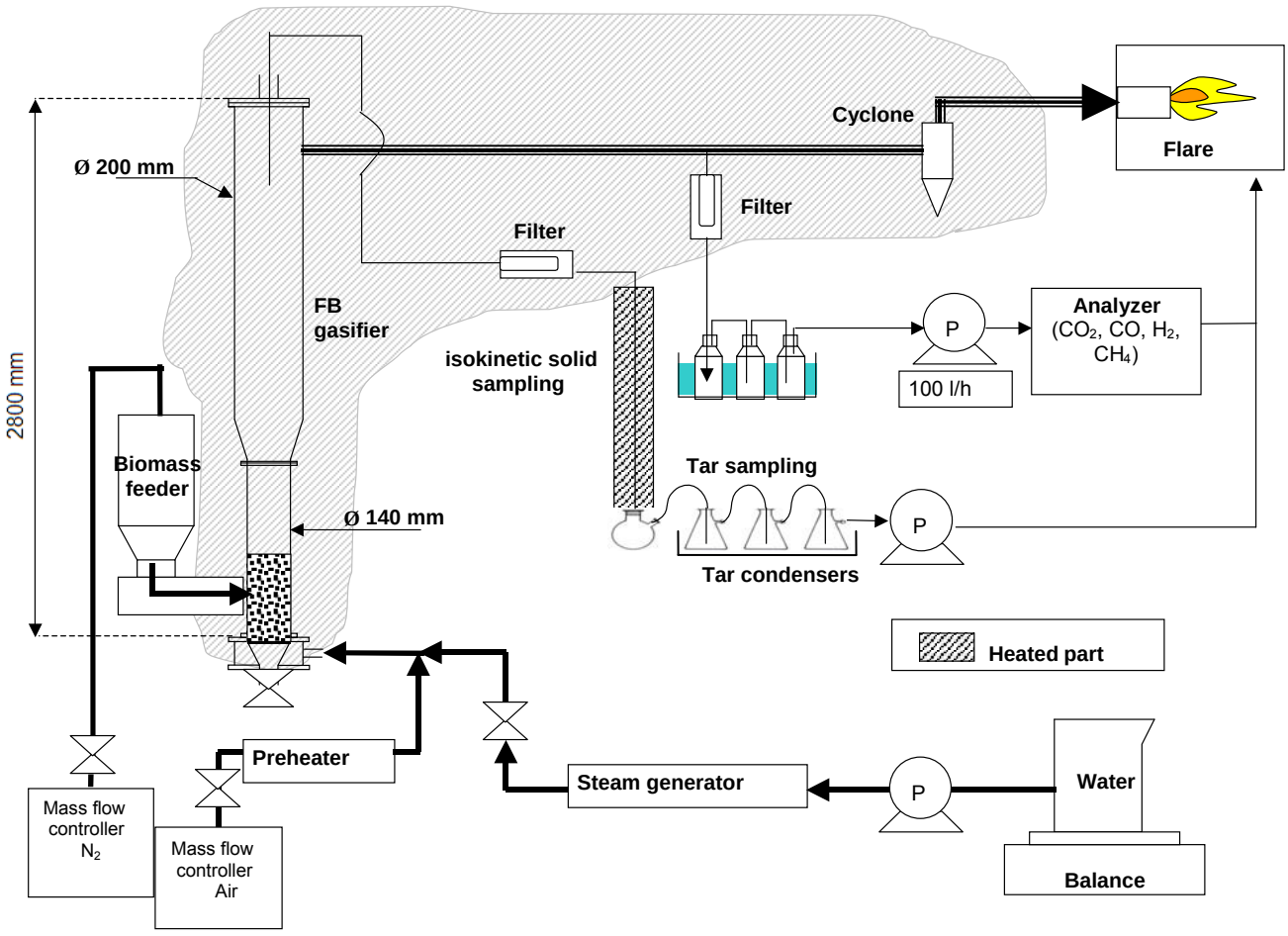

Figure 11. Scheme of the pilot-scale biomass fluidized bed gasifier.

The main gas stream flowing out the gasifier was sent to a cyclone, able to retain elutriated fine particles down to 20μm. The line and the cyclone were kept at 450°C to avoid the tar condensation. The outgoing gas was then sent to a flare equipped with a LPG pilot flame to burn the syngas coming from the gasifier in a chimney.

The analysis of the permanent gas was performed by an ABB continuous analyzer equipped with an IR detector for CO, CO_2 and CH_4 detection and a thermoconducibility detector for H_2. The gas was sampled from the main gas stream by a pump and was passed through a filter and an impinger train to eliminate both the condensable species and elutriated fine particles before the analysis system.

The sampling of the tar products has been performed according to the protocol CEN/TS 15439 (2006). In particular, elutriated solid fines and unconverted tars were sampled isokinetically

inside the reactor by means of a 15 mm ID stainless steel probe introduced in the reactor from the top (1 meter inside). A Zambelli high precision pump (DIGIT ISO) was used for the suction of the sampled gas, aerosol and solid. The sampled stream passed through a hot quartz fiber thimble to retain solid particles as small as 200 nm. Then the gaseous and condensable species were sent through a two step-condenser, the first one (a 500 ml glass tube) at ambient temperature for collection of heavier tars, the second one (three empty Erlenmeyer flasks of 250 ml each) at -10°C for lighter ones. The probe, the filter and the tube between the filter and the first condenser were kept at 450°C by a heating tape.

II-3.2 Test procedure

Steady state gasification tests have been carried out following a standard experimental procedure.

The reactor was heated up to the desired temperature (700-800°C) thanks to the air pre-heater and the electrical resistances. An air stream of around 8 $kg \cdot h^{-1}$ was fed. Generally, the plant was ready for gasification test within 2-3 hours. Then the fluidization air flow was set at the assigned value, the steam generator was turned on and the water was pumped to produce the desired steam flow rate at around 400°C. Afterwards, the biomass feeding was started, together with an inertizing nitrogen flow of 0.75 $kg \cdot h^{-1}$.

The operating conditions of the gasification tests are reported in Table 8. The bed temperature T, the fluidization velocity U, the equivalence ratio Φ, and the steam/fuel ratio Ψ have been kept constant. Different materials, such as sand, dolomite, olivine and Ni based catalyst, have been used as bed material. Two different bed heights have been adopted for sand and Ni catalyst.

Table 8. Operating conditions in the fluidized bed reactor.

Pressure (kPa)	101
Bed height (m)	0.18-0.30
Bed temperature (°C)	780
Fluidization velocity ($m \cdot s^{-1}$)	0.3
Equivalence ratio (-)	0.17
Steam/fuel ratio (-)	0.65

Under steady state conditions of the monitored variables, namely temperatures and gas molar fractions measured by the continuous analyzer, the measurements were recorded.

The solid particles collected both in the hot filter and in the hot cyclone were first weighed after the experiments. Then the CHN as well as the granulometric analyses, performed by the LECO analyzer and the Malvern Instruments granulometer described in § II-1.2 respectively, were carried out.

The liquid phase products were weighed, separately with respect to their Dew point. Then, both the condensate at ambient temperature and at low temperature were dissolved in dichloromethane, to separate water from tar. The speciation of the condensed heavy tars was performed by gas chromatography, using the Agilent gas chromatograph described in § II-2.2. The analysis was restricted only to the family of chemical species that are prescribed by the tar protocol CEN/TS 15439 (2006). The Total Organic Carbon Content analysis (TOC V-CSH, Shimadzu) of the extracted water was performed in order to verify that the concentration of carbon in the water was negligible compared to the total amount of collected tars.

For each test, gaseous samples, free of solids and tars, were also taken in 3 liters Tedlar bags and analyzed off-line by micro gas chromatography (see § II-2.2) for the determination of major light hydrocarbon species.

The different analyses performed during and after each gasification test are reported in Figure 12.

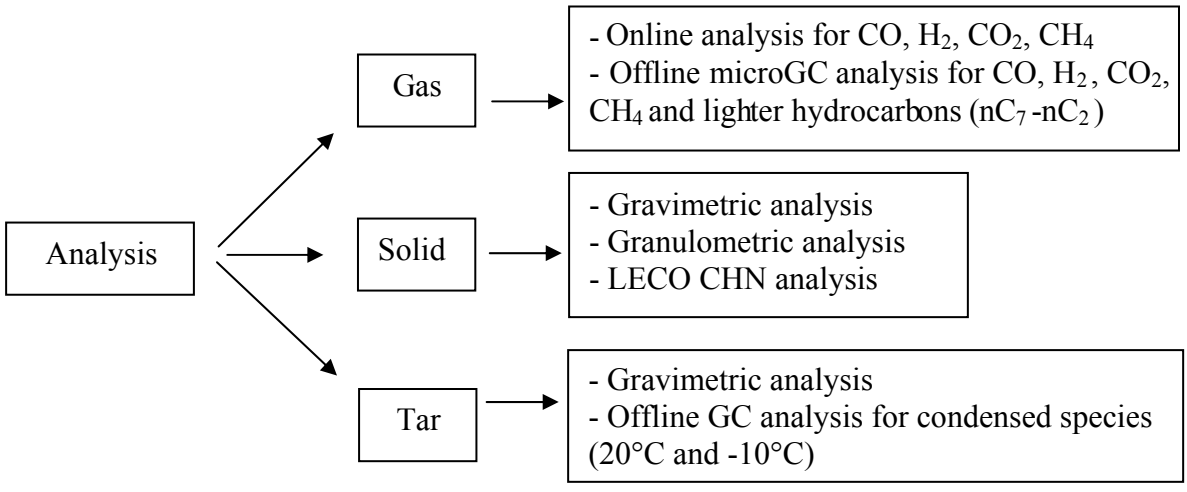

Figure 12. Summary of performed analyses related to the fluidized bed gasifier.

III-RESULTS

III-1 Materials characterization

III-1.1 Biomass

The main characteristics of the maple wood chips and commercial wood pellet used as fuel in the experiments carried out respectively in the dual fixed bed reactor and in the fluidized bed biomass gasifier are reported in Table 9.

Table 9. Properties of the used fuels.

	Maple wood chips	Commercial spruce wood pellets
LHV, $MJ \cdot kg^{-1}$	16.6	18.5
Proximate analysis, wt%		
Moisture	8.9	8.4
Volatiles	74	74.2
Fixed carbon	16.5	17.1
Ash	0.6	0.3
Ultimate analysis (dry basis), wt%		
Carbon	46.3	49.3
Hydrogen	5.6	5.9
Nitrogen	0	0
Ash	0.6	0.3
Oxygen (diff.)	47.5	44.5

Figure 13 reports the elemental analysis of the ash contained in the fuels. The amounts of inert compounds like silicium and aluminium under their oxide form were difficult to evaluate due to an uneasy dissolution in the acid solution used for the analysis. However, the other elements were quantifiable, such as alkaline and transition metals, also present in their oxide form. Calcium and potassium were the main alkaline elements found in these biomass fuels, followed by magnesium and sodium. Among transition metals, manganese was the most present in both fuels. Other transition metals, like titanium, iron, copper and zinc, were also found in much lower amounts. Zirconium, tin and lead were detected in the maple wood chips in much larger amounts than in commercial pellets, whereas barium was found mainly in the latter.

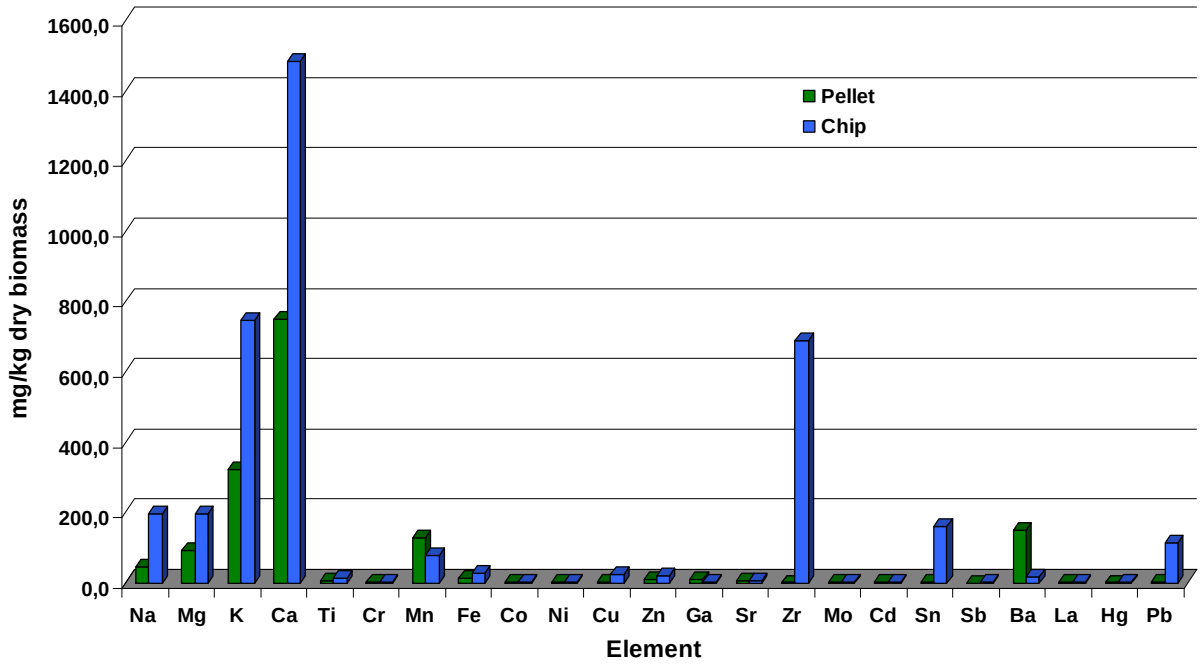

Figure 13. Elemental analysis of ash contained in the maple wood chips and commercial spruce wood pellets.

Thermogravimetric analysis coupled to a Fourier-transform infrared (FTIR) spectrometer has been selected as a suitable technique for the study of devolatilization products released during biomass thermal decomposition since this method allows to link the biomass weight loss with the emitted species during heating of the material. Good results have been obtained in biomass pyrolysis and oxidative pyrolysis by Bassilakis et al. (2001).

The maple wood chips, used as biomass fuel in the dual fixed bed reactor, were tested. In Figure 14 the temperature profile and the weight loss of the biomass are reported. Only water is emitted up to 100°C. Then the maple wood chips decompose pyrolytically in the temperature range

150°C-500°C, where the main weight loss is observed due to the emission of volatiles: CO, CO_2 (H_2 is not detected by IR), hydrocarbons (Tar 1) and oxygenates (Tar 2 and Tar 3). Burning of fixed carbon takes place when oxygen is introduced in the flow at 800°C.

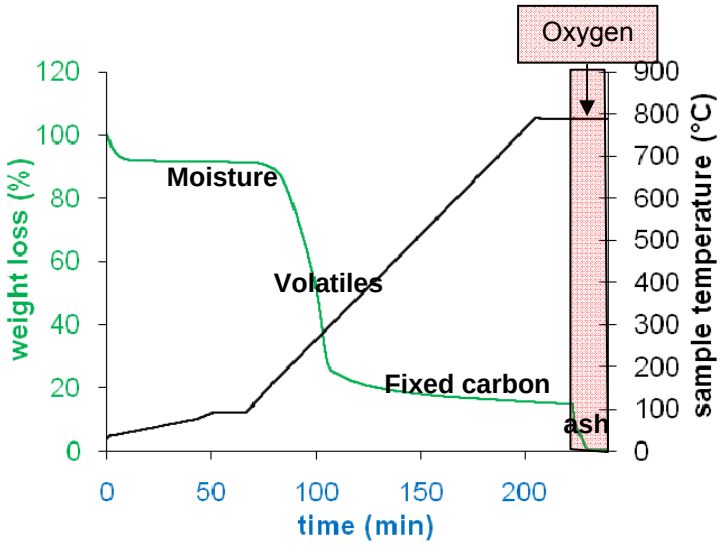

Figure 14. Weight loss of maple wood and furnace thermal ramp versus time. (particle size range 125-212 µm).

The Figures 15a and 15b show the evolution with temperature of released species during heating at 5°C·min^{-1} of the biomass wood chips up to 800°C and the relative weight loss rate. Since it results very difficult to separate the different species, they have been regrouped in classes. In Table 10 the IR bands attributed to single species or to a class of species are reported. The species are regrouped as: Tar 1 for alkanes (C-H bonds, green dashed line), Tar 2 for aldehydes and acids (C=O bonds, dashed brown line), and Tar 3 for esters and formic acid (C-O bonds, dashed blue line). CO (red line) and CO_2 (thin black line) have more easily distinguishable IR signals. Methane is largely produced during wood pyrolysis, but the corresponding signal (in yellow) is slightly visible, and is included in the Tar 1 group. As reported in Figure 15b, the decomposition of maple wood constitutive organic polymers is highlighted by the observation of the derivative weight loss of the sample. The shoulder at 225°C corresponds to the decomposition of hemi-cellulose, followed by a peak accounting for cellulose at 275°C, whereas lignin decomposes within the all temperature range.

The evolution of emitted species during wood thermal decomposition, reported in Figure 15, was in good agreement with literature (Yang, 2004).

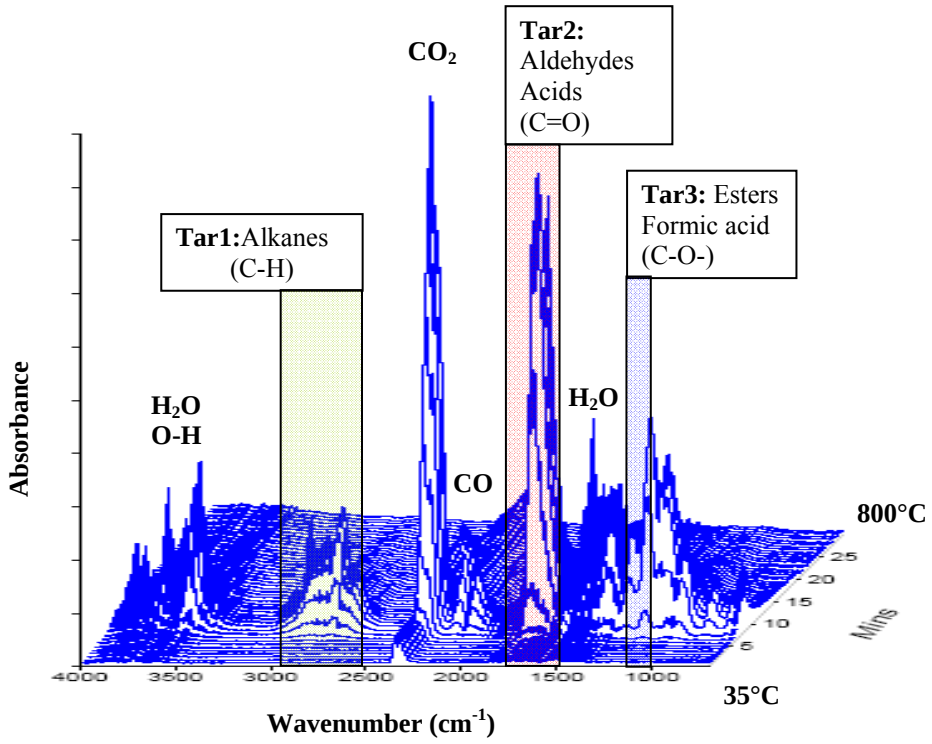

a

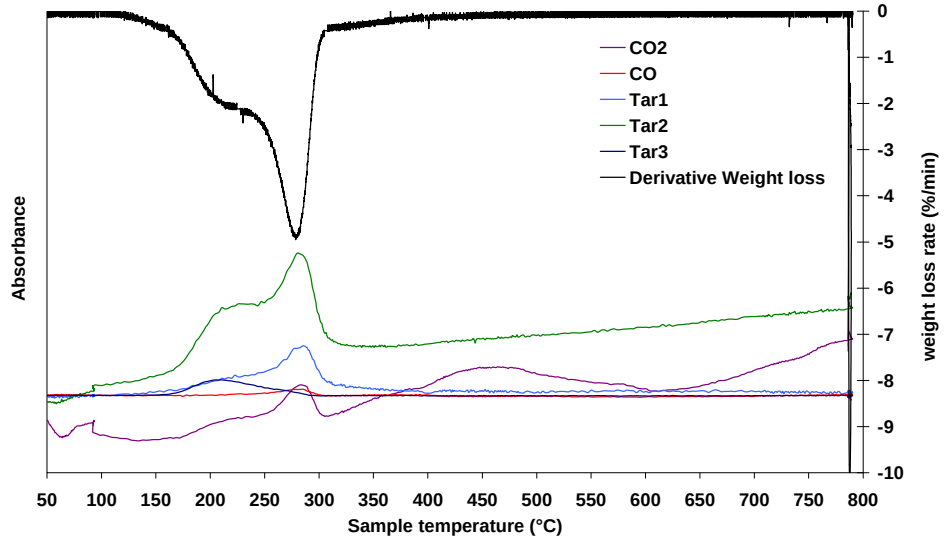

b

Figure 15. a) FTIR stack plot of compounds or compounds families; **b**) Related species profiles *versus* temperature and weight loss rate. Particle size: 125-212 µm; heating rate: 5°C·min^{-1}.

Table 10. Selected IR absorption bands of single or class of compounds (cm^{-1}).

H_2O	1297 – 2062 and 3455 – 3949
CO_2	2228 – 2396
CO	2054.5 – 2231
Tar1	2636 – 3052
Tar2	1588 – 1878
Tar3	1149 – 1218

In order to allow a correct choice of the biomass fuel-related parameters, the effect of heating rate as well as maple wood particle size on its weight loss (Figure 16a and Figure 16b, respectively) has been investigated. An increasing heating rate (from $1°C \cdot min^{-1}$ to $50°C \cdot min^{-1}$) resulted in a slight move of the weight loss curve of the biomass material toward higher temperatures, since the temperature gradient across the particle increased, resulting in a thermal resistance effect. This phenomenon was already reported by Haykiri-Acma (2006). Nevertheless, a too high heating rate does not allow a good separation of the pyrolysis products in the optic of a study of the catalytic activity versus different compounds. In agreement with the literature (Raveendran et al., 1996) a slight effect of particle size on the reactivity of the biomass material has been highlighted. In fact, the devolatilization temperature increases with increasing particle size (from 125-212 μm to 3-4 mm), but this effect was very slight for sizes lower than 1mm since the heat transfer from the particle surface to its centre is almost immediate. In both cases, the qualitative evolution of released species was similar to that reported in Figure 15.

An attempt to measure catalytic activity was made in the TGA-FTIR system by placing the catalyst (grinded in the same size-range as the biomass fuel) over the solid fuel. The catalyst weight loss was previously measured in a separate test, to evaluate its contribution to the sample (biomass + catalyst) weight loss. Nevertheless, due to the very low temperature range of decomposition of the biomass, far from the range of activity of the catalyst, no effect on the emitted products was detected. On the other hand, the biomass decomposition taking place at so low temperature allowed to exclude the possible occurrence of a solid-solid catalysis. To measure catalytic activity, it is necessary that the gas produced by biomass decomposition comes in direct contact with the catalyst, kept in its temperature range of activity. Therefore, in order to achieve these conditions using small amounts of catalyst for the preliminary screening, the dual fixed bed reactor, described in the § II 2.1. has been developed.

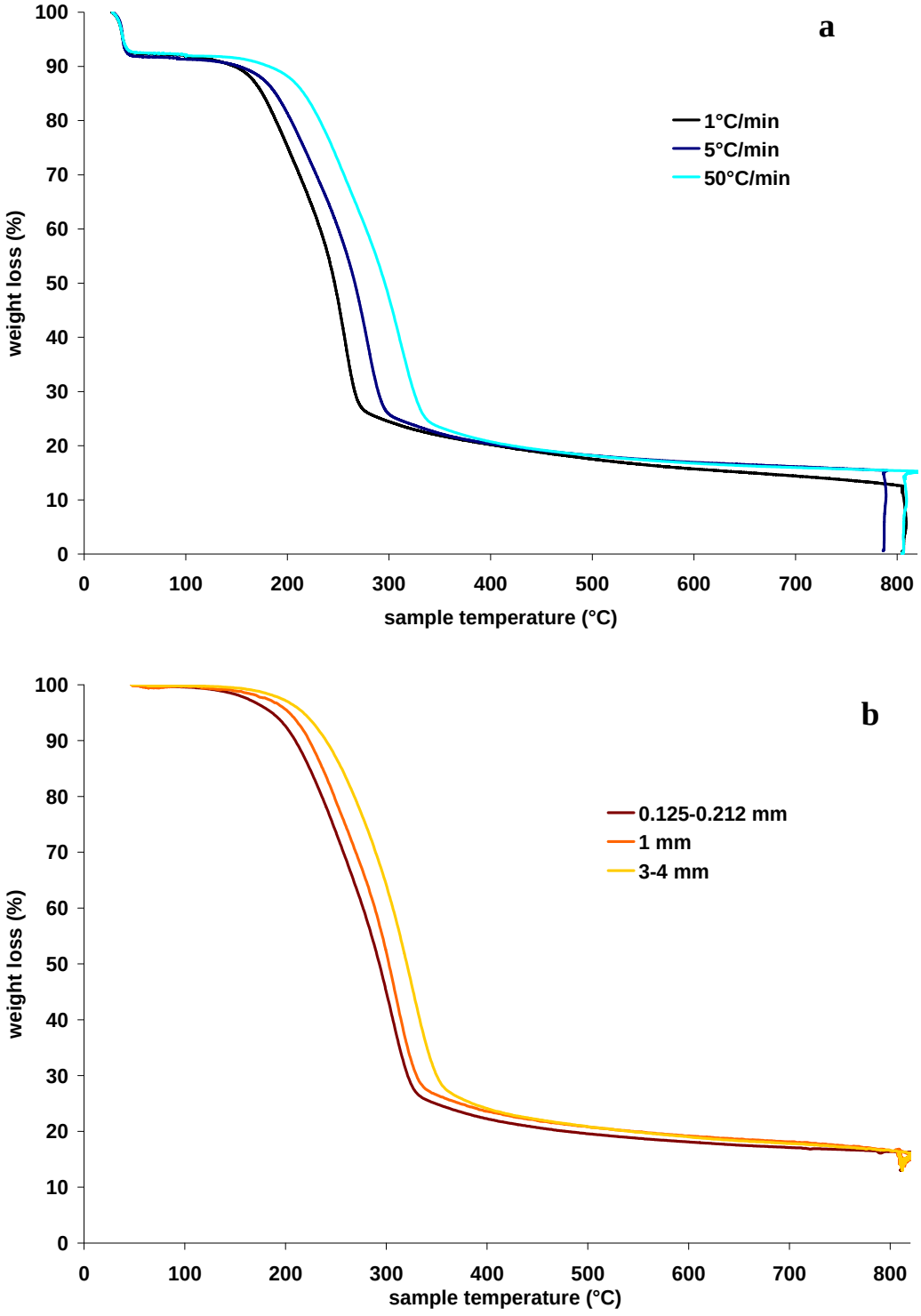

Figure 16. a) Effect of heating rate on weight loss. Particle size: 125-212 µm. **b)** Effect of biomass particle size on weight loss. Heating rate: 5°C·min^{-1}.

III-1.2 Catalysts

III-1.2.1 Physico-chemical and morphological characterization

Table 11 shows the results of elemental analysis of the catalysts as well as their specific surface areas.

Table 11. Elemental composition and specific surface areas of catalysts.

Notation	Active elements (wt %)						BET ($m^2 \cdot g^{-1}$)
	Co	Ni	Rh	Ca	Fe	Mg	
Olivine	-	-	-	0.05	2.27	21.90	<1
Dolomite	-	-	-	11.60	0.02	10.00	28
Ni/Al_2O_3	-	5.50	-	-	-	-	156
900/1Rh	-	-	0.80	-	-	-	139
900/p	4.60	-	-	-	-	-	117
900/p/1Rh	4.30	-	0.75	-	-	-	100
800/1Rh	-	-	0.84	-	-	-	134
800/p	4.70	-	-	-	-	-	101
800/p/1Rh	4.72	-	0.80	-	-	-	104
800/p/0.5Rh	4.50	-	0.45	-	-	-	99
800/p/0.1Rh	4.40	-	0.08	-	-	-	101

The BET measurements showed that the natural materials (olivine, dolomite) had low surface areas, in particular olivine, which has a surface area value as low as the one of sand (<1 $m^2 \cdot g^{-1}$). On the contrary, the synthetic catalysts demonstrated much higher values, thanks to the use of γ-aluminas as supports, which have a surface area of 140 or 160 $m^2 \cdot g^{-1}$. Quite high values of surface area are maintained even upon calcination at 900°C. As expected, for both calcination temperatures (800 and 900°C) the superficial area decreased with increasing the active phase

loading, i.e. superficial area was minimized when 20 wt% of $LaCoO_3$ was deposited, the very small amounts of rhodium did not further affect the value.

The elemental analysis highlighted the presence of very small amounts of iron in the used dolomite, whereas calcium and magnesium were present in typical amounts. The olivine denoted a composition similar to forsterite (Mg_2SiO_4), mainly made of magnesium, with insertion of small amounts of iron. Calcium was present in olivine at trace level.

The synthetic catalysts were found to contain the deposited active elements in amounts close to the desired ones. The Ni/Al_2O_3 catalyst contained 5.5 wt% of nickel. Rhodium was sometimes present in lower amounts than the expected nominal ones (800/p/1Rh, 900/p/1Rh, 800/1Rh and 900/1Rh), due to an undefined hydration of the Rh nitrate precursor. The different values of cobalt (incorporated in perovskite) concentration in the catalysts, lower than the nominal one (4.8wt%), denote a major sensitivity to experimental error during impregnation.

The XRD spectra of the catalysts containing rhodium and perovskite calcined at 800°C, reported in Figure 17 together with that of the alumina used as support, showed only a decrease in intensity of the γ-alumina peaks, whereas the presence of $LaCoO_3$ and RhO_x species could not be detected. This is due to a good dispersion of those species on the γ-alumina.

The XRD spectrum of the Ni/Al_2O_3 catalyst is reported in Figure 18. Also in that case, no formation of nickel oxides or aluminate could be detected due to the small amounts of deposited nickel and to the high dispersion of the formed phases.

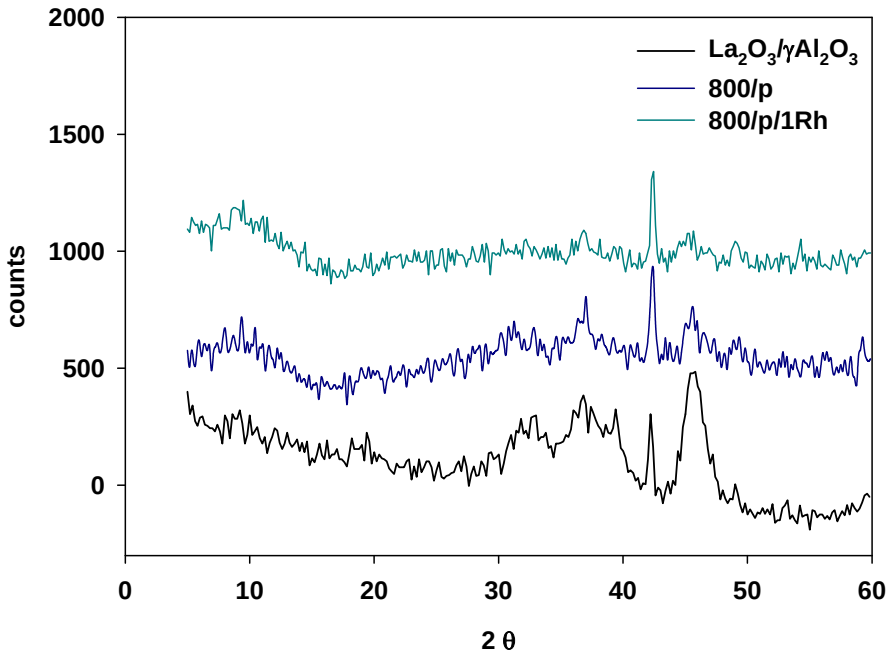

Figure 17. XRD spectra of catalysts containing perovskite and rhodium calcined at 800°C and of the alumina used as support.

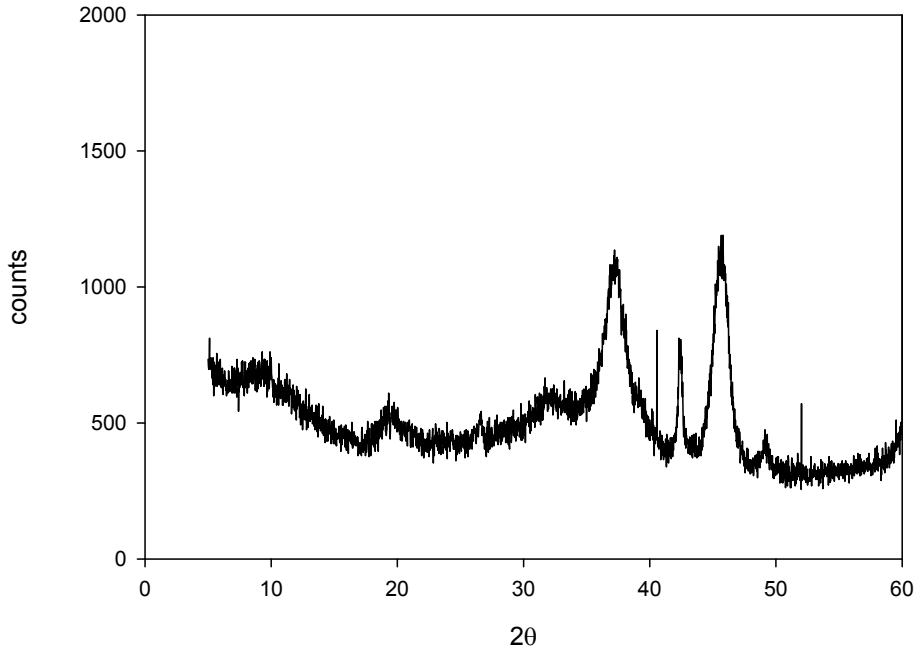

Figure 18. XRD spectra of Ni/Al_2O_3 catalyst calcined at 800°C.

In Figure 19, the TPR profiles of catalysts calcined at 800°C are reported. The TPR profile of 800/1Rh shows a low temperature peak at 250°C, that can be attributed to the reduction of rhodium oxide particles (RhO_x) having no interaction with the support, and a high temperature peak at 760°C, accounting for significantly more hydrogen uptake, related to the reduction of Rh strongly interacting with the alumina to form spinel type compounds ($Rh(AlO_2)_y$) (Hwang et al., 1999). In the TPR of the 800/p sample, the typical two stage reduction of cobalt from Co^{3+} to Co^{2+} and from Co^{2+} to Co^0 at 472 and 751°C respectively could be observed. The presence of those two peaks is characteristic of the $LaCoO_3$ bulk compound (Cimino et al., 2006). When 1 wt% rhodium was added to the perovskite (800/p/1Rh), the two peaks of cobalt reduction were still detectable, but less intense and shifted to higher temperature (one peak at 530°C for $Co^{3+} \rightarrow Co^{2+}$ and a shoulder at 760°C for $Co^{2+} \rightarrow Co^0$). This can be attributed to the double calcination step performed during the preparation of the sample, resulting in the further diffusion of cobalt into the alumina bulk. This evidence was confirmed by the presence of a peak under isotherm, that can be attributed to the reduction of $CoAl_2O_4$ spinel (Lisi et al., 1999). The low temperature signal of rhodium at 250°C for the sample 800/p/1Rh was more intense than for 800/1Rh suggesting that the perovskite layer has a barrier effect, preventing or limiting the interaction between rhodium and alumina.

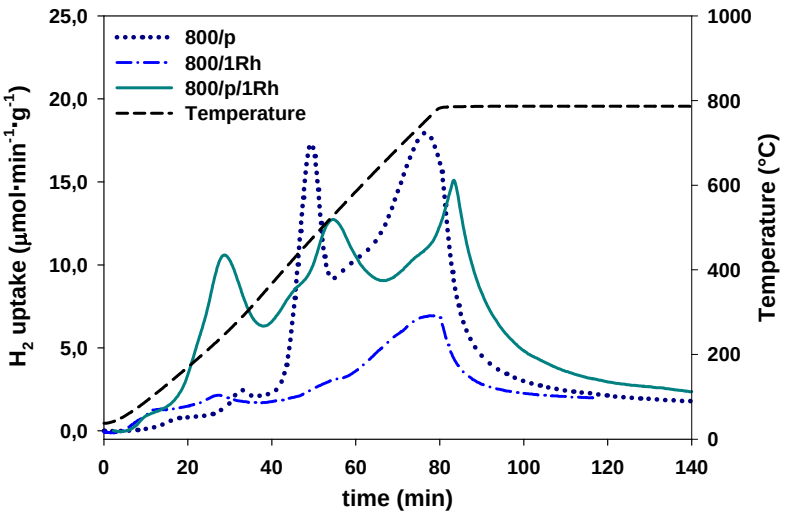

Figure 19. H_2-TPR profiles of catalysts containing perovskite and/or rhodium calcined at 800°C.

Table 12 reports the total hydrogen uptake and the H_2/metal ratios evaluated from integration of TPR profiles.

Table 12. H_2 uptake and H_2/metal ratio evaluated from integration of TPR profiles for catalysts calcined at 800°C.

Catalyst	Total H_2 uptake ($mmol \cdot g^{-1}$)	H_2/Co ($mol \cdot mol^{-1}$)	H_2/Rh ($mol \cdot mol^{-1}$)
800/1Rh	0.14	-	1.77
800/p	0.41	0.52	-
800/p/1Rh	0.73	0.74*	1.77**

*Calculated by subtracting the H_2/Rh ratio of the corresponding T/Rh sample.
**Assigned on the basis of the H_2/Rh ratio of the corresponding T/Rh sample.

The H_2/Co ratio evaluated for 800/p catalyst, lower than the stoichiometric one (1.5), indicated that the interaction probably occurring between cobalt and alumina, leading to the formation of a surface cobalt aluminate, limited the complete reduction of Co. On the other hand, rhodium was completely reduced to the metallic state in the 800/1Rh sample, as shown by H_2/Rh ratio even exceeding the theoretical one (1.5) likely due to a the not perfect recovering of TPR baseline, which affects the signal integration, or to the presence of some metal impurities. Assuming a complete rhodium reduction for the bi-functional catalyst 800/p/1Rh as occurred in the corresponding Rh/Al_2O_3 sample, the difference between the H_2 uptake of 800/p/1Rh catalyst and the one due to the total Rh reduction can be attributed to the reduction of Co; the resulting H_2/Co ratio, lower than the stoichiometric one (1.5), was in agreement with the value obtained for the 800/p catalyst.

TPR profiles of catalysts calcined at 900°C are reported in Figure 20, whereas quantitative results is reported in Table 13.

The 900/1Rh sample shows two peaks at 338 and 830°C as observed for 800/1Rh, however the low temperature signal, assigned to rhodium oxide, is smaller than that of 800/1Rh suggesting that the higher calcination temperature promotes the formation of spinel-type compounds $Rh(AlO_2)_y$ due to the interaction of rhodium with the support.The same effect, even more pronounced, was observed for the 900/p catalyst. The perovskite-type phase, present in the sample calcined at 800°C, has almost totally disappeared to the advantage of the $CoAl_2O_4$ spinel, difficult to reduce, since the diffusion of cobalt in the alumina bulk increases at higher temperature. Nevertheless, in the mixed sample, a greater amount of cobalt can be reduced at high temperature (>900°C) together with $Rh(AlO_2)_y$ species, as also shown by the greater amount of H_2 consumed. Furthermore, also in that case, the lanthanum-cobalt mixed oxide layer partially inhibits the migration of rhodium into the alumina lattice, as shown by the peak of RhO_x at low temperature (360°C).

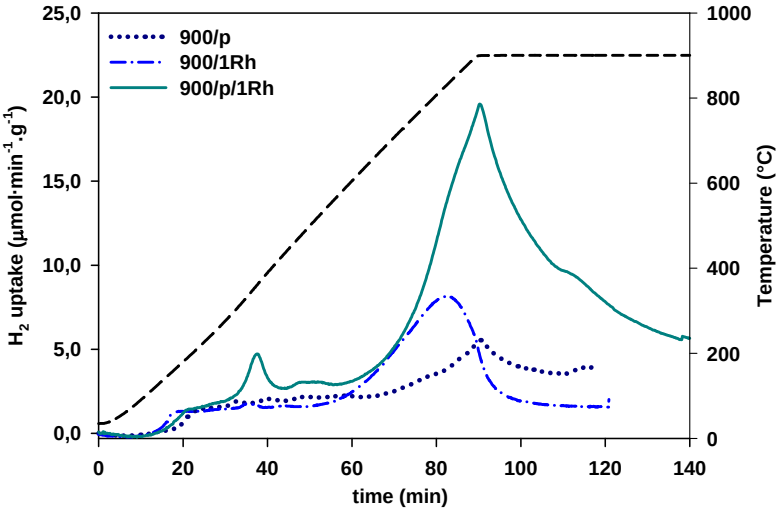

Figure 20. H_2-TPR profiles of catalysts containing perovskite and/or rhodium calcined at 900°C.

Table 13. H_2 uptake and H_2/metal ratio evaluated from integration of TPR profiles for catalysts calcined at 900°C.

Catalyst	H_2 uptake ($mmol \cdot g^{-1}$)	H_2/Co ($mol \cdot mol^{-1}$)	H_2/Rh ($mol \cdot mol^{-1}$)
900/1Rh	0.16	-	2.08
900/p	0.08	0.10	-
900/p/1Rh	0.53	0.52*	2.08**

*Calculated by subtracting the H_2/Rh ratio of the corresponding T/Rh sample.
**Assigned on the basis of the H_2/Rh ratio of the corresponding T/Rh sample.

TPR of catalysts with different rhodium loads have been carried out in the second experimental plant (see § II-1.2) and the H_2 profiles are reported in Figure 21. Due to the different fluidodynamic conditions in the two experimental plants which can affect the shape of the TPR curves, TPR analysis of 800/p and 800/p/1Rh have been repeated for comparison.

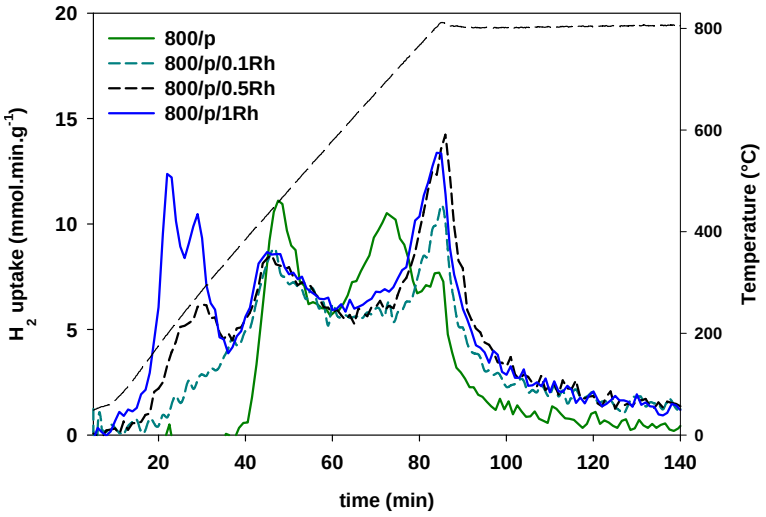

Figure 21. H_2-TPR profiles of Rh-perovskite catalysts with different rhodium loads.

The profiles obtained for 800/p and 800/p/1Rh are similar to those presented previously (Figure 19), even if obtained in different apparatus. In fact, the typical two stages of the reduction of cobalt from Co^{3+} to Co^{2+} and from Co^{2+} to Co^0, at 460°C and 695°C respectively in the 800/p catalyst are evidenced also in this tests. An additional peak recorded under the isothermal step highlight the presence of a small amount of cobalt aluminate ($CoAl_2O_4$), not evidenced previously. Similar results have been obtained also on the sample containing rhodium (800/p/1Rh), i.e. when rhodium was added to the perovskite: the reduction peak corresponding to the presence of cobalt aluminate, also due to the double calcination during synthesis, increased as previously observed. In this case, the presence of two low temperature peaks at 205 and 273°C can be attributed to the presence of two different oxidation states of the rhodium on the catalyst. As concerns the effect of rhodium content, these two low temperature peaks, present in the catalyst with 1wt% of rhodium, merge together for lower content of noble metal and, as expected, decrease in intensity along with decreasing rhodium load. The presence of the two low temperature peaks, accounting for rhodium reduction, together with the small reduction peak of the aluminate in 800/p could not be measured in the first apparatus. This can be explained by the increased contact time in the second plant, resulting in a better sensitivity.

The total H_2 uptake and the H_2/metal ratios evaluated from the integration of TPR curves are reported in Table 14. As expected, the H_2 consumption decreases with decreasing Rh content. Since it was evidenced above that Rh is always completely reduced from Rh^{3+} to Rh^0, assuming a complete theoretical reduction of rhodium (H_2/Rh = 1.5), the difference between the total H_2 uptake

of bi-functional catalysts and the one due to the respective total Rh reduction can be attributed to the reduction of Co. The resulting H_2/Co ratios, lower than the stoichiometric one (1.5), were in agreement with those obtained with the Micromeritics 2900 TPD/TPR analyzer and reported in Table 12.

Table 14. H_2 uptakes and H_2/metal ratios evaluated from TPR experiments of catalysts with different Rhodium loads.

Catalyst	Total H_2 uptake ($mmol \cdot g^{-1}$)	H_2/Co ($mol \cdot mol^{-1}$)	H_2/Rh ($mol \cdot mol^{-1}$)
800/p/1Rh	0.69	0.70*	1.5
800/p/0.5Rh	0.62	0.69*	1.5
800/p/0.1Rh	0.51	0.62*	1.5
800/p	0.38	0.48	-

*calculated supposing a complete theoretical reduction of rhodium.

Redox properties of the nickel on alumina catalyst were also measured using the Micromeritics 2900 TPD/TPR analyzer described in § II-1.2. The TPR profile of this material is reported in Figure 22.

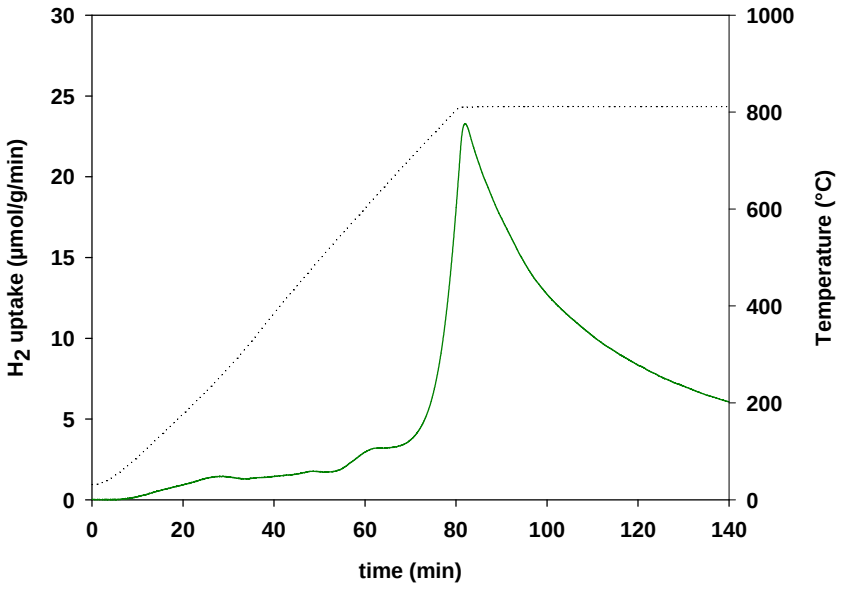

Figure 22. H_2-TPR profiles of Ni/Al_2O_3 catalyst.

The small peak at 630°C can be assigned to the reduction of a small amount of NiO while the main peak at high temperature under the isothermal step can be assigned to the reduction of Ni^{2+} ions in the lattice of the $NiAl_2O_4$ spinel (Zhang et al., 2003), since Ni^{2+} ions incorporated in the crystalline lattice are more difficult to be reduced than NiO (Shan et al., 2003).

Table 15 reports the hydrogen uptake evaluated on the basis of signal integration as well as the ratio hydrogen consumed/metal for the Ni/Al_2O_3 catalyst. The H_2 uptake ratio is smaller than the stoichiometric one (1), thus, the Ni/Al_2O_3 could not be completely reduced during the TPR.

Table 15. H_2 uptakes and H_2/metal ratios evaluated from the TPR experiment for Ni/Al_2O_3 catalyst.

Catalyst	H_2 uptake ($mmol \cdot g^{-1}$)	H_2/Ni ($mol \cdot mol^{-1}$)
Ni/Al_2O_3	1.12	0.66

III-1.2.2 Characterization of mechanical and fluidization properties

The fluidization properties of the materials used in the fluidized bed gasifier are reported in Table 16. The size distribution of different materials linked with their densities allowed to determine the respective Geldart's group. The minimum fluidization velocity and terminal velocity were calculated on the basis of the material properties at 800°C in air ($Re < 5$) (Perry handbook 5th Ed.). The different bed materials have been introduced inside the reactor in amounts related to their bulk densities in order to have the same volume of bed inventory. The attrition measurements, performed in the plant described in § II-1.2, confirmed the high attrition sensitivity of calcined dolomite, due to a low mechanical resistance, also reported by Rapagnà et al. (2000). The Ni/Al_2O_3 catalyst, on the contrary, had a low attrition rate constant, thanks to the relatively high resistance of γ-Al_2O_3 used as support. Sand and olivine were not tested, since they are known to be insensitive to attrition.

Table 16. Fluidization properties of catalyst used in the fluidized bed gasifier.

	Size range (μm)	Loaded amount (kg)	Particle density ($kg \cdot m^{-3}$)	U_{mf} in air at 800°C ($m \cdot s^{-1}$)	U_t in air at 800°C ($m \cdot s^{-1}$)	Attrition rate constant (-)	Geldart's group
Sand	100-400	5.0	2600	$2.9 \cdot 10^{-2}$	1.5	-	B
Dolomite	212-400	-	1600	$2.5 \cdot 10^{-2}$	1.3	$70.5 \cdot 10^{-7}$	B
Olivine	100-400	6.4	3200	$3.5 \cdot 10^{-2}$	1.8	-	B
Ni/Al_2O_3	125-212	3.5	1800	$1.0 \cdot 10^{-2}$	0.5	$2.5 \cdot 10^{-7}$	A-B

Besides these materials used in the fluidized bed gasifier, the individuation of a support with a density as close as possible to that typical of the biomass (500-1000 $kg \cdot m^{-3}$), in order to limit the physical segregation of biomass inside the bed, and its chemical and mechanical characterization constituted a preliminary part of this experimental research activity. The relative results are reported in the Annex A.

III-2 Catalytic screening results

III-2.1 Preliminary tests

Three preliminary runs were carried out before catalytic screening, their results are reported below. Firstly, the quantitative and qualitative analysis of the biomass pyrolysis products was done, excluding the second reactor. In the second run, the second reactor was connected and loaded with inert sand in order to verify the occurrence of thermal cracking reactions at high temperature (700°C) in a volume similar to that used during the catalytic tests. To conclude this preliminary study, La_2O_3 stabilized γ–Al_2O_3, used as the support for catalysts containing perovskite and/or rhodium, was loaded, after calcination at 800°C, in the second reactor in order to evaluate its possible contribution to the catalytic reaction.

The solid, liquid and gaseous yields of these three preliminary tests are reported on dry basis in Table 17.

The products of the biomass pyrolysis were constituted of gaseous species, condensable hydrocarbons and char. Both char yield (16.6 wt%) and total yield of liquid (74.6 wt%) and gas (7.8 wt%) were in agreement with the results of proximate and TG analysis (see § III-1.1). When sand was loaded in the second reactor, the gaseous yield increased up to 32.3 wt% with respect to the 7.8 wt% obtained in the absence of the secondary reactor. Accordingly, the condensable tars decreased from 74.6 to 48.3 wt%. As expected, the presence of the second reactor did not affect the char yield which stayed in the range 16.6 - 17.6 wt%. In the test with alumina, the gaseous yield increased up to 51.5 wt% with respect to the 32.3 wt% obtained with sand. Accordingly, the condensable tars decreased down to 29.2 wt% compared to the 48.3 wt% of sand. Once again, the amount of remaining char is the same obtained in the previous cases since the biomass pyrolysis condition have not been changed.

Table 17. Solid, liquid and gas yields on dry basis during the preliminary tests.

Sample in the second reactor	Solid yield (wt%)		Liquid yield (wt%)	Gas yield (wt%)
	char	coke		
-	16.6	-	74.6	7.8
Sand	17.6	-	48.3	32.3
$La_2O_3/\gamma\text{-}Al_2O_3$	16.8	5.1	29.2	51.5

Concerning the gas phase, the concentration profiles of the main constituents of detected gaseous products, obtained during the three experiments, as a function of the biomass temperature are reported in Figure 23. In all cases the gaseous products mainly consisted of carbon oxides, hydrogen and methane. It is to note that the use of He as carrier gas for the micro GC analysis with only sand did not allow the measurement of H_2 concentration (see § II-2.2). Light hydrocarbons (acetylene, ethylene, ethane, propane, propene, nC_4, nC_5, 1-pentene, 1-hexene) were also emitted at very low concentration. The amounts of light hydrocarbons obtained by integration of their emission profiles are reported in Table 18.

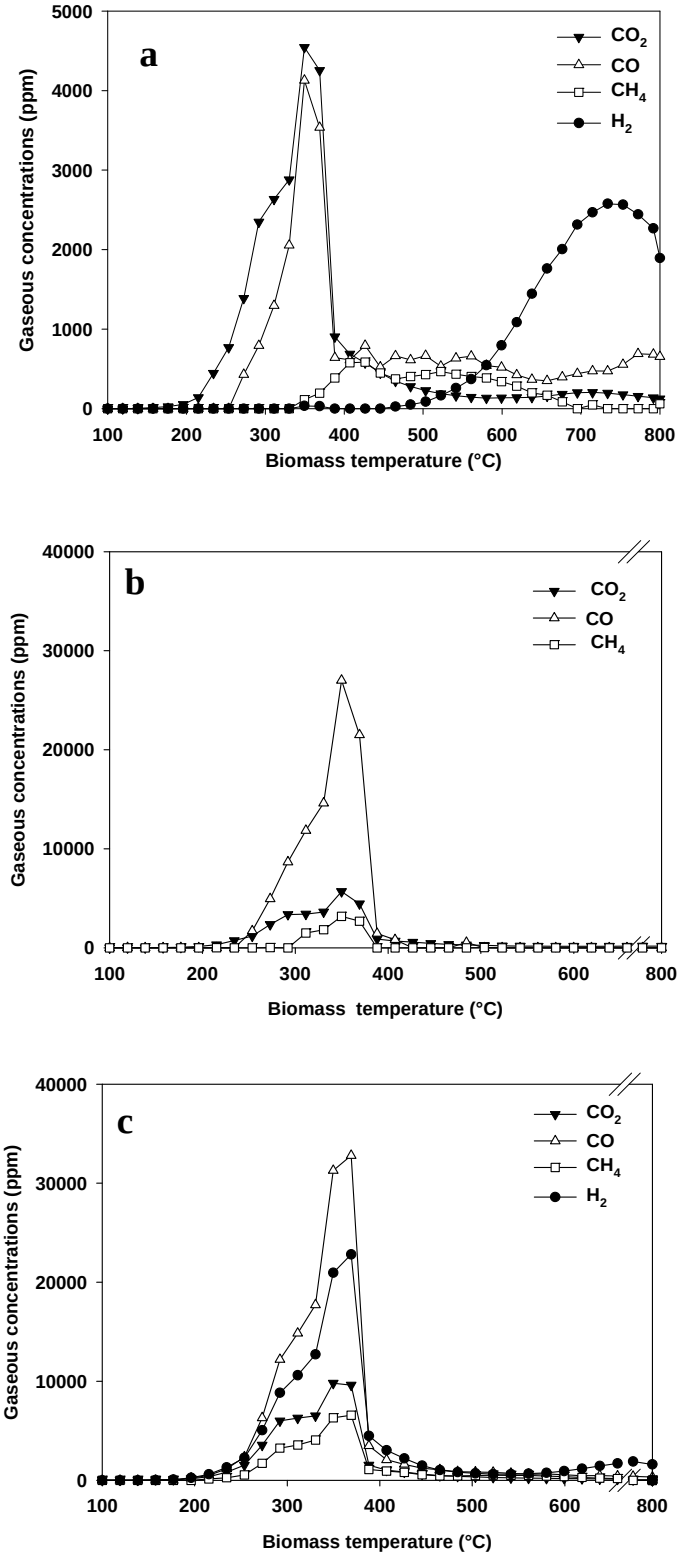

Figure 23. Micro GC thermal profiles of main gaseous products obtained during maple wood pyrolysis: **a**) excluding the second reactor (N_2 flow rate = 12 Nl·h^{-1}); **b)** with sand in the second reactor (amount = 500 mg, temperature = 700°C and N_2 flow rate = 12 Nl·h^{-1}); **c)** with La_2O_3/γ-Al_2O_3 in the second reactor (amount = 500 mg, temperature = 700°C and N_2 flow rate = 12 Nl·h^{-1}).

Table 18. Light hydrocarbons (μmol) detected in the gas phase during the preliminary tests.

Sample in the second reactor	C_2H_2	C_2H_4	C_2H_6	C_3H_6/C_3H_8	nC_4	nC_5	1-pentene	1-hexene
-	1.3	0.7	0.6	0	1.1	0.2	1.3	1.6
Sand	50.0	307.0	42.0	56.0	38.0	2.7	6.7	1.3
La_2O_3/γ-Al_2O_3	0	441.0	52.0	82.0	37.0	2.3	0	0

During maple wood pyrolysis experiment CO_2 was the first compound to be released at about 150°C with a maximum concentration of about 4500 ppm at 350°C. At about 370°C its concentration sharply decreased. The emission of CO_2 continued at a lower extent (about 150 ppm) until the end of the experiment. The CO production started at about 270°C with a maximum concentration value of 4100 ppm at 350°C. At 370°C its concentration sharply decreased. The emission of CO continued at a lower extent (about 500 ppm) until the end of the experiment. Methane started to be released at about 350°C with a maximum concentration of about 600 ppm at 430°C end to 700°C. Hydrogen started to be released at about 460°C until the end of experiment with a maximum concentration of about 2600 ppm at 730°C. Light hydrocarbons (acetylene, ethylene, ethane, propane, propene, nC4, nC5, 1-pentene, 1-hexene) were also released at very low concentration (< 50 ppm) at about 370°C.

When sand was present in the second reactor the main components were again CO, CO_2 and CH_4. However, their concentration (except from CO_2) was about one order of magnitude higher than in the absence of the second reactor. The CO_2 profile followed the same trend as the one observed for the biomass. Actually, CO_2 started to be released at about 150°C with a maximum value of about 5700 ppm at 350°C. Traces of CO_2 (> 200 ppm) were also observed until the end of the experiment. CO started to be released at 270°C and up to 370°C, similarly to that observed without the second reactor, but at higher concentration reaching a maximum value of about 27000 ppm at 350°C. The methane started to be released at about 300°C, i.e. earlier than during the test with only biomass, up to 370°C, with a maximum concentration of about 3200 ppm at 350°C. The methane released by biomass in the temperature range 350-700°C was not detected anymore. The amounts of light hydrocarbons significantly increased with respect to the test carried out in the

absence of the second reactor (Table 18). They were released at different concentrations in the temperature range 170-560°C; in particular, maximum concentration values of about 2500 ppm for ethylene and hundreds of ppm for nC_4, ethane, acetylene, propane and propene have been observed at 350°C, the maximum concentration of remaining species being lower than 50 ppm. The increase in CO, CO_2 and light hydrocarbon concentrations in the temperature range 150-400°C and the contemporary appearance of CH_4 highlighted the further conversion of species coming from the biomass decomposition in the second reactor at 700°C. Moreover, the disappearance of CH_4 released from biomass at higher temperatures may be explained by its further conversion in the second reactor, also confirmed by the slight increase of CO_2 concentration in the same temperature range.

The carbon oxides profiles, obtained when alumina was present in the second reactor, were qualitatively similar to those observed for sand, but with a significant gas yield increase. Methane detection started at about 250°C with a maximum concentration of about 7700 ppm at 350°C. A shoulder in methane profile was also observed with a maximum of about 600 ppm, corresponding to the unconverted methane released by the biomass up to 700°C. Differently to that observed without the second reactor, hydrogen started to be released earlier at about 150°C with a maximum concentration of about 23000 ppm at 370°C. In the same way as observed for methane, the hydrogen produced by biomass in the temperature range 470-800°C was still detected in the same amount (maximum of about 2300 ppm at 730°C). Light hydrocarbons were produced in the temperature range 200-600°C in similar amounts with respect to the test with sand. As for sand, the increase in CO, CO_2 and light hydrocarbon concentrations in the temperature range 150-400°C and the contemporary appearance of CH_4 and H_2 highlighted the further conversion of species coming from the biomass decomposition in the second reactor at 700°C. Nevertheless, the CH_4 and H_2 released from biomass at higher temperatures were still present in the products.

The Figure 24 summarizes in a more comprehensive way the CO, CO_2, CH_4 and light hydrocarbons yields obtained for the three runs. H_2 is reported only for biomass and alumina. As previously said, very few amounts of gas were formed in the first biomass pyrolysis test.

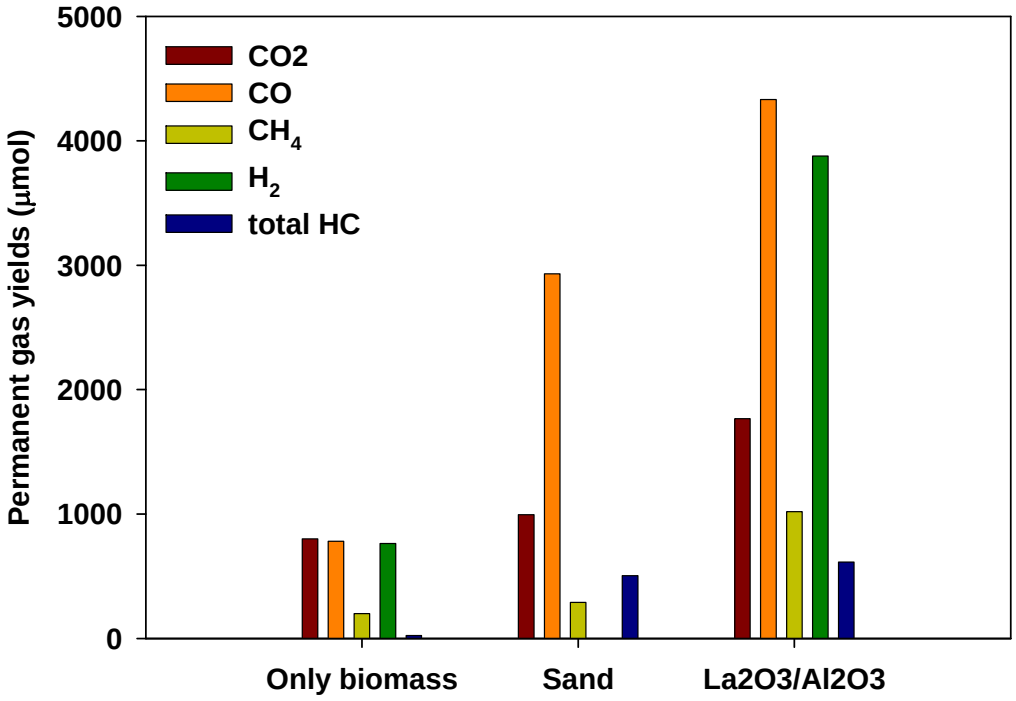

Figure 24. Compared gaseous and light hydrocarbon yields of the preliminary tests.

The chromatogram of condensed tars, collected during these preliminary tests, are reported in Figure 25, while their relative amounts are reported in Table 17.

The tar produced during biomass pyrolysis (excluding the second reactor) was, as expected, a very complex mixture and many different compounds were present. The peaks identified, as request by the CEN/TS 15439 (2006) protocol before mentioned, correspond to phenols, PAHs and guaiacols, characteristic compounds of biomass decomposition. In the presence of the second reactor a qualitatively different product distribution have been obtained if compared to that obtained in the absence of the second reactor. In particular when sand is used in the second reactor, among the oxygenated compounds creosol and guaiacols disappeared while phenols were reduced, accompanied by the increase in CO_x production and light hydrocarbon before observed. PAHs species were still detectable together with aromatic compounds. Moreover, a shift towards heavier polycyclic compounds have been observed, highlighted by the presence of not well resolved peaks in the range of retention time 40-50 min. These findings suggest the occurrence of cracking phenomena followed by secondary reactions of polycondensation promoted by presence of the second reactor at 700°C. In the presence of alumina in the second reactor, a qualitatively similar product distribution to that obtained with sand has been observed, but with lower intensities.

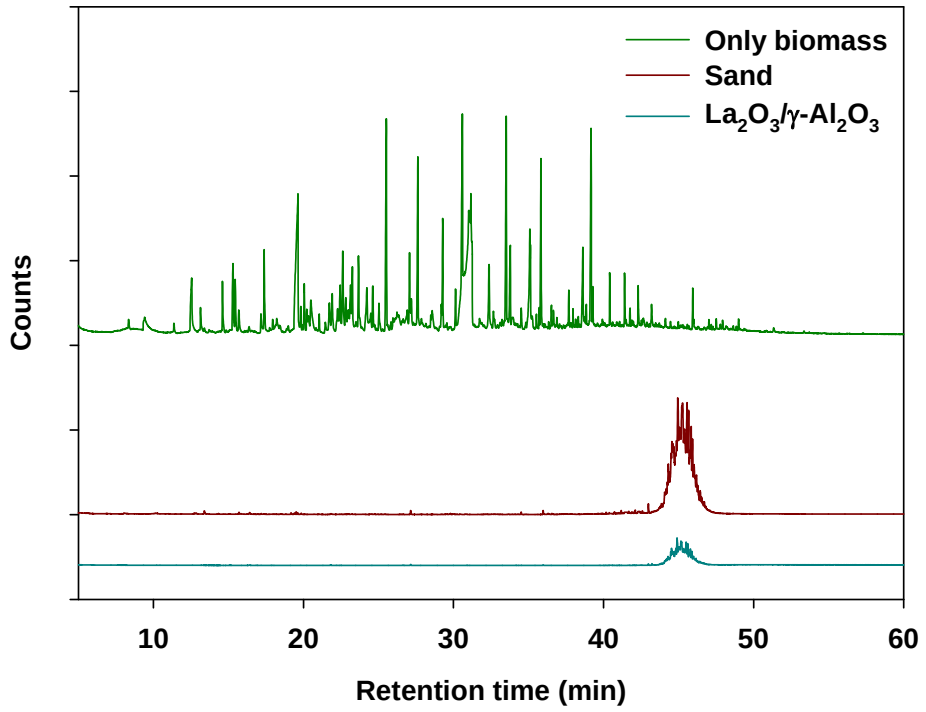

Figure 25. GC spectra of tars obtained during the preliminary tests.

Table 19. GC compounds (μmol) detected during the preliminary tests following the CEN/TS 15439 (2006) protocol.

Compound	Biomass	Sand	La_2O_3/γ-Al_2O_3
Creosol	8.19	-	-
Guaiacol	10.09	-	-
Indene	-	0.07	0.02
Phenol	2.51	1.84	-
3-Methylphenol	2.52	0.03	-
Naftalene	-	0.02	<0.01
Fluorene	0.02	-	-
Phenanthrene	0.11	<0.01	-
Antracene	-	-	-
Fluoranthene	<0.01	<0.01	<0.01
Pyrene	<0.01	<0.01	<0.01
Benz(a)Anthracene	<0.01	0	<0.01
Chrysene	<0.01	<0.01	<0.01
Benzo(k)Fluoranthene	<0.01	-	<0.01
Benzo(b)Fluoranthene	<0.01	-	<0.01
2-MetylPhenol	0.98	0.02	-
4.MethylPhenol (p-cresol)	2.34	0.57	-
2,4-DimethylPhenol (2,4-Xylenol)	0.03	0.13	-
2,4,5-Trichlorophenol	<0.01	-	-
2,3,5,6-Terachlorophenol	<0.01	-	-
TOTAL (μmol)	8.54	2.61	0.03

Figure 26 shows the CO_2 profiles determined by the temperature programmed oxidation of coke deposited on the sand and the La_2O_3/γ-Al_2O_3 at the end of the experiment (see § II-2.2). Only one main CO_2 peak was observed at about 550°C for alumina, whereas no coke was formed on sand, essentially due to its very low surface area (<1 $m^2 \cdot g^{-1}$).

The amount of deposited coke, evaluated by integration of the obtained CO_2 profile, expressed in wt% on dry basis, is reported in Table 17.

The amount of coke has been considered as an index of the cracking activity of the samples since it is formed by the deposition of organic residues from cracking of molecules taking place on the surface of the investigated materials. The presence of coke on alumina then confirms its cracking ability, due to the activation of tar decomposition on its acid surface, favouring coke deposition.

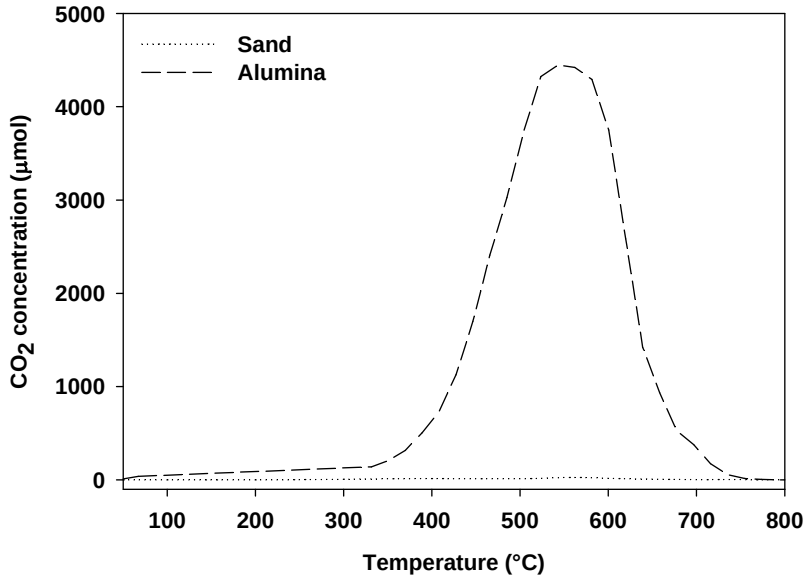

Figure 26. CO_2 profile obtained during oxidation of coke produced during preliminary tests (O_2 concentration = 0.5%vol. in He and flow rate = 17 $Nl \cdot h^{-1}$).

In order to allow a direct comparison of the results obtained during these preliminary tests, the normalized product yields are reported in Figure 27.

The observation of this figure clearly shows the increase in gas phase yield, to the detriment of the tar formation, when the second reactor was introduced and loaded with an inert material. More specifically, as confirmed by the tar analysis, the increase in the total gas yield can be explained by the thermal decomposition of part of the vaporized tarry species over the hot surface (700°C) of the inert fixed bed material. In addition, the presence of alumina in the second reactor

further increased the gas yield (to the detriment of liquid phase) since it was more active than sand in tar conversion, due to its stronger cracking activity related to its higher surface area and acidity, also confirmed by the formation of coke.

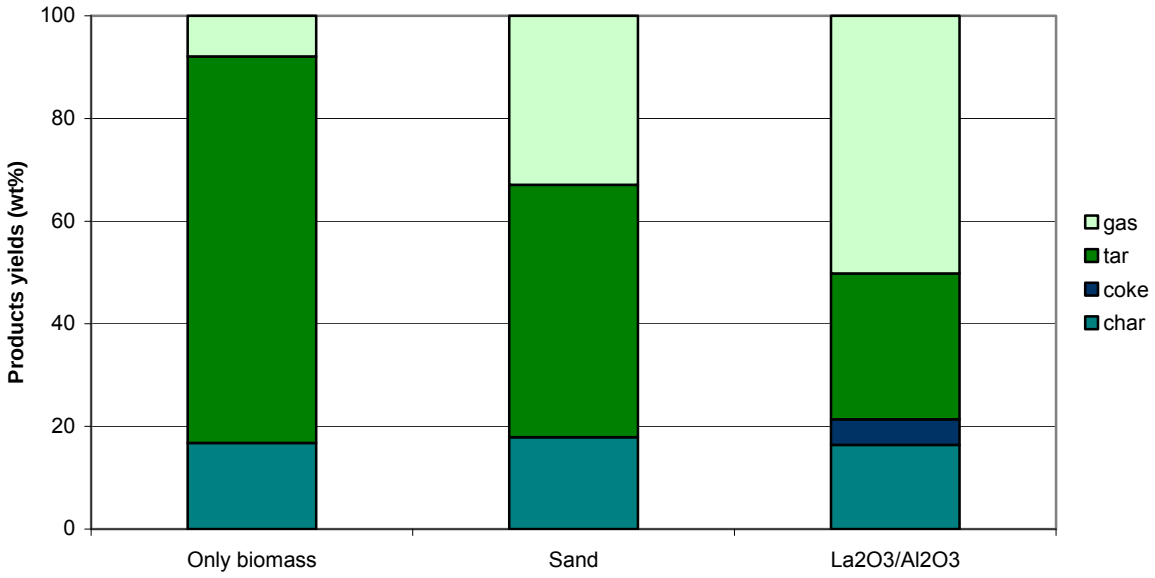

Figure 27. Normalized product yields in wt% of the dry biomass for preliminary tests.

III-2.2 Screening of conventional catalysts

This section compares the performances, in the transformation of tar produced during the biomass pyrolysis, of the catalysts traditionally used for tar conversion, especially as primary catalysts in fluidized bed gasifiers (Devi et al., 2003), such as olivine, dolomite (natural catalysts) and Ni/Al_2O_3, prepared as reported in § II-1.2.

The solid, liquid and gaseous yields of these tests are reported on dry basis in Table 20. The presence of a catalyst in the second reactor led, except for olivine, to an increase in gas yield, in comparison with that obtained with alumina, due to the enhanced conversion of condensable tars. However, all catalysts (natural and synthetic) left condensable products unconverted in different amounts. The char yield was in the range 16.6 to 17.5 wt% for all the experiments, still in agreement with the data of proximate analysis reported before (see § III-1.1).

Table 20. Solid, liquid and gas yields on dry basis for conventional catalysts (catalyst amount = 500 mg, temperature = 700°C and N_2 flow rate = 12 Nl·h^{-1}).

Sample in the second reactor	Solid yield (wt%)		Liquid yield (wt%)	Gas yield (wt%)
	char	coke		
Ni/Al_2O_3	17.1	5.5	16.3	61.9
Dolomite	16.9	4.9	16.1	56.7
Olivine	17.5	-	32.8	40.7

The Figure 28 reports the concentration profiles of the main gaseous species in function of the biomass temperature. H_2 concentration is not available for these tests.

The CO profile (Figure 28a) followed a similar trend for all catalysts in the temperature range 230-550°C with a unique maximum at about 350°C. The Ni/Al_2O_3 catalyst produced more CO than the other two materials while olivine the less. The CO_2 production (Figure 28b) occurred in the temperature range 200-700°C, showing two main CO_2 peaks at 290°C and 350°C. Dolomite showed the largest CO_2 yield, followed by Ni/Al_2O_3, whereas olivine had a halved CO_2 yield. The highest concentration of methane in the gaseous products (Figure 28c) was found for dolomite and Ni/Al_2O_3 catalyst, followed by olivine. Methane was mainly produced between 215 and 390°C, being the product of further conversion of species coming from the biomass decomposition. The methane released by biomass in the temperature range 350-700°C remained essentially unconverted only for dolomite and olivine. On the contrary, the Ni/Al_2O_3 catalyst was able to convert this methane, without a further increase of CO_2 with respect to that obtained with only biomass in this temperature range, thus highlighting the methane cracking activity of this catalyst.

As reported in Table 21, few light hydrocarbons were found using the Ni/Al_2O_3, whereas the other two catalysts were less able to convert these compounds.

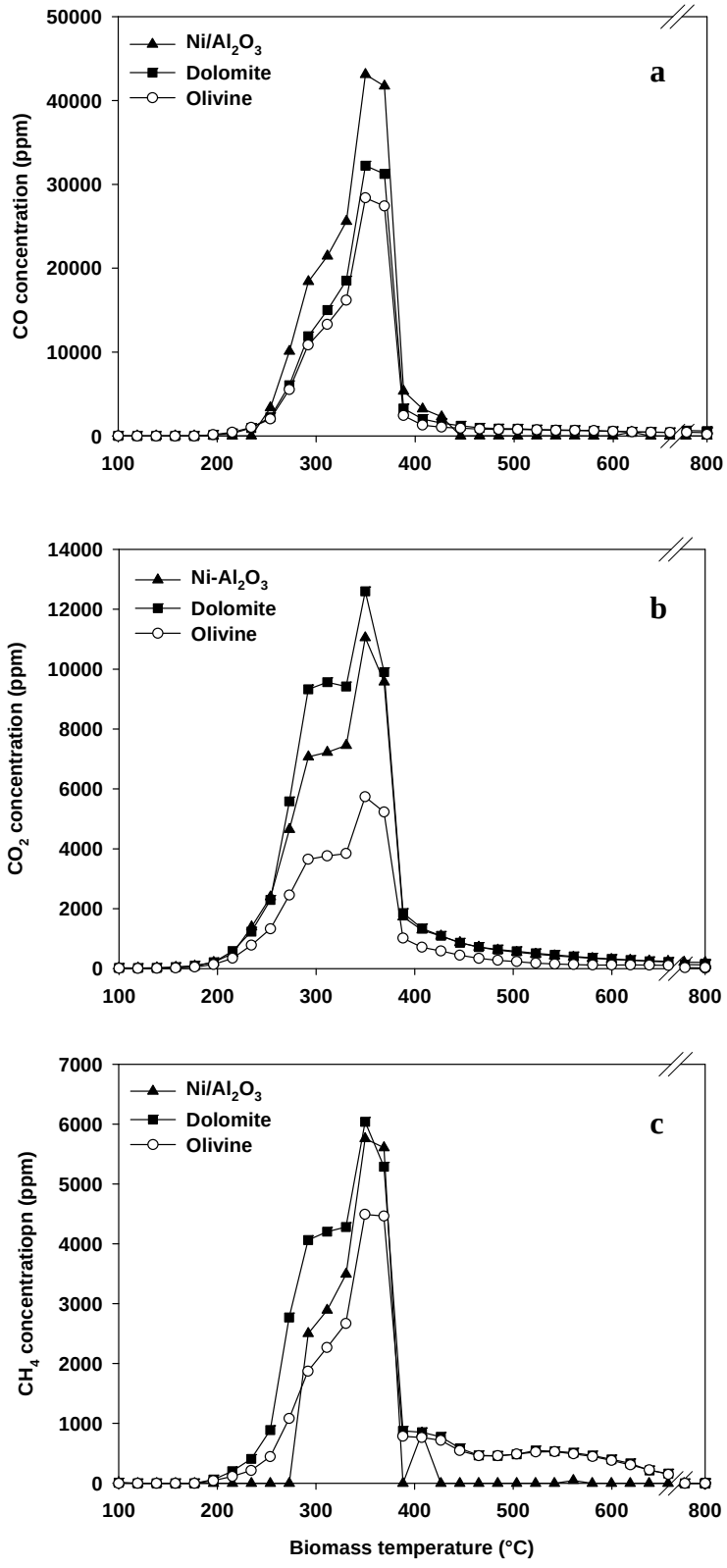

Figure 28. Micro GC thermal profiles of CO **(a)**, CO_2 **(b)** and CH_4 **(c)** obtained during maple wood pyrolysis with conventional catalysts in the second reactor (catalyst amount = 500 mg, temperature = 700°C and N_2 flow rate = 12 $Nl \cdot h^{-1}$).

Table 21. Light hydrocarbons (μmol) detected in the gas phase for conventional catalysts (catalyst amount = 500 mg, temperature = 700°C and N_2 flow rate = 12 Nl·h^{-1}).

Sample in the second reactor	C_2H_2	C_2H_4	C_2H_6	C_3H_6/C_3H_8	nC_4	nC_5	1-pentene	1-hexene
Ni/Al_2O_3	-	240.7	35.0	31.6	8.5	0.5	-	-
Dolomite	21.0	351.3	48.1	71.1	-	4.3	17.7	1.6
Olivine	58.7	356.0	44.7	60.3	41.2	3.1	11.9	1.4

Figure 29 reports the compared CO, CO_2, CH_4 and total light hydrocarbon gas yields. The CO production, which increased following the order olivine < dolomite < Ni/Al_2O_3, can be addressed to an increasing reforming activity of the catalysts, thus explaining also the decrease in methane and light hydrocarbons production.

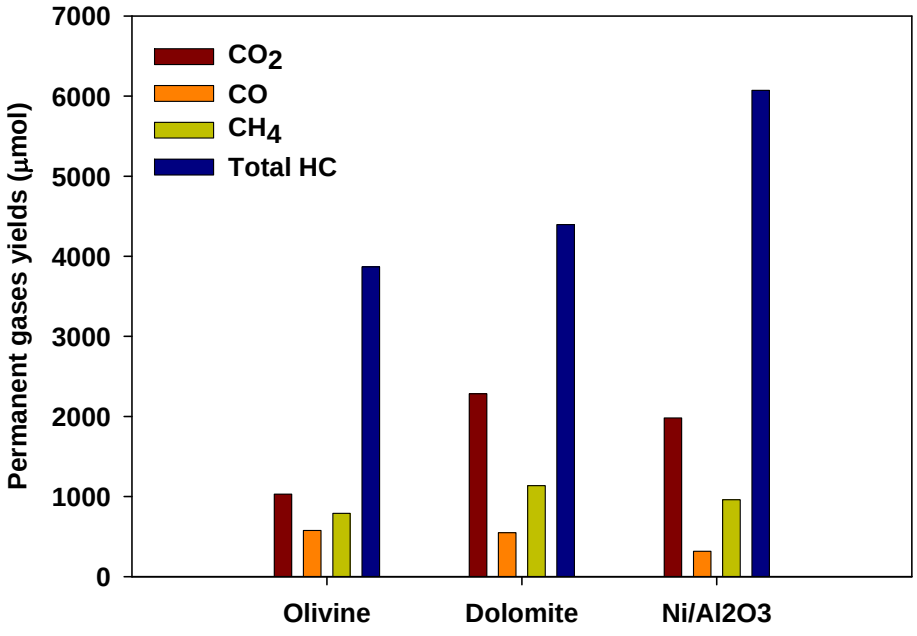

Figure 29. Compared gaseous and light hydrocarbon yields of conventional catalysts (catalyst amount = 500 mg, temperature = 700°C and N_2 flow rate = 12 Nl·h^{-1}).

In Figure 30 and Table 22 the chromatographic profiles and the quantitative analysis of the GC detected compounds included in the CEN/TS 15439 (2006) normative are reported,

respectively. Many compounds have been detected by the chromatographic analysis of condensed tar. Few amounts of oxygenated compounds (phenols) were present in the condensate in the tests with dolomite and olivine (only traces of naphthalene were found among tars produced in the test with Ni/Al_2O_3 catalyst), whereas PAHs, lumped in the broad peak at 45 minutes, were always detectable, as already observed in the tests with sand and alumina.

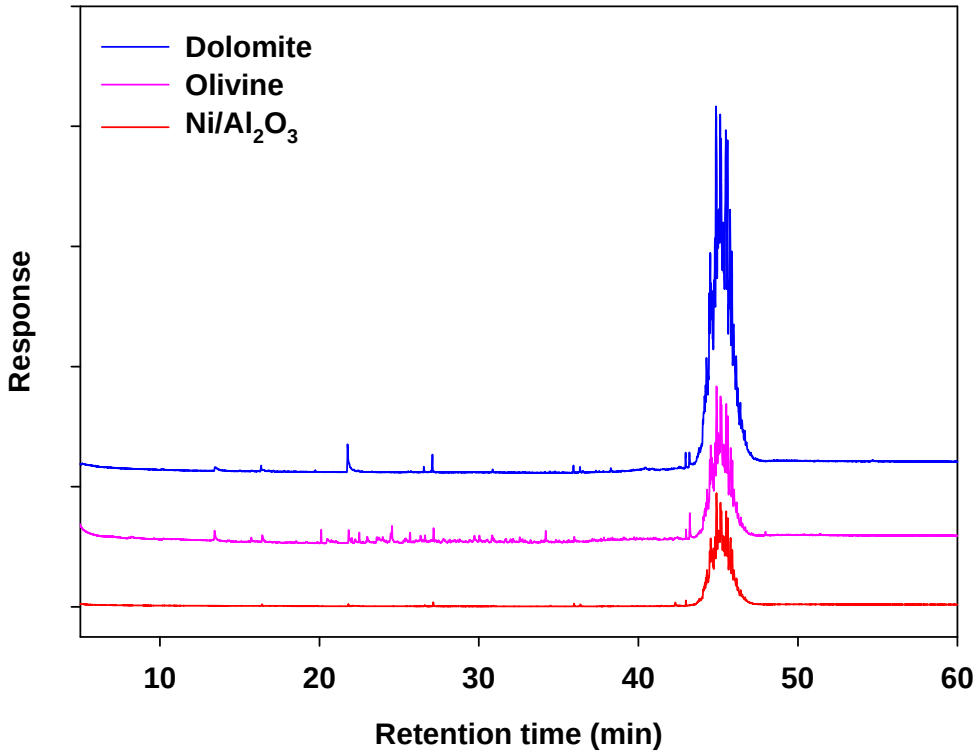

Figure 30. GC spectra of tars obtained for conventional catalysts (catalyst amount = 500 mg, temperature = 700°C and N_2 flow rate = 12 $Nl \cdot h^{-1}$).

Table 22. GC compounds (μmol) detected for conventional catalysts following the CEN/TS 15439 (2006) protocol.

Compound	Dolomite	Olivine	Ni/Al_2O_3
Creosol	-	-	-
Guaiacol	-	-	-
Indene	0.06	0.04	-
Phenol	1.64	1.99	-
3-Methylphenol	0.16	0.58	-
Naftalene	0.04	0.01	<0.01
Fluorene	<0.01	<0.01	-
Phenanthrene	<0.01	<0.01	-
Antracene	-	<0.01	-
Fluoranthene	<0.01	<0.01	-
Pyrene	<0.01	0,01	-
Benz(a)Anthracene	<0.01	<0.01	-
Chrysene	<0.01	<0.01	-
Benzo(k)Fluoranthene	<0.01	-	-
Benzo(b)Fluoranthene	<0.01	-	-
2-MetylPhenol	<0.01	0.02	-
4.MethylPhenol (p-cresol)	0.01	0.53	-
2,4-DimethylPhenol (2,4-Xylenol)	0.02	0.10	-
2,4,5-Trichlorophenol	-	-	-
2,3,5,6-Terachlorophenol	-	-	-
TOTAL in μmol	1.91	3.26	<0.01

Figure 31 shows the CO_2 profiles obtained during oxidation of coke deposited on the different materials. The CO_2 profile obtained for Ni/Al_2O_3 catalyst showed two peaks at about 550 and 650°C, whereas that of dolomite presented a tri-modal distribution with an additional peak at t about 420°C with respect to Ni/Al_2O_3 catalyst. These peak distributions of CO_2 profiles observed can be explained by the formation of different coke species on the catalysts. Li and Brown (2001) studied the oxidation kinetics of single amorphous carbon (charcoal) and graphite particles, not deposited on a surface. They found that the CO_2 profiles resulting from their TPO experiments reached a peak value at 730°C, 760°C and 805°C for powdered charcoal, granular charcoal and graphite, respectively. Their findings led us to consider a possible comparison with our temperature programmed oxidation experiments. Thus, the low temperature peaks observed at 450 and 550°C may be the result of the oxidation process of coke agglomerates deposited on the catalyst surface at two different scales; the first one corresponding to powdered amorphous carbon species and the

second one to granular amorphous carbon species. The high temperature oxidation peak (around 650°C) would be attributable to a more stable graphitic-like species. The fact that the oxidation of carbon species occurs at lower temperature than those observed in literature on oxidation of single carbon particles can reasonably be attributed to a catalytic effect. This is confirmed by the work of the same research group, who also found the presence of three peaks in CO_2 profiles at lower temperatures (470, 672 and 714°C) obtained during the temperature programmed oxidation of coke deposited on cracking catalysts under similar experimental conditions (Le Minh et al., 1997).

The amount of deposited coke expressed in wt% on dry basis is reported in Table 19. The olivine did not tend to form coke, probably due to its very low superficial area (< 1 $m^2 \cdot g^{-1}$). On the contrary, the Ni catalyst and the dolomite were very sensitive to coking.

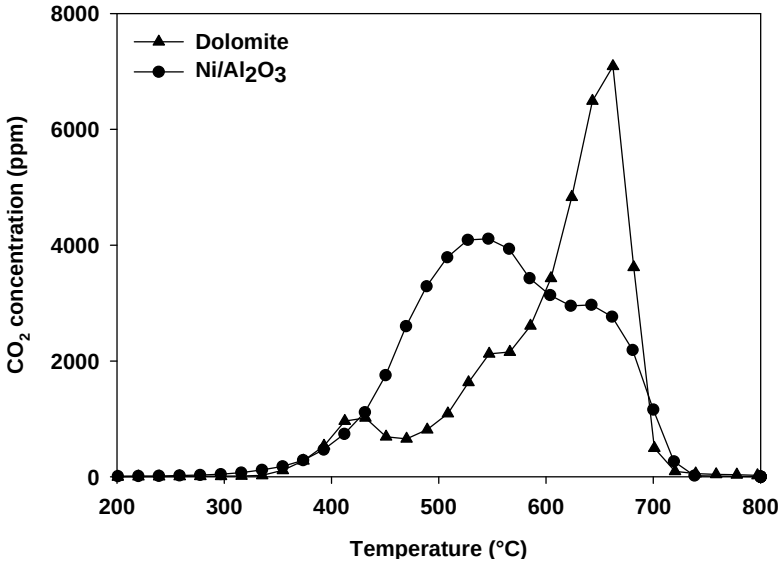

Figure 31. CO_2 profile obtained during oxidation of coke deposited on conventional catalysts (O_2 concentration = 0.5%vol. in He and flow rate = 17 $Nl \cdot h^{-1}$).

Figure 32 reports the normalized solid, liquid and gaseous yields, obtained during these tests. The observation of this figure clearly shows that olivine was the least active catalyst in tar conversion, followed by dolomite and Ni/Al_2O_3 catalyst. Coking phenomena was observed only for dolomite and Ni/Al_2O_3 catalysts.

In conclusion, the results of catalytic tests can be summarized as follows. All conventional catalysts were able to convert tars, even if not totally, in different ways, promoting the cracking, the total oxidation or the reforming of species released during biomass decomposition. In particular, the activity of dolomite was more addressed to cracking, favouring the formation of cracked

compounds leading to coke deposition, similarly to that obtained for the La_2O_3/γ-Al_2O_3, and, in a lesser extent, to total oxidation, as confirmed by the observed slight increase of CO_2 production with respect to the sand and La_2O_3/γ-Al_2O_3 (§ III.2.1). In comparison, olivine showed much less cracking activity, thus showing a similar comportment to that of inert sand. On the other hand, the activity of Ni/Al_2O_3 sample was addressed mainly to the cracking, favoring the coke formation, and, in a lesser extent, to the reforming and total oxidation of species released during biomass decomposition, as confirmed by a slight increase of CO and CO_2 production and a decrease of methane and light hydrocarbons production with respect to the La_2O_3/γ-Al_2O_3 (§ III.2.1). The comparison between the Ni/Al_2O_3 and dolomite showed that the first one had a reforming activity which led to a decrease of CO_2, methane and light hydrocarbon and to an increase of CO.

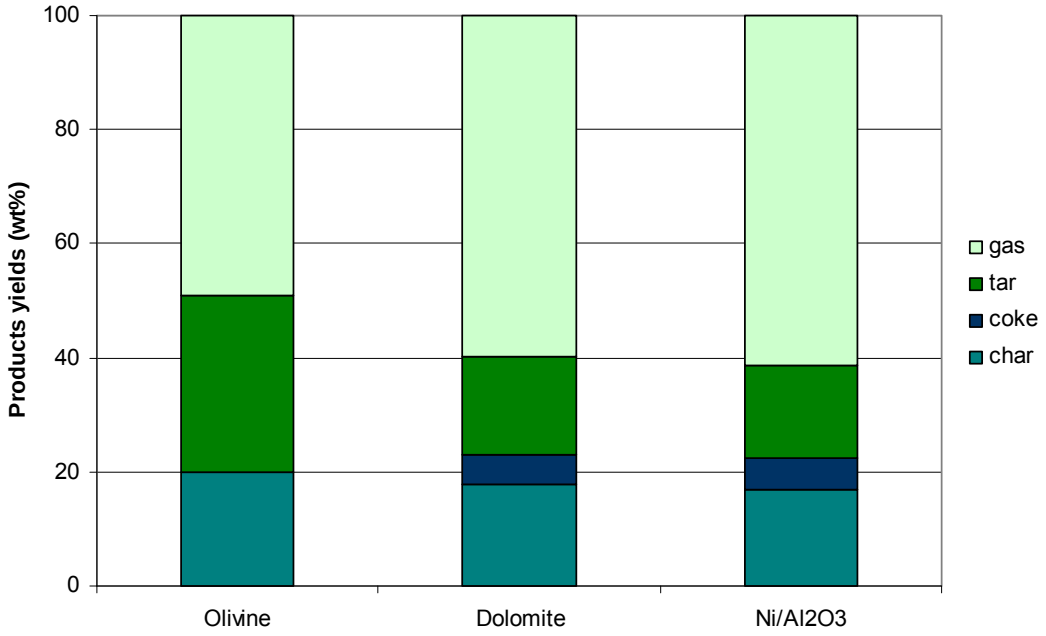

Figure 32. Normalized product yields in wt% of the dry biomass for conventional catalysts (catalyst amount = 500 mg, temperature = 700°C and N_2 flow rate = 12 $Nl \cdot h^{-1}$).

III-2.3 Screening of the novel catalysts

In this section, the results of catalytic tests carried out on the proposed lanthanum cobalt alumina supported perovskite catalysts, doped or not with 1 wt% of rhodium and calcined at different temperatures (800 and 900°C), will be described.

These tests aimed to determine the role of both noble metal and perovskite and how the calcination temperature can affect the performances of the systems.

At the end of the section, the activity of the best conventional catalyst i.e. the Ni/Al_2O_3 catalyst (§ III.2.2), will be compared to the one showing the best performances selected after the study.

The gas, solid and liquid yields obtained with the novel catalysts are reported on dry basis in Table 23. Except for 900/p which favoured some liquid formation (mainly water), no liquid condensation was observed in the flasks for all the others catalysts, neither at room temperature or at -20°C. All catalysts tested showed a gas yield higher than 75.9 wt %, except for the 900/p sample, which provided a lower gas yield of 57.4 wt% (similar to alumina reported in § III-2.1). The char yield was in the range 16.5 to 18.3 wt% for all the experiments, in good agreement with the data of TG analysis (§ III-1.1) and the previous catalytic results (§ III-2.1 and § III-2.2) since the pyrolysis condition of biomass in the first reactor has not been changed**.**

Table 23. Solid, liquid and gas yields on dry basis for novel catalysts (catalyst amount = 500 mg, temperature = 700°C and N_2 flow rate = 12 $Nl \cdot h^{-1}$).

Sample in the second reactor	Solid yield (wt%)		Liquid yield	Gas yield
	char	coke	(wt%)	(wt%)
800/1Rh	16.5	2	-	76.5
800/p	18.3	3.5	-	75.9
800/p/1Rh	18.0	1.1	-	77.6
900/1Rh	17.3	2.6	-	76.5
900/p	18.3	5.6	11.0*	57.4
900/p/1Rh	18.0	1.0	-	77.9

*mainly water

As concerns the gaseous product distribution, H_2, CO, CO_2 and CH_4 were the main detected gas products for all samples. Their concentration profiles are reported in the Figure 33 a - d, respectively.

The H_2 and CO profiles for all catalysts qualitatively similar to those obtained with alumina (§ III-2.1). The amounts of CO and H_2 produced on the 900/p were comparable to those found using alumina. All the other samples showed similar H_2 and CO yields, significantly higher than that observed the 900/p sample. All samples showed two main CO_2 peaks at 290°C and 350°C. A broad peak extending from 390°C to the end of the experiment was present for all catalysts except for the 900/p sample, the latter providing the highest total CO_2 concentration. Methane was produced at temperatures (215-390°C) at which it was not present for simple pyrolysis (§ III-2.1) and thus it should be the product of further conversion of species coming from the biomass decomposition. On the contrary, the methane released by the biomass in the range 350-700°C remained essentially unconverted for 900/p as also observed for sand (§ III-2.1). Since CO_2 formation in the final stage (from 390 to the end of experiments) overlapped the conversion zone of methane (350-700°C), the activity of all the other catalysts probably consisted in the methane oxidation in this temperature range.

The amounts of light hydrocarbons obtained by integration of their emission profiles are reported in Table 24. No light hydrocarbons were found when rhodium was present in the catalyst also in combination with $LaCoO_3$ while the light hydrocarbons formed with the 900/p catalyst were qualitatively and quantitatively similar to those found with alumina. Only ethane and ethylene, in small amount, were produced on 800/p.

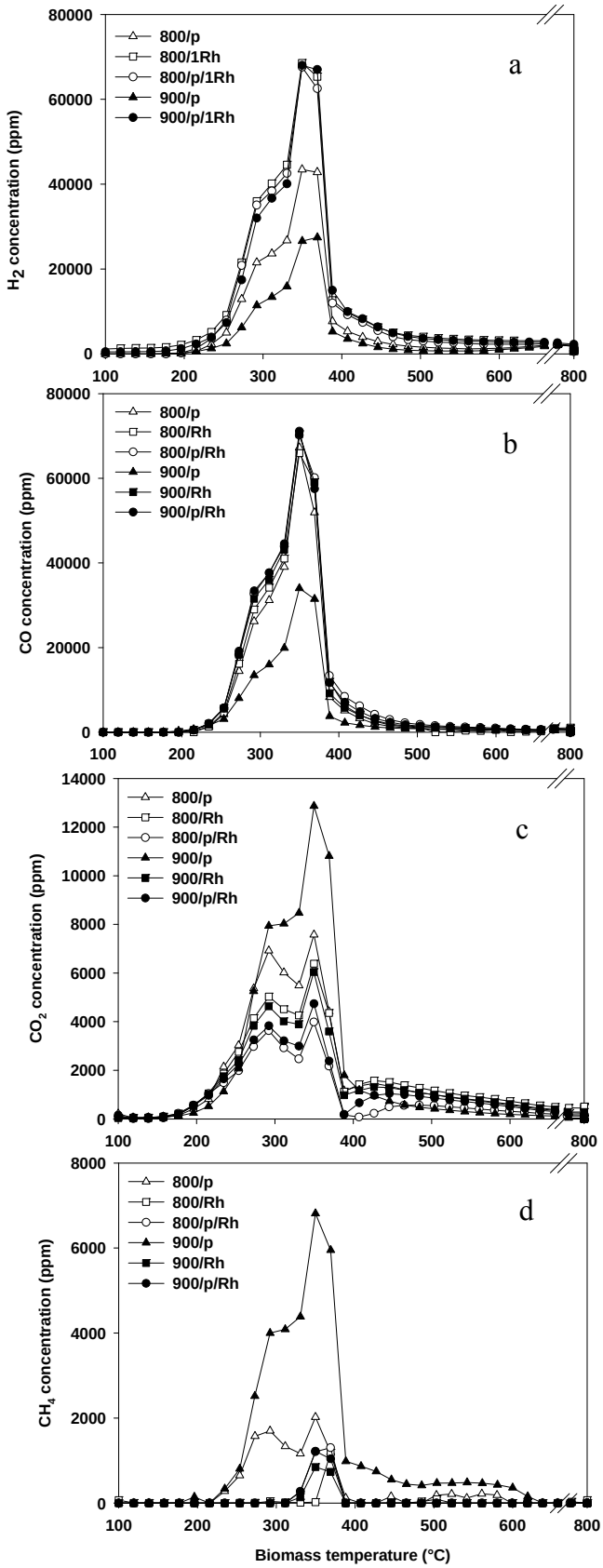

Figure 33. Micro GC thermal profiles of H_2 **(a)**, CO **(b)**, CO_2 **(c)** and CH_4 **(d)** obtained during maple wood pyrolysis with novel catalysts in the second reactor (catalyst amount = 500 mg, temperature = 700°C and N_2 flow rate = 12 $Nl \cdot h^{-1}$).

Table 24. Light hydrocarbons (µmol) detected in the gas phase for novel catalysts (catalyst amount = 500 mg, temperature = 700°C and N_2 flow rate = 12 Nl·h^{-1}).

Sample in the second reactor	C_2H_2	C_2H_4	C_2H_6	C_3H_6/C_3H_8	nC_4	nC_5	1-pentene	1-hexene
800/p	0	2.1	2.8	0	0	0	0	0
900/p	3.5	401	50	85	38	3.2	1.4	0.3

Figure 34 reports in a more comprehensive way the H_2, CO, CO_2, CH_4 and light hydrocarbons yields.

The higher selectivity to H_2 and CO of the catalysts containing rhodium, linked to the total conversion of light hydrocarbons and the few amounts of produced methane, was evidenced. On the contrary, the catalysts containing only perovskite, especially the 900/p sample, were less able to convert the species emitted during biomass devolatilization to syngas.

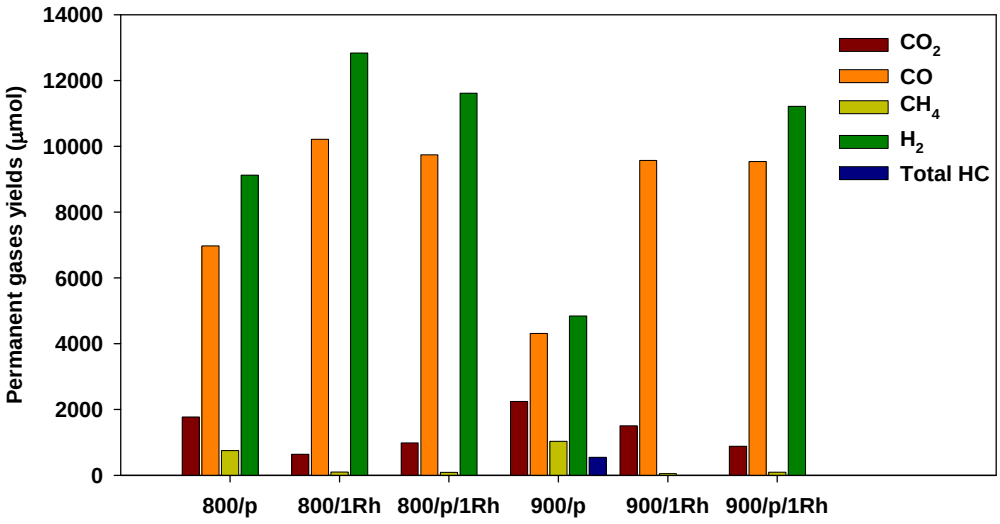

Figure 34. Compared gaseous and light hydrocarbon yields of novel catalysts (catalyst amount = 500 mg, temperature = 700°C and N_2 flow rate = 12 Nl·h^{-1}).

The quantitative results of GC analysis performed on the condensate products obtained during the test of 900/p sample are reported in Table 25. The GC analysis showed that no primary tars (oxygenated species) were produced, but non negligible amounts of different secondary and tertiary tars were measured. Nevertheless, the broad peaks corresponding to heavier PAHs observed before for other catalytic systems in the range of retention time 40-50 min disappeared. The relatively small amounts of detected tar in comparison to the 11 wt% of total liquid yield found for the 900/p confirmed the main presence of water. For all the other catalytic systems, the isopropanol used for cleaning the flasks was analysed. No trace of tars could be detected, according to the fact that no tar were gravimetrically measured.

Table 25. GC compounds (μmol) detected for novel catalysts following the CEN/TS 15439 (2006) protocol.

compound	Catalyst
	900/p
Phenanthrene	0
Fluoranthene	0.004
Pyrene	0.006
Benz(a)anthracene	0.005
Chrysene	0.010
Benzo(k)fluoranthene	0.004
Benzo(b)fluoranthene	0.004
Benzo(a)pyrene	0.007
TOTAL in μmol	0.04

Figure 35 shows the CO_2 profiles obtained during the temperature programmed oxidation of coke at the end of the experiment (see § II-2.1) for the different materials. All profiles showed a different CO_2 peaks distribution, still attributable to the formation of different species of coke (see § III-2.2). In particular, the catalysts containing only rhodium presented only one peak at 550°C, attributable to granular amorphous carbon. On the other hand, the catalysts containing only perovskite and the 800/p/1Rh catalyst presented a bi-modal distribution with the main peak at about 450-500°C, attributable to powdered amorphous carbon, and the second minor peak at about 650-700°C, due to the formation of graphitic-like carbon. On the contrary, the high temperature peak

was not present in the CO_2 profile of the 900/p/1Rh catalyst, that showed only the peak at about 450°C.

The amount of deposited coke expressed in wt% on dry basis is reported in Table 23. The coke formation ranged from 1 wt% for the least sensitive catalyst (800/p/1Rh) to 5.6 wt% for the most sensitive one (900/p). In particular, the catalysts containing only perovskite were found to be more sensitive to coking, specially the one calcined at 900°C, which had a similar behaviour to the La_2O_3/γ-Al_2O_3 (§ III-2.1). The catalysts containing only rhodium appeared less susceptible to coking, however calcination at 900°C tended to increase slightly the coke formation. Nevertheless, the least coked materials were those containing both active phases (900/p/1Rh and 800/p/1Rh).

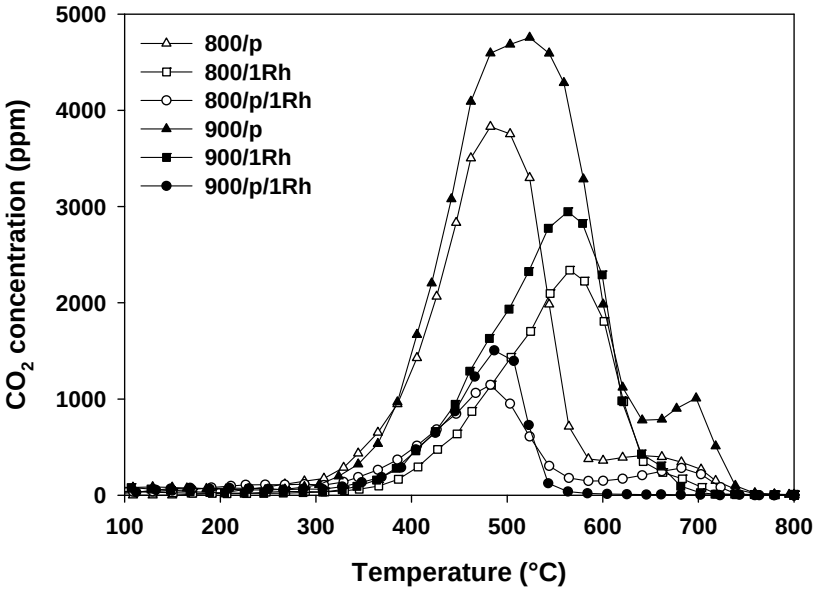

Figure 35. CO_2 profile obtained during oxidation of coke deposited on novel catalysts (O_2 concentration = 0.5%vol. in He and flow rate = 17 $Nl \cdot h^{-1}$).

The Figure 36 reports the compared yields (normalized) of the novel catalysts. The complete conversion of tar for all catalysts is evident. As said above, the liquids found during the test with 900/p were mainly composed of water.

In conclusion, the results of catalytic tests of novel catalysts can be summarized as follows. all catalysts were able to convert tars (except for the 900/p sample), promoting reforming, total oxidation or, in a lesser extent, cracking of species released during biomass decomposition. The amount of CO and H_2 produced has been related to the reforming ability of the catalysts, whereas that of CO_2 to total oxidation activity. On the other hand, the presence of light hydrocarbons in the

gas phase as well as the formation of coke on the catalyst surface have been correlated to the occurrence of cracking reactions breaking the high molecular weight species emitted by the biomass into lighter species, which partly re-condensate on the catalyst surface. The activity of the 900/p sample was more addressed to cracking and total oxidation (confirmed by the presence of water in the liquid phase) rather than to reforming reactions with respect to other samples. This sample also favoured the coke formation. With respect to the 900/p, the 800/p sample had a higher reforming activity. On the other hand, the presence of Rh was fundamental to favour the reforming of methane and light hydrocarbons, not totally converted by samples not containing the noble metal, confirmed by the strong increase of CO and H_2 and a decrease of CO_2. The Rh containing samples could also oxidize methane emitted from biomass pyrolysis in the range 350-700°C to CO_2. In particular, the samples containing both Rh and perovskite phases also showed the lowest cracking activity, lower amounts of coke having been observed on these samples.

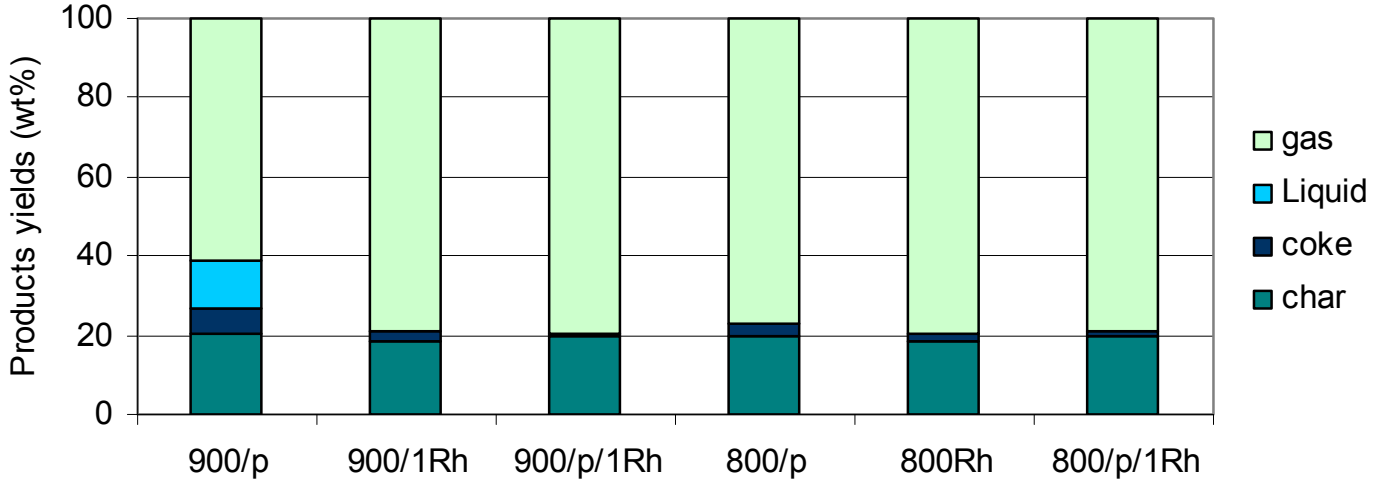

Figure 36. Normalized product yields in wt% of the dry biomass for novel catalysts (catalyst amount = 500 mg, temperature = 700°C and N_2 flow rate = 12 $Nl \cdot h^{-1}$).

The results of TPR analysis (see § III-1.2) and, then, the different reducibility of novel catalysts can provide a possible explanation of their different catalytic activities. In fact, reforming and oxidation activity as well require a good oxygen mobility in the temperature range close to that of the reaction (700°C). As a consequence, only catalysts with a sufficient oxygen availability at this temperature can promote these reactions. On the contrary, cracking reactions are favoured by a high surface acidity, as already observed for the La_2O_3/γ-Al_2O_3 (§ III-2.1). Therefore, the hardly

reducible catalysts (800/p and 900/p) fundamentally provide a good cracking activity coupled with a slight oxidation activity. On the contrary, the samples reducible at lower temperature due to the presence of easily reducible rhodium oxide alone or even of cobalt oxide (800/1Rh, 800/p/1Rh, 900/1Rh and 900/p/1Rh) promotes reforming of tars into syngas and depresses coke formation. In particular, thanks to the barrier effect provided by the cobalt-lanthanum oxide, highlighted by TPR analysis, both in the perovskite (800/p/1Rh) or spinel (900/p/1Rh) form, the rhodium was more easily reducible than when deposited directly on the alumina support. Those two catalysts were, by far, the best candidates for tar conversion.

The activity of the 800/p/1Rh catalyst has been compared to that of Ni/Al_2O_3, which was found to be the most active in biomass tar conversion among conventional catalysts (see § III-2.2). Same consideration could be reached comparing the performance of 900/p/1Rh catalyst to the performance of Ni/Al_2O_3.

The Figure 37 reports the compared solid, liquid and gaseous yields (normalized) of these two catalysts. The 800/p/1Rh catalyst was able to completely convert tars with respect to the Ni/Al_2O_3 catalyst which left 16.3 wt% of unconverted tars. Moreover, the Ni/Al_2O_3 catalyst was about 5 times more sensible to coking.

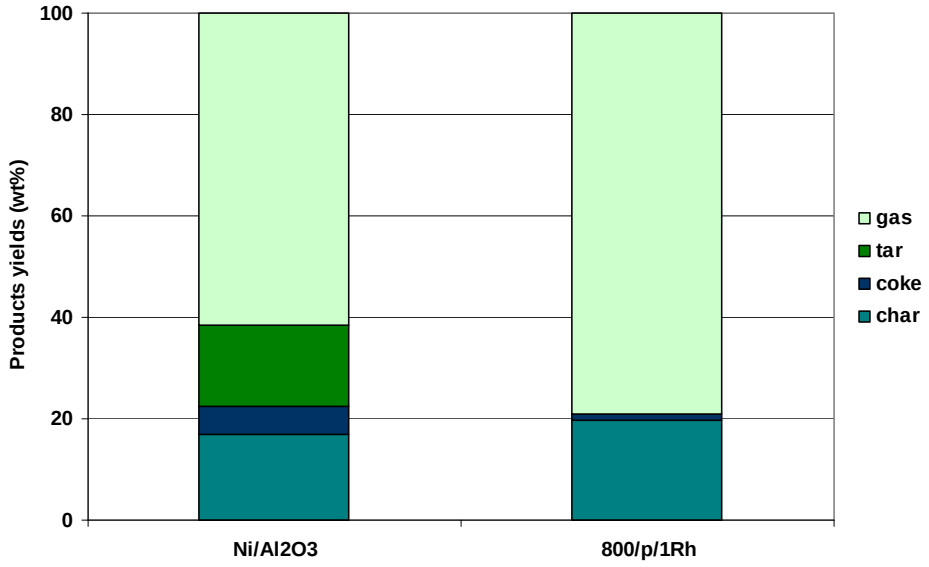

Figure 37. Normalized product yields in wt% of the dry biomass for Ni/Al_2O_3 and 800/p/1Rh catalysts (catalyst amount = 500 mg, temperature = 700°C and N_2 flow rate = 12 $Nl \cdot h^{-1}$).

Concerning the gaseous products, Figure 34 reports H_2, CO, CO_2, CH_4 and light hydrocarbons yields, highlighting that the 800/p/1Rh catalyst showed better catalytic performances than the conventional Ni/Al_2O_3 Actually, the 800/p/1Rh catalyst totally converted all light hydrocarbons, whereas the Ni/Al_2O_3 catalyst could not promote their complete conversion, and strongly reduced the methane production with respect to the Ni/Al_2O_3 sample. At the same time, the 800/p/1Rh catalyst produced more CO than Ni/Al_2O_3. Considering the fact that the H_2 concentration profiles followed those of CO in every test, (no data on H_2 for Ni/Al_2O_3), it can reasonably be said that the 800/p/1Rh catalyst provided a higher reforming activity. The 800/p/1Rh catalyst showed the least CO_2 production tendency, which can be explained by its involvement in reforming reactions. Moreover, the 800/p/1Rh sample (and not the Ni/Al_2O_3 sample) was also able to oxidize methane emitted from biomass pyrolysis in the range 350-700°C to CO_2.

The very good tar, light hydrocarbon and methane reforming activities and the poor sensibility to coking of the 800/p/1Rh catalyst make it a better candidate than the Ni/Al_2O_3 conventional catalyst, whose cracking and oxidative activities are not sufficient to completely convert these products.

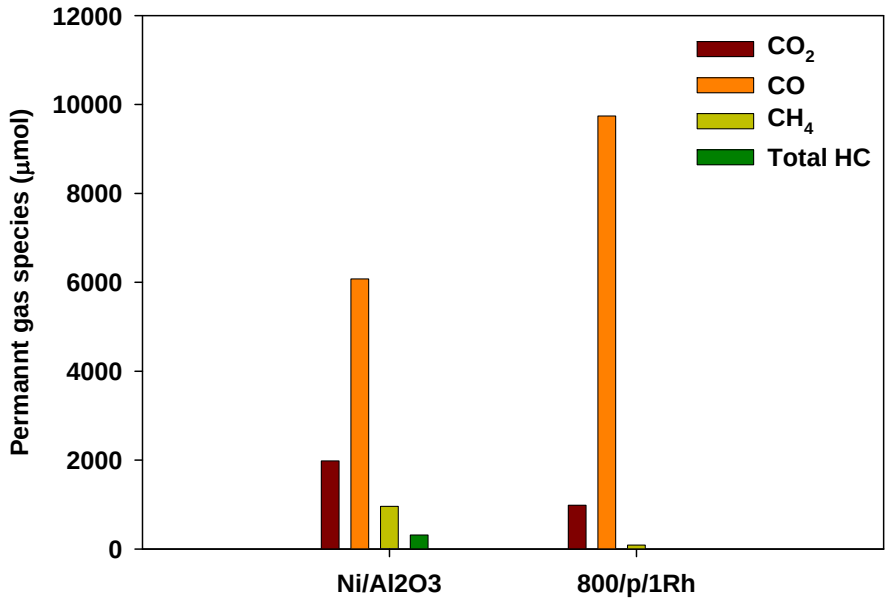

Figure 38. Compared gaseous and light hydrocarbons yields for Ni/Al_2O_3 and 800/p/1Rh catalysts (catalyst amount = 500 mg, temperature = 700°C and N_2 flow rate = 12 $Nl \cdot h^{-1}$).

In order to understand the different performances of the two synthetic catalysts, their reducibility should be considered (§ II-1.2.1). The Rh promoted catalyst showed three reduction

peaks, the two first ones at 240°C and 530°C, and the third one under the isothermal step. Concerning the Ni/Al_2O_3 catalyst, except for a smaller shoulder at 630°C, it showed a main reduction peak under the isothermal step at 800°C. Therefore, the Ni/Al_2O_3, less reducible at the temperature used for catalytic tests (700°C), fundamentally provided a good cracking activity coupled with a slight oxidation activity. On the contrary, the 800/p/1Rh sample, almost completely reduced at 700°C, promoted the conversion of tars and depressed coke formation due to the large oxygen availability.

III-2.4 Effect of rhodium load

The previous studies have shown that, under the conditions used for the screening, the catalyst calcined at 800°C and containing both 20 wt% of perovskite and 1 wt% of rhodium was one the best formulation for biomass tar conversion and syngas production. In the aim of an eventual scale-up of the process, the possible control of operative costs due to the catalyst has been also investigated. In particular, the effect of the decrease of the expensive rhodium load was studied, being the noble metal the more expensive component of the catalytic system. In particular, the rhodium load has been lowered down to 0.1 wt% in order to define the limit Rh load necessary to completely convert tar.

The values of the product yields are reported in Table 26. No tars were formed, either during the tests with 0.1, 0.5 or 1 wt% rhodium (reported here as a reference). Moreover, the gas yields were found to be very similar.

Table 26. Solid, liquid and gas yields on dry basis for catalysts with different rhodium loads (catalyst amount = 500 mg, temperature = 700°C and N_2 flow rate = 12 $Nl \cdot h^{-1}$).

Sample in the second reactor	Solid yield (wt%)		Liquid yield (wt%)	Gas yield (wt%)
	char	coke		
800/p/1Rh	18.0	1.1	0	77.6
800/p/0.5Rh	16.7	1.7	0	70.7
800/p/0.1Rh	16.8	3.6	0	73.0

The main gaseous products were once again H_2, CO, CO_2, and CH_4. The gaseous concentration profiles of 800/p/0.5Rh and 800/p/0.1Rh were very similar to those obtained for the 800/p/1Rh, already reported in Figure 33, and, since they overlapped each other, they are not reported here.

Therefore, only the yields of H_2, CO, CO_2, and CH_4, obtained from the integration of these profiles, are reported in Figure 39, as a function of rhodium load. It was highlighted the slight decrease of the reforming activity and the slight increase of the oxidation activity of the catalysts with decreasing rhodium load, confirmed by the slight decrease of CO and H_2 yields together with an increase in CO_2 production observed along with decreasing rhodium load.

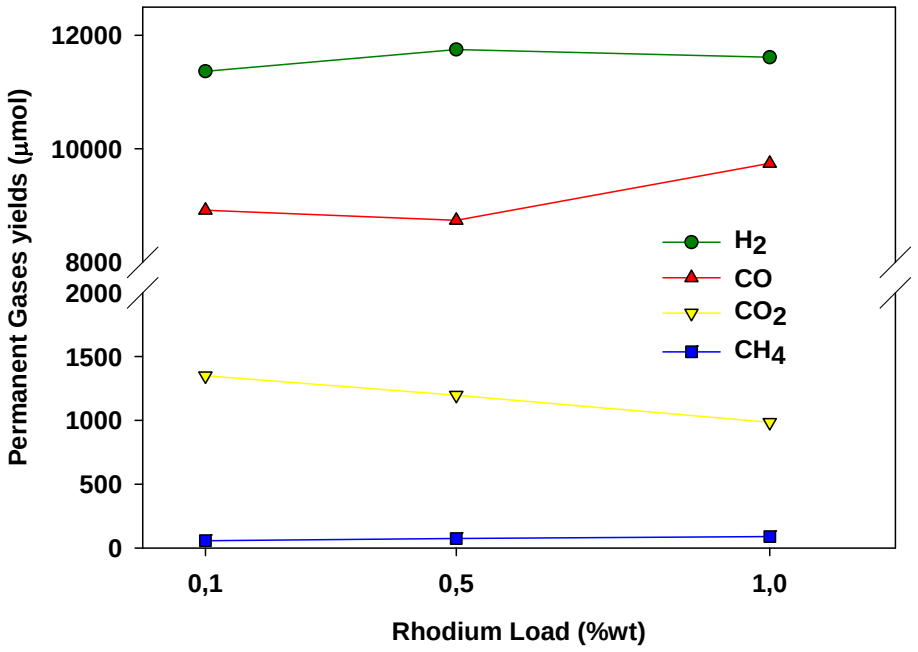

Figure 39. Compared gaseous yields for catalysts with different rhodium loads (catalyst amount = 500 mg, temperature = 700°C and N_2 flow rate = 12 Nl·h^{-1}).

No light hydrocarbons were detected with any of the catalysts. Furthermore the analysis of the isopropanol used for the cleaning of the condensation train did not show trace of tars for all catalysts, according to the fact that no tars were gravimetrically measured.

The CO_2 profiles obtained during oxidation of the coke deposited on the catalysts containing different rhodium loads are shown in Figure 40. They presented the same bi-modal peaks distribution with the main CO_2 peak at 450°C and the minor one at 650°C, due to the formation of powdered amorphous and graphitic-like carbon species, respectively.

The amount of deposited coke (already reported in the Table 26) increased with decreasing rhodium load from 1.1 wt% for the 800/p/1Rh catalyst up to 3.6 wt% for the 800/p/0.1Rh catalyst. The latter value was very close to the one obtained with the catalyst 800/p without rhodium (§ III-2.3), suggesting that the 800/p/0.1Rh had a very similar coke sensitivity to the one of the 800/p catalyst, already reported in Figure 35. Nevertheless, on the catalyst containing 0.1 wt% rhodium, a smaller amount of more hardly oxidizable coke was formed with respect to that containing only the perovskite.

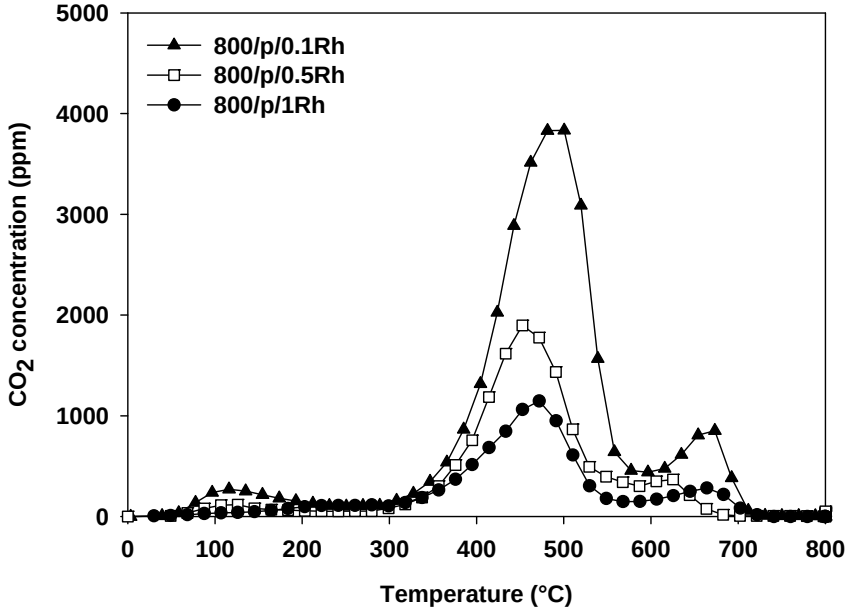

Figure 40. CO_2 profile obtained during oxidation of coke deposited on catalysts with different rhodium loads (O_2 concentration = 0.5%vol. in He and flow rate = 17 $Nl \cdot h^{-1}$).

The study of the effect of the rhodium load on the catalytic performances of the bi-functional catalyst showed that, even when the rhodium load was lowered by one order of magnitude, the catalyst was still able to convert all the tars and light hydrocarbons to syngas, even if a slight decrease of the reforming activity and an increase of coke sensibility have been observed. However, the performance of the catalyst with the lesser rhodium load was by far better than the most active conventional Ni based catalyst.

III-2.5 Effect of operation temperature

The 800/p/1Rh catalyst has been proved to be very active at 700°C (§ III-2.3). In the following study, the reaction temperature was decreased in order to find the lower temperature limit allowing the catalyst to provide the same performances as obtained at 700°C. Table 27 reports the product yields obtained during these tests.

Table 27. Solid, liquid and gas yields on dry basis for 800/p/1Rh catalyst at different operating temperature (catalyst amount = 500 mg and N_2 flow rate = 12 $Nl \cdot h^{-1}$).

Catalyst temperature	Solid yield (wt%)		Liquid yield (wt%)	Gas yield (wt%)
	char	coke		
700°C	18.0	1.1	0	77.6
650°C	17.5	2.4	0	75.5
600°C	17.0	4.9	0	77.4
550°C	17.8	5.7	4.6	65.4
500°C	17.3	7.9	9.5	68.0

The 800/p/1Rh catalyst was able to totally convert tars in gas in the range 600-700°C. A decrease of the operating temperature to 550°C and, in a greater extent, to 500°C involved a decrease in gas yield, due to a not complete conversion of tars, which reached 4.6 wt% at 550°C and 9.5 wt% at 500°C.

Concerning the evolution of the gas profiles, H_2, CO, CO_2 and CH_4 were the main detected gas products for all tests. Their concentration profiles are reported in the Figure 41. No data on H_2 production are available for the tests at 550 and 650°C. Nevertheless, these are intermediate temperatures, thus, allowing to predict a continuous decrease in hydrogen production with decreasing temperature. The gas concentration profiles qualitatively presented the similar shape with the same peaks. Nevertheless, the continuous increase in CO and H_2 yields with increasing temperature, accompanied by the continuous decrease in CO_2 and CH_4, was observed.

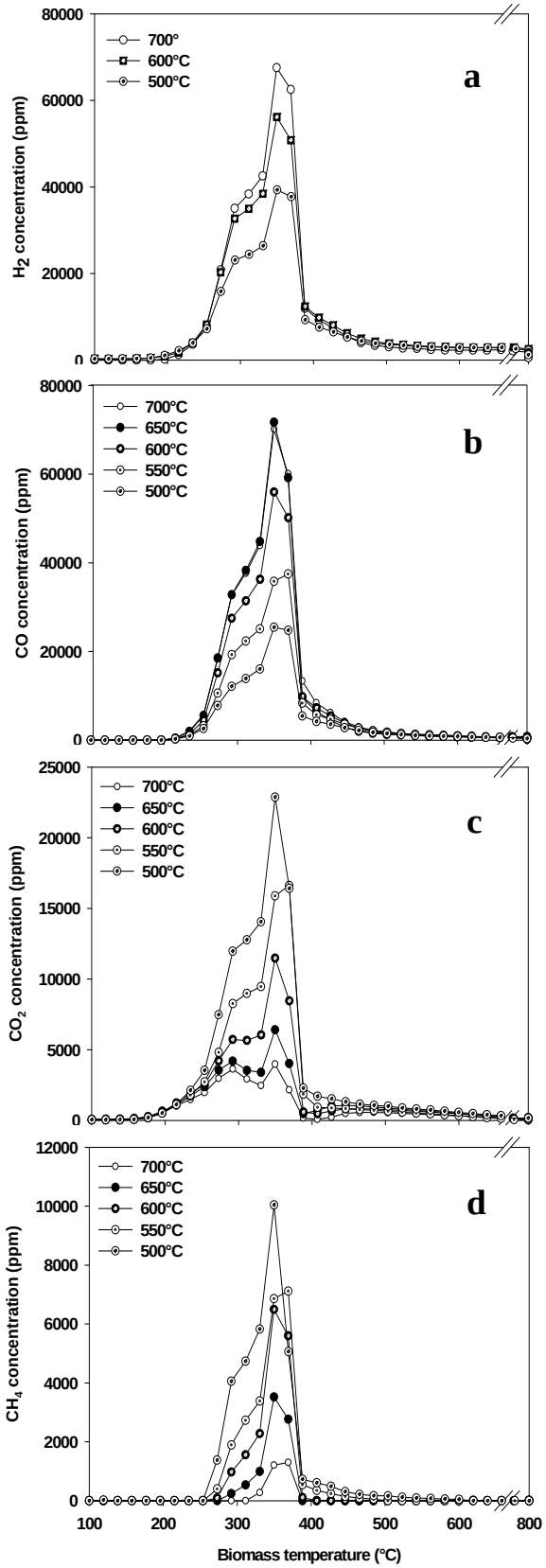

Figure 41. Micro GC thermal profiles of H_2 **(a)**, CO **(b)**, CO_2 **(c)** and CH_4 **(d)** obtained during maple wood pyrolysis with the 800/p/1Rh catalyst in the second reactor at different temperatures (catalyst amount = 500 mg and N_2 flow rate = 12 $Nl \cdot h^{-1}$).

The amounts of light hydrocarbons obtained by integration of their emission profiles are reported in Table 28. No light hydrocarbons were formed at 700°C and 650°C and a very few amount of ethylene was detected at 600°C, whereas at lower temperatures non negligible amounts of light hydrocarbons were measured.

Table 28. Light hydrocarbons (μmol) detected in the gas phase for the 800/p/1Rh catalyst operated at different temperatures (catalyst amount = 500 mg and N_2 flow rate = 12 $Nl \cdot h^{-1}$).

Catalyst temperature (°C)	C_2H_2	C_2H_4	C_2H_6	C_3H_6 /C_3H_8	nC_4	nC_5	1-pentene	1-hexene
500	2.16	1.80	0	0	0.30	2.43	3.73	2.86
550	2.90	0.71	0	0	0.30	1.01	1.78	1.58
600	0	0.15	0	0	0	0	0	0

The Figure 42 reports the H_2, CO, CO_2, CH_4 and light hydrocarbons yields obtained at different temperatures, calculated by integration of the respective gaseous profiles. The CO and H_2 yields increased, whereas the CO_2, CH_4 and light hydrocarbons yields decreased with increasing temperature. These observations are in agreement with an increase of the reforming activity of the catalyst when operated at higher temperatures. This behaviour can be explained by the fact that reforming reactions are favoured at higher temperatures.

The quantitative results of GC analysis performed on the condensate products obtained during the test at 500 and 550°C showed traces of pyrene according to the protocol CEN/TS 15439 (2006) and the broad peaks of heavier compounds at retention times of 40-50 min was still detected. The analysis of the isopropanol used for the cleaning of the condensation train for all the other temperatures did not show trace of tars, according to the fact that no tars were gravimetrically measured.

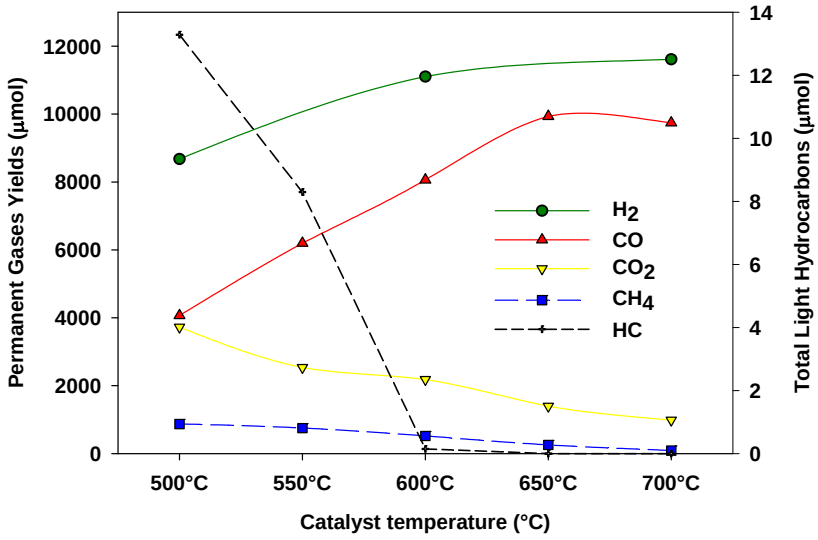

Figure 42. Compared gaseous and light hydrocarbons yields for the 800/p/1Rh catalyst operated at different temperatures (catalyst amount = 500 mg and N_2 flow rate = 12 $Nl \cdot h^{-1}$).

The CO_2 profiles obtained during oxidation of the coke deposited on the catalysts operated at different temperatures are reported in Figure 43. All the samples presented a CO_2 peak at about 450°C and only the catalysts operated in the temperature range 600-700°C were characterized by the presence of an additional CO_2 peak at about 650°C.

The amount of deposited coke, evaluated by integration of the obtained CO_2 profile, expressed in wt% on dry basis, is reported in Table 27. The coke formation increased along with decreasing temperature from 1.1 wt% at 700°C to 7.9 wt% at 500°C. This result is in line with the decrease in activity of the catalyst in tar and light hydrocarbons conversion, leading to the formation of more coke. This tends to confirm the fact that, when used at high temperatures, the oxidation capability of the material increased (the oxygen mobility in the perovskite increased, and so did the oxygen release).

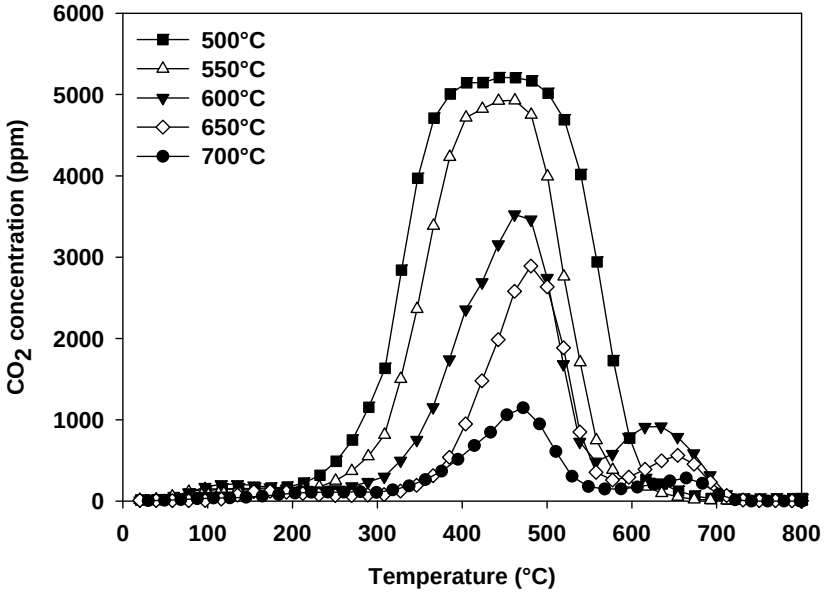

Figure 43. CO_2 profile obtained during oxidation of coke deposited on the 800/p/1Rh catalyst operated at different temperatures (O_2 concentration = 0.5%vol. in He and flow rate = 17 $Nl \cdot h^{-1}$).

The Figure 44 shows the normalized product yields of 800/p/1Rh operated isothermally in the temperature range 500-700°C. The presence of tar at temperature lower than 600°C is evidenced, as well as the continuous decrease in coke deposition with increasing temperature.

In conclusion, the 800/p/1Rh catalyst was active in tars and light hydrocarbons conversion in the temperature range 600-700°C. Nevertheless, at 600°C a slight decrease in reforming activity, highlighted by the decrease in syngas production and the increase in CO_2, and an increase in coke sensitivity were observed with respect to that obtained at 650 and 700°C. At temperatures lower than 600°C the catalyst was not able to convert all the tars and light hydrocarbons and was less able to oxidize the deposited coke. These behaviours can be explained by the fact that reforming reactions are favoured at higher temperatures.

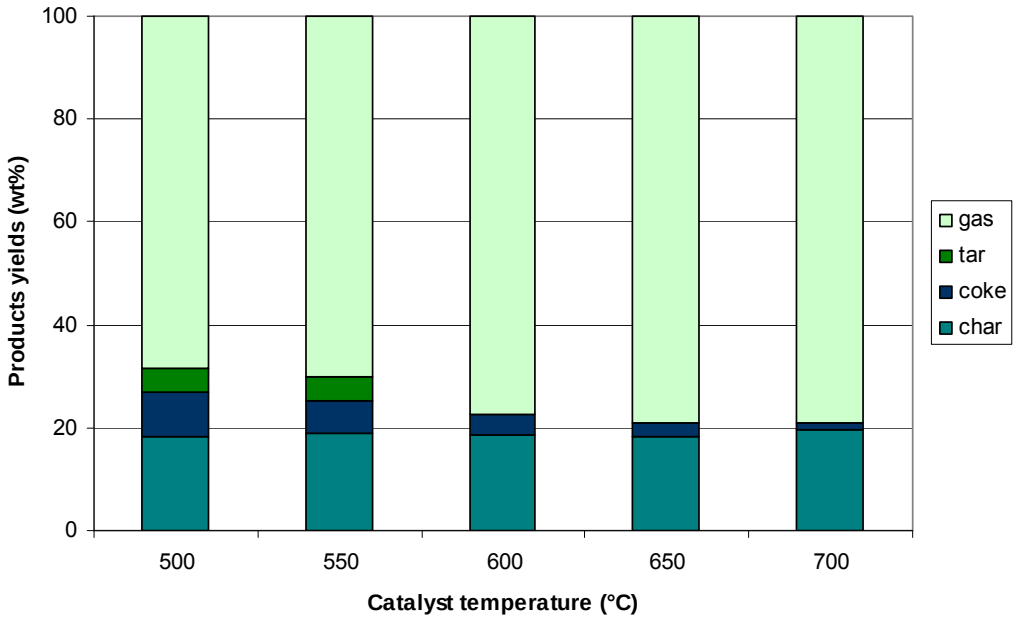

Figure 44. Normalized product yields in wt% of the dry biomass for 800/p/1Rh operated at different temperatures (catalyst amount = 500 mg and N_2 flow rate = 12 Nl·h^{-1}).

III-2.6 Effect of contact time

After the study of the effect of operating temperature, the study of the performances of the 800/p/1Rh catalyst at different contact times has been carried out. Experiments have been performed both changing the amount of catalyst inside the reactor (1, 0.5 and 0.25 g) at a constant nitrogen flow rate (12 Nl·h^{-1}) and changing the nitrogen flow rate (12, 24, 48 and 60 Nl·h^{-1}) passing through a fixed amount of catalyst (0.5 g).

III-2.6.1 Effect of catalyst amount

Table 29 reports the values of the product yields obtained by varying the amount of 800/p/1Rh catalyst inside the reactor. Note that in this section the reference test is the one with 0.5 g of catalyst, since it has been the amount used for all the tests presented in the previous sections.

Table 29. Solid, liquid and gas yields on dry basis for different amounts of 800/p/1Rh catalyst (temperature = 700°C and N_2 flow rate = 12 $Nl \cdot h^{-1}$).

Amount of catalyst in the second reactor (g)	Solid yield (wt%)		Liquid yield (wt%)	Gas yield (wt%)
	char	coke		
1	17.2	2.0	0	78.6
0.5	18.0	1.1	0	77.6
0.25	17.1	1.7	6.6	73.2

Doubling the catalyst amount from 0.5 to 1 g, and, consequently, the contact time from 0.15 to 0.3 $g \cdot s \cdot Ncm^{-3}$, had no effect on the gas yield, on conversion of tars, still absent in the products, and on the production of light hydrocarbons, also still absent in the gaseous products. On the contrary, dividing by 2 the amount of catalyst, thus decreasing the contact time from 0.15 $g \cdot s \cdot Ncm^{-3}$ to 0.075 $g \cdot s \cdot Ncm^{-3}$, led to the detection of a condensable phase (6.6 wt%) to the detriment of the gas yield (73.2 wt%) and many unconverted light hydrocarbons were detected as reported in Table 30. Varying the amount of catalyst had no significant effect on the general trends of the gaseous profiles and, for this reason, they are not reported here.

Table 30. Light hydrocarbons (μmol) detected in the gas phase for different amounts of the 800/p/1Rh catalyst (temperature = 700°C and N_2 flow rate = 12 $Nl \cdot h^{-1}$).

Amount of catalyst in the second reactor (g)	C_2H_2	C_2H_4	C_2H_6	C_3H_6 /C_3H_8	nC_4	nC_5	1-pentene	1-hexene
0.25	0	15.87	1.19	0	1.78	0.15	0.28	0

The Figure 42 reports the H_2, CO, CO_2, CH_4 and light hydrocarbons yields obtained at different temperatures, calculated by integration of the respective gaseous profiles. No differences in the permanent gas yields were measured between the tests with 0.5 and 1 g of catalyst. On the contrary, the test at lower contact time, with 0.25 g of catalyst, led to a general decrease in CO, CO_2 and H_2, accompanied by an increase in CH_4 and light hydrocarbon.

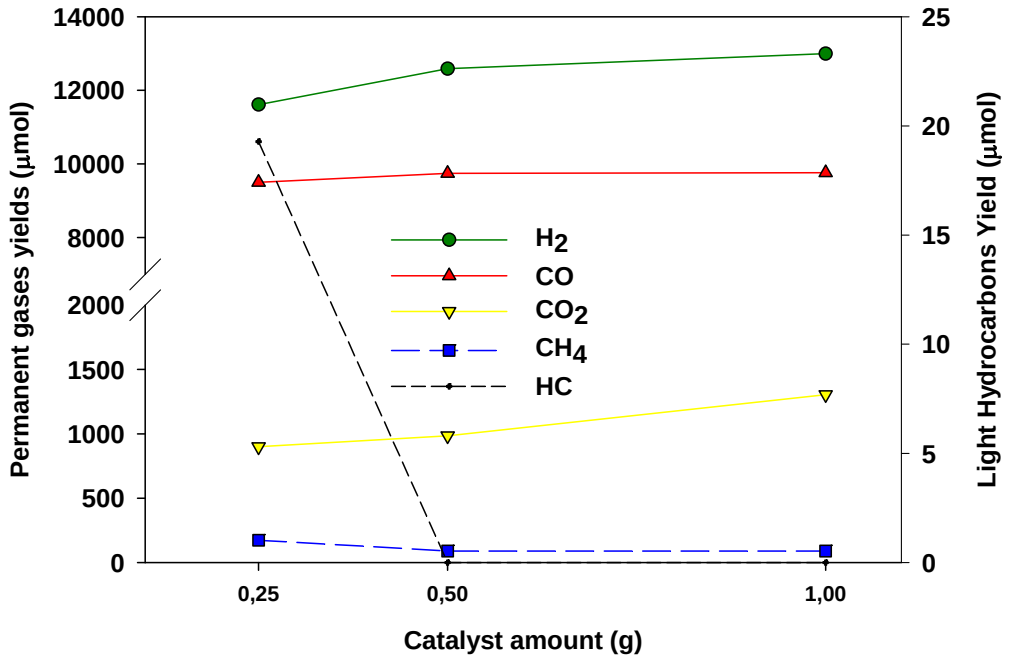

Figure 45. Compared gaseous and light hydrocarbons yields for different amounts of the 800/p/1Rh catalyst (temperature = 700°C and N_2 flow rate = 12 $Nl \cdot h^{-1}$).

The quantitative results of GC analysis performed on the condensate products obtained during the test at 0.25 g showed only traces of pyrene and naphthalene, according to the protocol CEN/TS 15439 (2006). The analysis of the isopropanol used for the cleaning of the condensation train for tests at higher contact times did not show trace of tars, according to the fact that no tars were gravimetrically measured.

The oxidation profiles of coke deposited on different amounts of the 800/p/1Rh catalyst, reported in Figure 46, showed that all the samples presented a bi-modal peaks distribution of CO_2 with the first peak at 450°C and the second at 650°C.

In Figure 47 the results obtained with different catalyst amounts have been reported all together for a better comparison. These data suggested that for the test with 0.25 g of 800/p/1Rh catalyst the corresponding contact time (0.075 $g \cdot s \cdot Ncm^{-3}$) was too low to completely convert tars and light hydrocarbons. On the other hand, the product yields distribution was very similar for the test with 0.5 and 1 g of catalyst, highlighting that under the operative conditions tested, 0.5 g of catalyst, corresponding to a contact time of (0.150 $g \cdot s \cdot Ncm^{-3}$), were enough to provide good tar conversion performances.

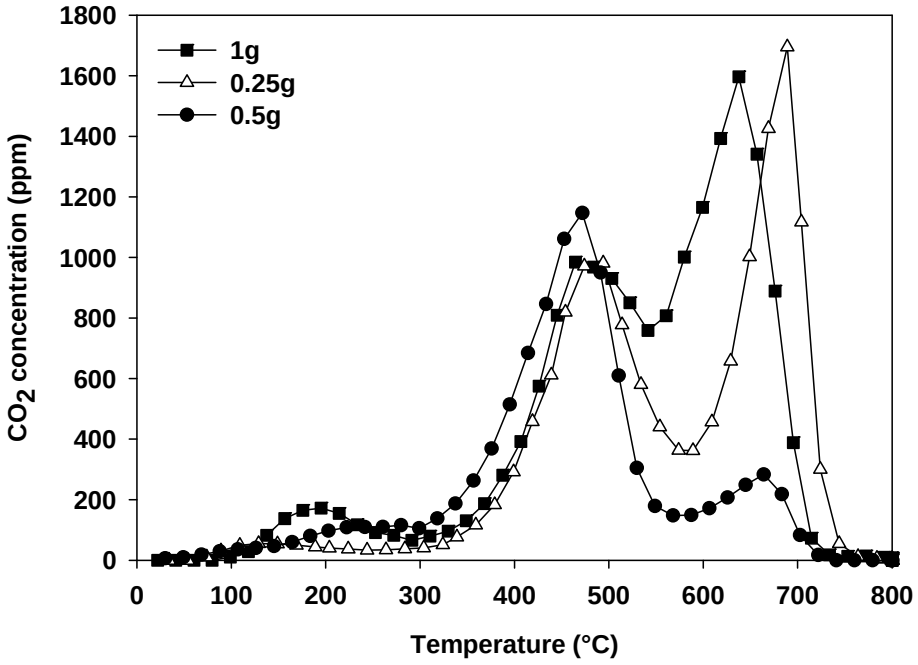

Figure 46. CO_2 profile obtained during oxidation of coke deposited on different amounts of the 800/p/1Rh catalyst (O_2 concentration = 0.5%vol. in He and flow rate = 17 Nl·h^{-1}).

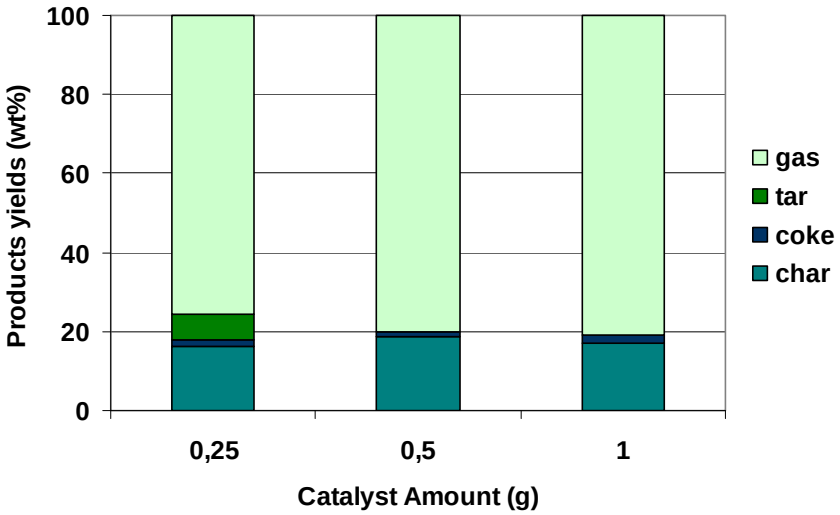

Figure 47. Normalized product yields in wt% of the dry biomass for different amounts of the 800/p/1Rh catalyst (temperature = 700°C and N_2 flow rate = 12 Nl·h^{-1}).

III-2.6.2 Effect of nitrogen flow rate

Four different flow rates were tested to modify the contact time, 12, 24, 48 and 60 $Nl \cdot h^{-1}$, with 0.5 g of catalyst operated at 700°C. The obtained product yields are reported in Table 31. Very similar gas yields were observed for all tests and no liquids were measured except at 60 $Nl \cdot h^{-1}$.

Only for the N_2 flow rate of 60 $Nl \cdot h^{-1}$ the presence of few amounts of ethylene as unconverted light hydrocarbons were detected, as reported in Table 32.

Table 31. Solid, liquid and gas yields on dry basis for 800/p/1Rh catalyst at different N_2 flow rates (catalyst amount = 0.5 g and temperature = 700°C).

N_2 flow rate ($Nl \cdot h^{-1}$)	Solid yield (wt%)		Liquid yield (wt%)	Gas yield (wt%)
	char	coke		
12	18.0	1.1	0	77.6
24	17.1	2.7	0	80.8
48	16.7	5.2	0	82.6
60	17.1	2.4	4.5	79.3

Table 32. Light hydrocarbons (μmol) detected in the gas phase for the 800/p/1Rh catalyst at different N_2 flow rates (catalyst amount = 0.5 g and temperature = 700°C).

N_2 flow rate ($Nl \cdot h^{-1}$)	C_2H_2	C_2H_4	C_2H_6	C_3H_6 /C_3H_8	nC_4	nC_5	1-pentene	1-hexene
60	0	3.25	0	0	0	0	0	0

The Figure 48 reports the values of the gas and light hydrocarbons yields obtained by varying the nitrogen flow rate from 12 $Nl \cdot h^{-1}$ (reference test) up to 60 $Nl \cdot h^{-1}$. An increase in H_2, CO and CO_2 yield, when the N_2 flow was increased from 12 to 24 $Nl \cdot h^{-1}$, has been observed probably due to an increase in mass transfer rate between gas phase and catalyst surface, which overcame the negative effect of the corresponding reduction of contact time. This observation suggested a mass transfer control of the process at 700°C. On the contrary, a further increase of the flow rate up to 60 $Nl \cdot h^{-1}$ led to an incomplete conversion of tars and light hydrocarbons, accompanied by a consequent

decrease in CO, CO_2 and H_2 yields. This can be explained by the fact that at the highest flow rate the negative effect of contact time reduction prevailed on the increased mass transfer rate.

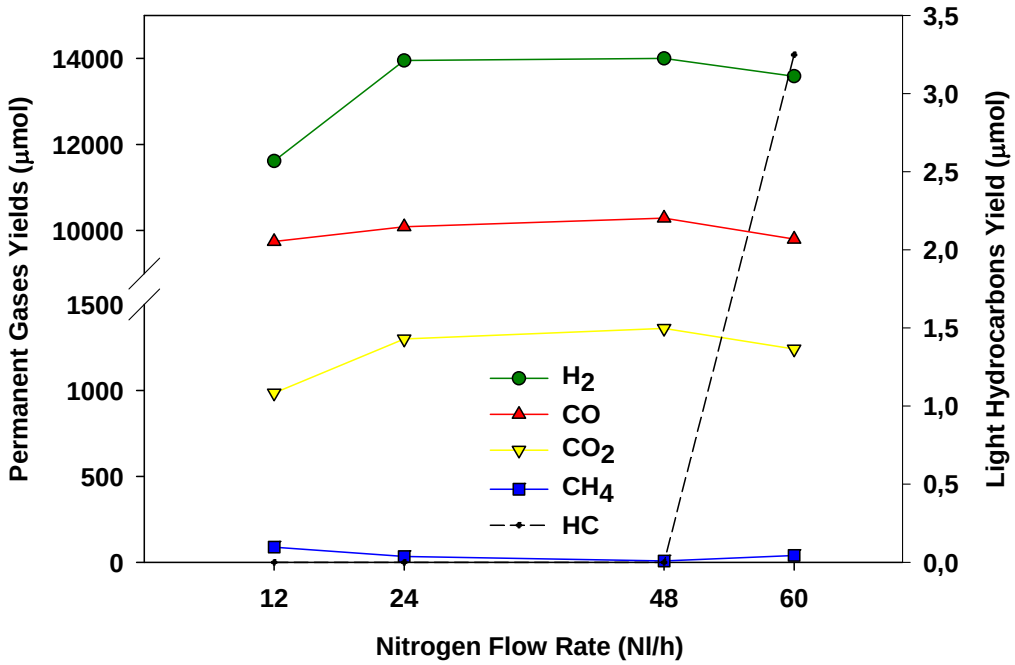

Figure 48. Compared gaseous and light hydrocarbons yields for the 800/p/1Rh catalyst different N_2 flow rates (catalyst amount = 0.5 g and temperature = 700°C).

The quantitative results of GC analysis performed on the condensate products obtained during the test at 60 $Nl \cdot h^{-1}$ showed only traces of phenanthrene and naphthalene, according to the protocol CEN/TS 15439 (2006). The analysis of the isopropanol used for the cleaning of the condensation train for tests at higher contact times did not show trace of tars, according to the fact that no tars were gravimetrically measured.

Figure 49 reports the CO_2 profiles obtained during combustion of the coke deposited on the catalysts. The CO_2 peaks followed a bi-modal distribution for all samples, with one main peak at 450°C, accounting for amorphous granular carbon species, and a minor one at 650°C, corresponding to graphitic-like carbon.

The amounts of deposited coke are reported in Table 31. When the N_2 flow was increased from 12 to 48 $Nl \cdot h^{-1}$, an increase in deposited coke was observed. A maximum in coke formation was measured at 48 $Nl \cdot h^{-1}$. On the contrary, a further increase of the flow rate up to 60 $Nl \cdot h^{-1}$ led to a decrease in coke formation. These findings confirms the observations made for gaseous products. Actually, the decrease in contact time resulted in an increase in mass transfer rate, thus increasing the coke formation on the catalyst, but when the contact time reached a too low value (at 60 $Nl \cdot h^{-1}$)

a by-pass of gaseous species through the catalytic fixed bed occurred, resulting in a lower coke deposition.

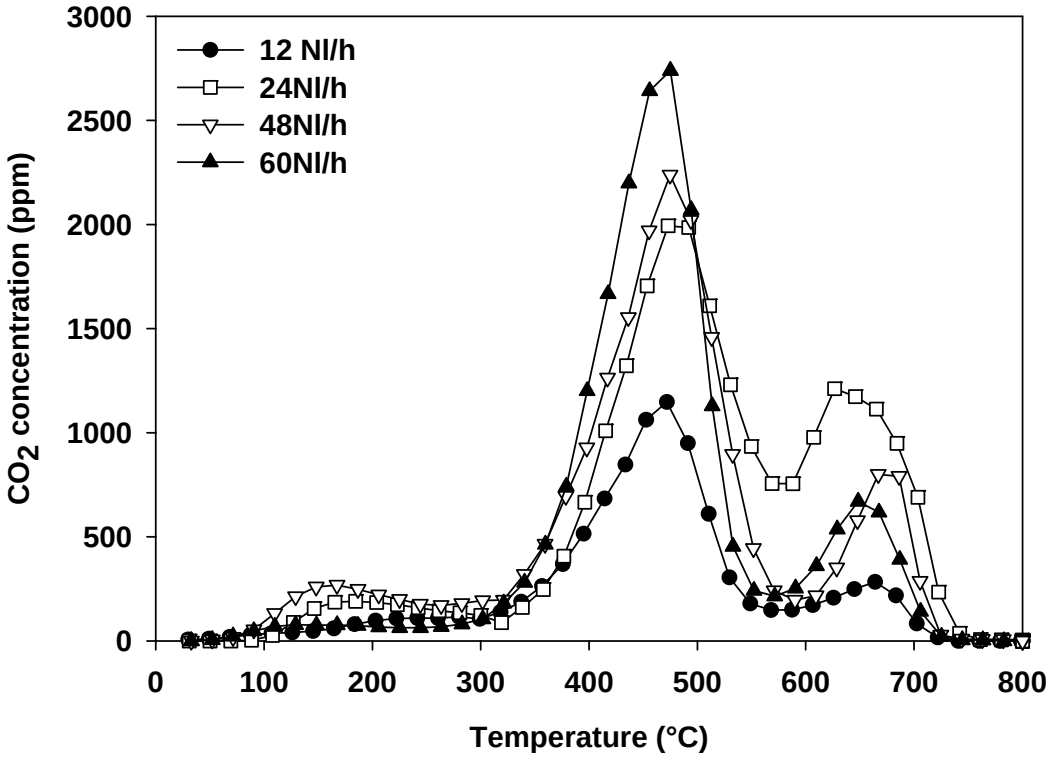

Figure 49. CO_2 profiles obtained during oxidation of coke deposited on the 800/p/1Rh catalyst for different N_2 flow rates (O_2 concentration = 0.5%vol. in He and flow rate = 17 $Nl \cdot h^{-1}$).

The summary of the results obtained at different N_2 flow rates is reported in Figure 50 as comparison of the product yields obtained under the different conditions. These data suggested that for the test of 800/p/1Rh catalyst at 60 $Nl \cdot h^{-1}$ the corresponding contact time (0.03 $g \cdot s \cdot Ncm^{-3}$) was too low to completely convert tars and light hydrocarbons. On the other hand, the product yields distribution was very similar for the test with 0.5 and 1 g of catalyst, highlighting that under the operative conditions tested, 0.5 g of catalyst, corresponding to a contact time of (0.150 $g \cdot s \cdot Ncm^{-3}$), were enough to provide good tar conversion performances.

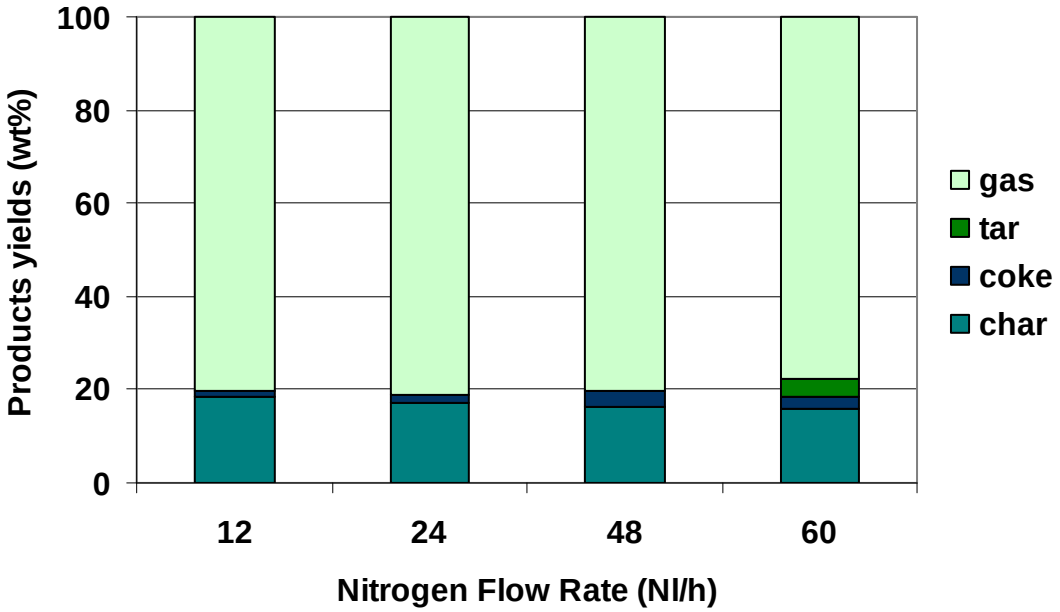

Figure 50. Normalized product yields in wt% of the dry biomass for the 800/p/1Rh catalyst for different N_2 flow rates (catalyst amount = 0.5 g and temperature = 700°C).

The effect of external diffusive limitation was highlighted by the comparison (Figure 51) of two tests carried out at the same contact time (0.075 g·s·cm^{-3}), but varying the amount of catalyst or the flow rate.

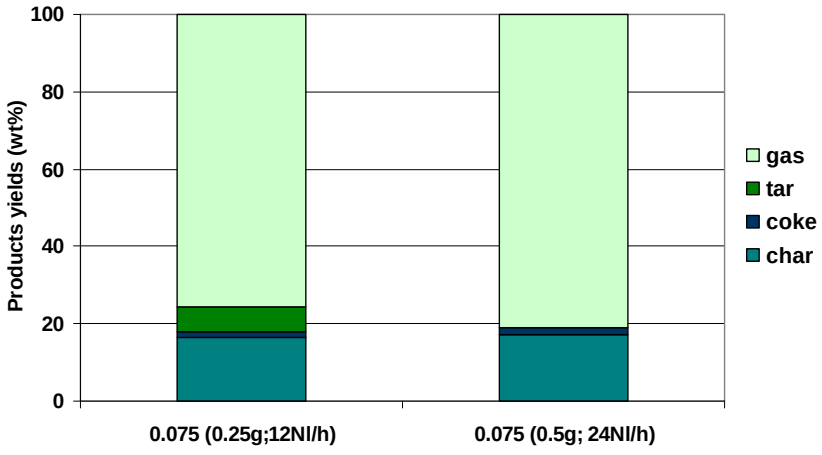

Figure 51. Normalized product yields in wt% of the dry biomass for the 800/p/1Rh catalyst operated at the same contact time (0.075 g·s·cm^{-3}) varying the catalyst amount or the N_2 flow rate.

At high flow rate and low catalyst amount, tar cannot be completely converted, whereas when increasing the N_2 flow rate to 24 $Nl \cdot h^{-1}$ and doubling the catalyst amount, neither tars nor light HC were found among the products and thus these can be related to diffusion limitation occurring at low flow rate.

III-3 Fluidized bed gasifier

III-3.1 Effect of bed material

Many different experiments have been carried out in the biomass fluidized bed gasifier in order to stabilize the experimental procedure. After this, tests with constant steam-to-biomass ratio (Ψ), equivalent ratio Φ (= the actual air-fuel ratio/the air-fuel ratio for complete combustion) and bed temperature have been carried out using different bed materials: sand, dolomite, olivine and Ni/Al_2O_3. The operative parameters are shown in Table 33.

Table 33. Operative conditions, spruce-wood pellet

Pressure, kPa	101
Bed height, m	0.18-0.30
Bed temperature, °C	780
Fluidization velocity, m/s	0.3
Equivalence ratio, -	0.17
Steam/fuel ratio, -	0.65

The fluidization velocity at the reaction temperature (780°C) was 0.3 $m \cdot s^{-1}$ in all experiments, which corresponds to 37 times the U_{mf} evaluated for the Ni/Al_2O_3 catalyst which has the lower U_{mf} and 8 times the one of the olivine which has the higher U_{mf} (the other materials have U_{mf} in this range). Thus, allowing to have in all cases a well developed bubbling fluidization regime and to operate at a value of gas velocity lower than the terminal velocity (U_t) of the Ni/Al_2O_3 as it is possible to see from the data reported in the § III-1.2.2.

The Figure 52 shows the results of the gas analysis performed during the experiment with the sand bed as an example. In this case CO_2, CO and methane concentrations were stable after about few minutes, the hydrogen concentration required a longer stabilisation time (about 30 minutes).

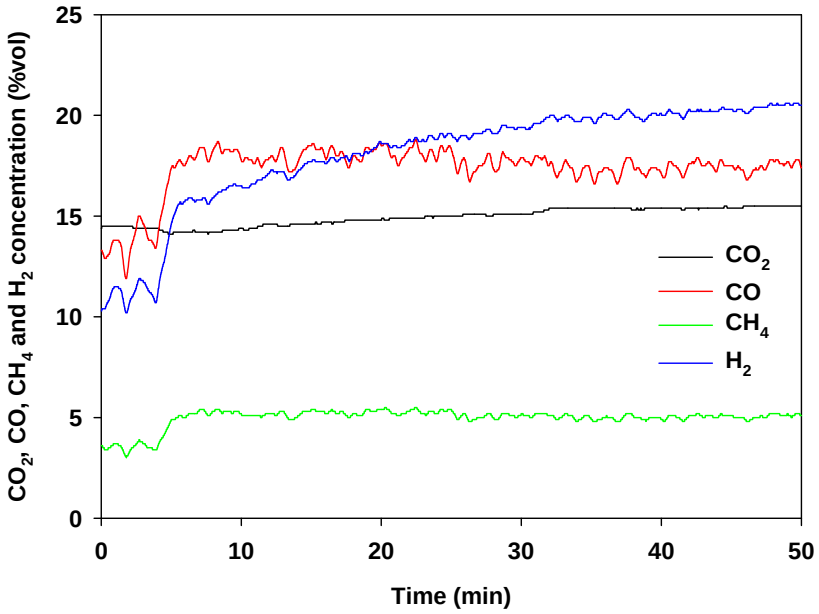

Figure 52. Evolution of CO_2, CO, CH_4 and H_2 profiles. Sand bed (T = 780°C, Φ =0.17, Ψ = 0.65, U= 0.3 m/s)

As soon as the stationary regime was reached, in addition to gas analysis, the sampling of the gas, solid and tar in the producer gas was started. The average concentrations of gas species obtained using the four different materials, are reported in Figure 53 and Table 34.

A stable activity of the Ni/Al_2O_3 catalyst has been observed for the whole duration of the reaction tests, up to 120 minutes, suggesting that no deactivation phenomena occurred, due to coke deposition or morphological modifications. The value of the surface area of the used sample measured by BET analysis is the same of that obtained for the fresh catalyst (156 $m^2 \cdot g^{-1}$). This result indicates that no particle sintering or nickel migration and agglomeration along the alumina surface may occur, under reaction conditions. Furthermore, for a sample of catalyst taken during a gasification test, the elemental analysis highlights the deposition of small amounts of coke on the catalyst surface, less than 1%. These good features can be ascribed to the strong interaction between nickel and support, as confirmed by TPR analysis showing the presence of nickel aluminate phase, which limit the nickel sintering and coking in agreement with finding reported by Pfeifer and Hofbauer (2008).

Table 34. Composition of dry gas, tar concentration, carbon load (ζ_c) and water conversion (X_w) obtained during the biomass gasification tests with different bed materials (T = 780°C, Φ =0.17, Ψ = 0.65, U= 0.3 m/s).

	Sand	Olivine	Dolomite	Ni/Al_2O_3
CO_2 (%)	16.40	16.90	17.70	14.50
CO (%)	15.20	13.80	11.70	16.70
H_2 (%)	20.20	20.30	22.80	28.70
CH_4 (%)	4.70	4.40	4.10	2.02
C_2H_4 (%)	1.25	0.15	0.04	0.02
C_2H_6 (%)	0.11	0.11	-	-
TAR_I (g/m^3_n)	14.60	10.5	8.90	8.40
TAR_{II} (g/m^3_n)	4.60	2.70	2.50	0.60
ζ_c (kg/kg)	0.21	0.33	0.30	0.38
X_w (kg/kg)	0.31	0.43	0.43	0.57

The inert bed of sand is assumed as reference case for the other tests; as expected, it gives the worst performance in term of syngas quality (e.g. H_2/CO =1.33).

The use of olivine slightly improves the hydrogen content in the syngas and significantly contributes to tar conversion in lighter hydrocarbons, both effects being emphasized with dolomite as bed material. The catalyst exerts the largest role in improving the gasification performance: the H_2 molar fraction reached the largest value and a H_2/CO ratio of 1.72.

Furthermore, the comparison of the gas concentrations reached with different bed materials (Figure 53) shows that the hydrocarbon steam reforming reactions (CH_4 and C_2H_4) are largely accelerated by the presence of the catalyst, whereas the dolomite mainly enhances the reaction path of the water gas shift reaction, by increasing H_2 and CO_2 level in the syngas. More specifically, the methane concentration followed a decreasing trend from sand to olivine and finally Ni/Al_2O_3. Whereas CO was present in lower amounts in the producer gas in presence of olivine and dolomite and in higher concentrations using Ni/Al_2O_3.

The water conversion (X_w) is referred to the total amount of water entering the gasifier. The values for each test are reported in Table 34. In all tests, the water conversion value is far from 1, in agreement with a large excess of steam used in the test. The higher X_w value has been reported for the Ni/Al_2O_3 catalyst, in agreement with the occurrence of steam reforming reaction.

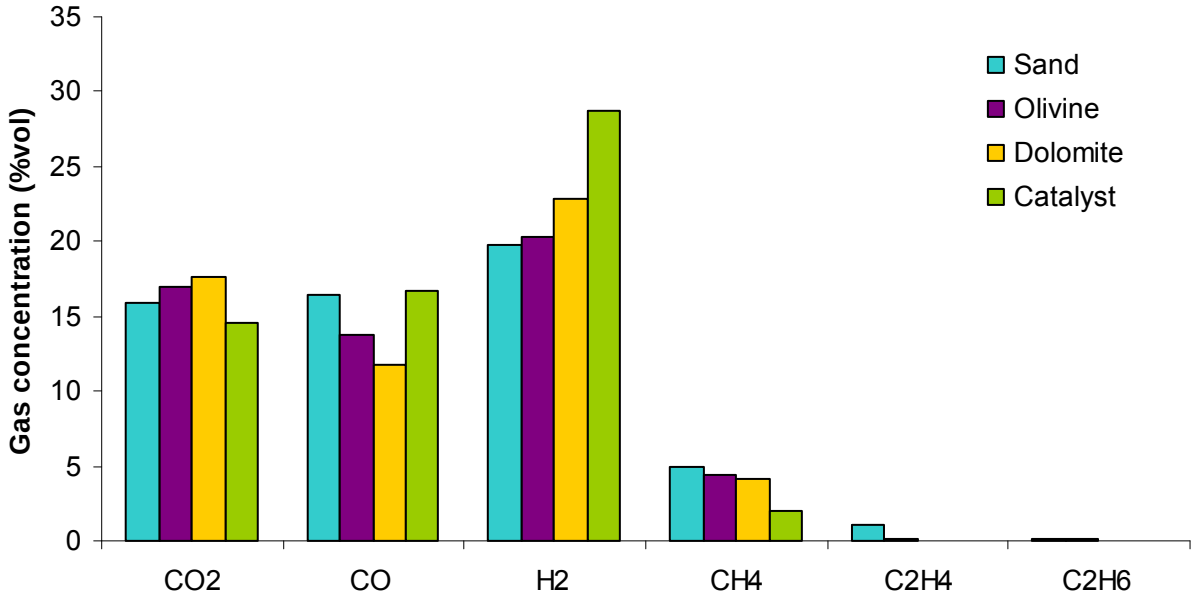

Figure 53. Compared gaseous product distribution of the gasification tests (T = 780°C, Φ =0.17, Ψ = 0.65, U= 0.3 m/s).

The tar concentration in the syngas evaluated on the basis of both condensation steps (i.e. at room temperature and at -10°C) is reported in Figure 54. It is worth to note that the concentration of light tar (TAR II) is always significantly lower than that of heavy tar (TAR I). With respect to the test with sand, when the olivine bed was used, the amount of tar was only slightly reduced, while a more marked effect is observed using dolomite. A tar reduction up to 50% was observed in presence of the Ni/Al_2O_3 catalyst, which gave rise to the lowest tar level. The measured values are in agreement with the data reported by Gil et al. (1999) obtained under rather similar gasification conditions in inert bed with a gasification ratio [(H_2O+O_2)/Biomass] = 0.90 and H_2O/O_2 = 3, instead of 0.8 and 2.3 used in this work.

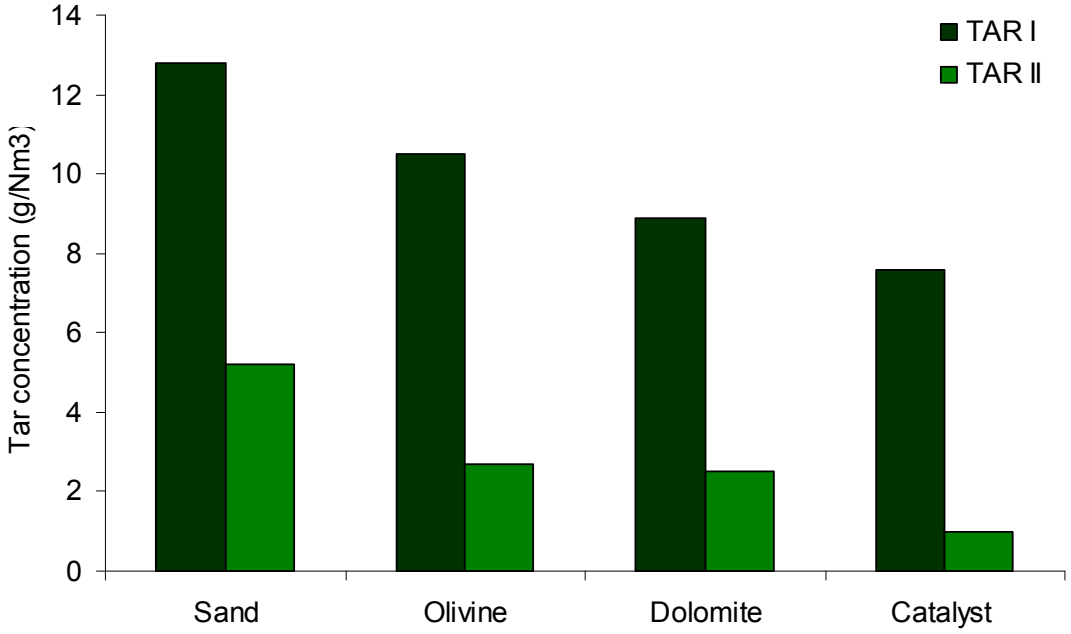

Figure 54. Tar I and Tar II concentrations obtained during the catalytic campaign (T = 780°C, Φ =0.17, Ψ = 0.65, U= 0.3 m/s).

Figure 55 reports the chromatograms obtained by GC analysis of the tar. It is worth noting that different Y-scales have been used in the four panels, 800 pA for sand and olivine and 140 pA for dolomite and Ni/Al_2O_3. In agreement with a higher sample dilution due to the lower amounts of collected tars in the latter samples. A progressive reduction of the number of chemical species detected in the tar can be noted, following the order sand<olivine<dolomite<Ni/Al_2O_3.

The produced tar was a very complex mixture where a large number of different species could be detected. Using sand and dolomite as bed material, the more abundant products were napthalene, acenaphthylene, fluorene, phenanthrene, fluranthene, indene and pyrene. This result is in agreement with that reported by Pfeifer et al. (2004), using a bed of olivine and similar steam/biomass ratio in the temperature range 750-900°C. The tar nature was also affected by the presence of the Ni/Al_2O_3 catalyst. In particular, no hydrocarbons with five rings were present because they were probably converted to hydrocarbons with three or four rings, while hydrocarbons with a single or double ring, such as phenol and indene, were completely reformed.

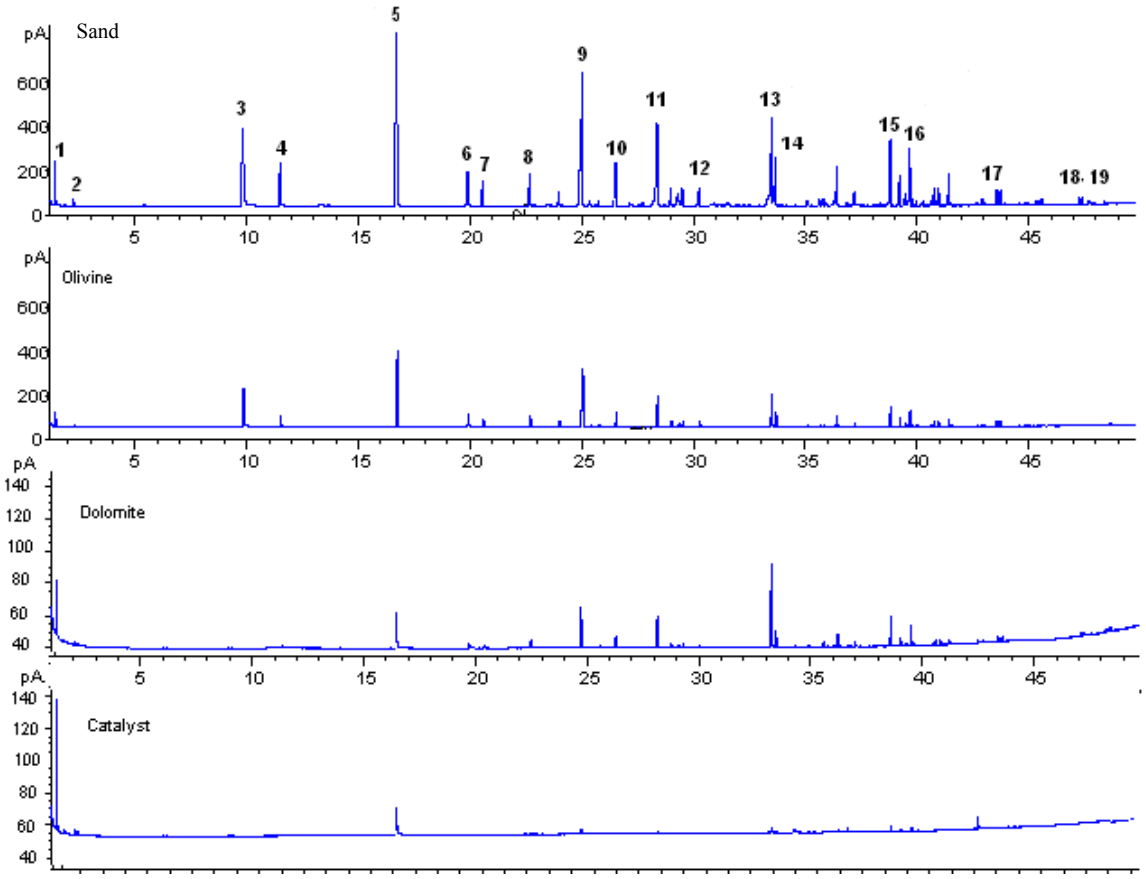

1. Benzene
2. Toluene
3. Phenol
4. Indene
5. Naphthalene
6. 2-Methilnaphthalene
7. 1-Methilnaphthalene
8. 2,4,5 Trichlorophenol
9. Acenaphthylene
10. Acenaphthene
11. Fluorene
12. 4,6 Dinitro-o-Cresol
13. Phenantrene
14. Anthracene
15. Fluoranthene
16. Pyrene
17. Benzo-(a)-Anthracene
18. Benzo-(b)-Fluranthene
19. Benzo-(a)-Pyrene

Figure 55. GC profiles and compounds identification of the tars obtained using catalysts. (T = 780°C, Φ =0.17, Ψ = 0.65, U= 0.3 m/s)

Table 36 reports the measured amounts of particulate found in the hot ceramic filter and in the cyclone. Limited generation and in turn elutriation of fine particles, evaluated by weighing the solid collected at both the cyclone and filter respectively, have been observed using sand and olivine as bed materials.

Table 36. Particulate present in the producer gas (T = 780°C, Φ =0.17, Ψ = 0.65, U= 0.3 m/s).

	Sand	Olivine	Ni/Al_2O_3
Hot filter ($g \cdot h^{-1}$)	3.12	1.6	28.0
Cyclone ($g \cdot h^{-1}$)	26.6	58.9	152.1

More in detail, the dimensionless elutriation rates evaluated with respect to dry fuel feeding rate are $6.3 \cdot 10^{-3}$ and $1.1 \cdot 10^{-2}$ for sand and olivine, respectively. The elutriated particles are predominantly composed by residual char, as confirmed by the elemental analysis showing that the carbon content is 75% and hydrogen 1.5% by weight. This result confirms the high mechanical resistance reported for both sand and olivine (Rapagnà, 2000). Higher elutriation rates, evaluated by a mass balance on the bed material before and after the gasification test, have been obtained for both dolomite and catalyst: $1.3 \cdot 10^{-1}$ and $3.7 \cdot 10^{-2}$ respectively. The larger elutriation rate of dolomite with respect to the catalyst is congruent with a significantly higher attrition constant, denoting a better mechanical resistance and suitability for fluidized bed process of the catalyst.

It is worth to note that the U/U_{mf} ratio adopted in the gasification tests for Ni/Al_2O_3 is largely higher than that of other materials. Since the attrition and elutriation rates are strongly enhanced by increasing U/U_{mf} ratio, a larger elutriation rate could be expected. Congruently, the samples collected at the filter and cyclone for the Ni/Al_2O_3 catalyst have a lower carbon content, less than 10% by weight.

III-3.2 Effect of bed height

The influence of the bed height i.e. on the contact time between biomass and the bed particles has been evaluated using Ni/Al_2O_3 and sand by doubling the bed height unchanging the operating variables (Table 33). Two bed heights have been adopted for sand and catalyst, namely 0.18 m and 0.30 m (the latter is noted: “I” in the following).

From the comparison of tests with different bed height reported in Table 35 and Figure 56 it appears that the bed height, in the range explored, has a marginal influence on the gas composition, the largest effect being appreciable for H_2 concentration that only increases of around 1% with the taller bed of Ni/Al_2O_3 catalyst.

Table 35. Gaseous and tar concentrations measured at different bed heights of Sand and Ni/Al_2O_3 (T = 780°C, Φ =0.17, Ψ = 0.65, U= 0.3 m/s).

	Sand	Sand (I)	Ni/Al_2O_3	Ni/Al_2O_3 (I)
CO_2 (%)	16.40	15.90	14.50	14.30
CO (%)	15.20	16.40	16.70	17.60
H_2 (%)	20.20	19.80	28.70	30.30
CH_4 (%)	4.70	4.90	2.02	1.49
C_2H_4 (%)	1.25	1.11	0.02	0.02
C_2H_6 (%)	0.11	0.11	-	-
TAR_I (g/m^3_n)	14.60	12.80	8.40	7.60
TAR_{II} (g/m^3_n)	4.60	5.20	0.60	1.00

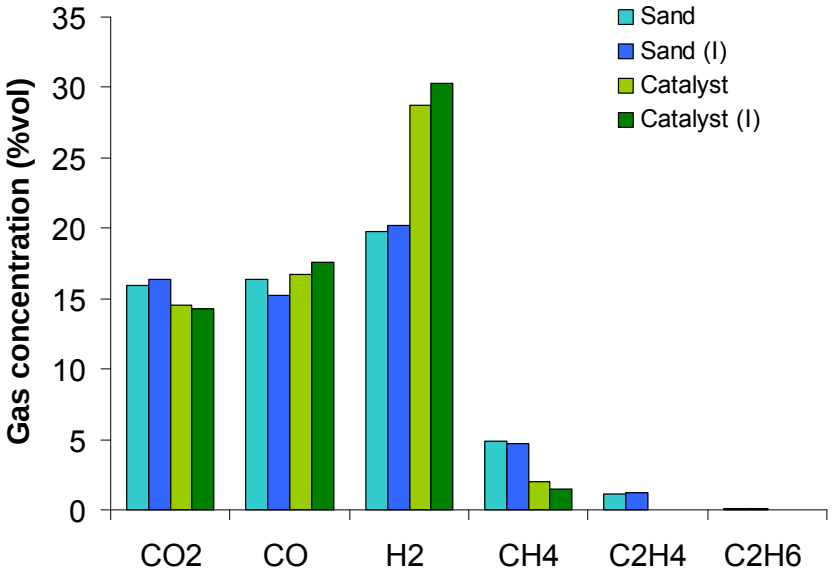

Figure 56. Influence of bed height on gaseous product distribution.
(T = 780°C, Φ =0.17, Ψ = 0.65, U= 0.3 m/s)

Furthermore, the increase in bed height did not significantly improve the tar conversion activity, as evidenced in Figure 57. This observation is valid both for tar I and tar II.

This result indicates that the residence time of the gas in the bed and the amount of catalyst are high enough, even for the shallow bed, but bed bypass phenomena may occur.

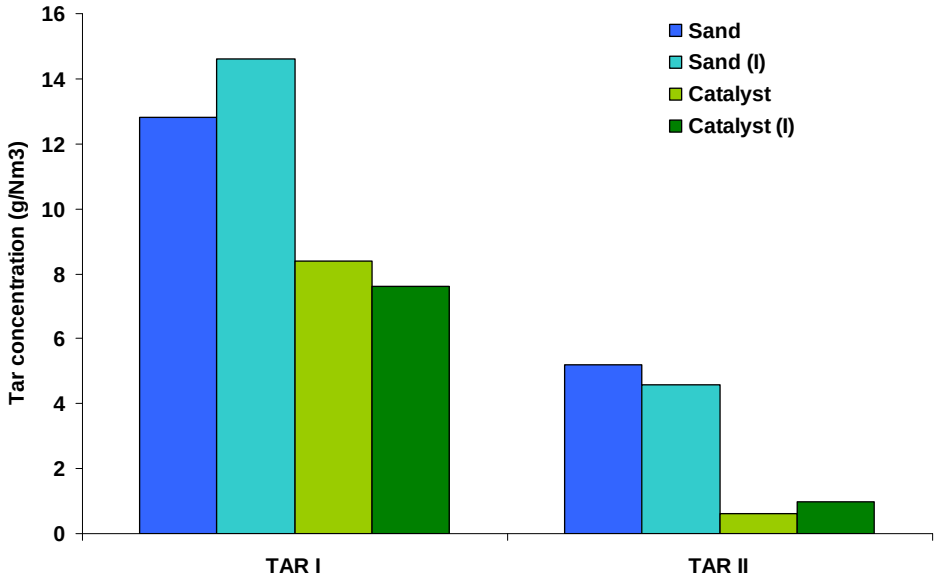

Figure 57. Influence of bed height on tar I and tar II production.

(T = 780°C, Φ =0.17, Ψ = 0.65, U= 0.3 m/s)

IV-CONCLUSIONS

The proposed innovative catalytic system developed in this work is an alumina-supported lanthanum-cobalt perovskite (20 wt%) promoted with rhodium (0.1 to 1 wt%). The activity measurements were performed in a double fixed bed plant developed specifically to perform catalytic screening tests at laboratory scale. This set up allowed to study the reforming, oxidation and cracking activity towards tar reforming by contacting the catalysts with a real mixture of biomass devolatilization products.

The novel catalyst demonstrated much better tar conversion activity and an increased syngas quality than the conventional catalysts of biomass gasification i.e. Ni/Al_2O_3, dolomite and olivine tested in the same dual fixed bed plant.

The performances of the novel catalytic formulation has been studied by modifying parameters such as the rhodium content, the calcination temperature and the contact time. It was found that the novel catalyst was able to completely convert tars and light hydrocarbons contained in the biomass devolatilization products, but also to significantly increase the H_2/CO ratio. Moreover, the catalyst had limited sensitivity to coke deactivation.

These good results were correlated to the rhodium reforming activity, enhanced by the deposition on the perovskite material. The rhodium content on the catalyst could be significantly reduced from 1 wt% to 0.1 wt% with no significant decrease in tar conversion activity. Moreover, although the unfavourable conditions used (complete absence of oxidant in the gas phase), the process temperature could be decreased to 600°C with still good catalytic activity in tar conversion. Finally, it was showed that in the absence of diffusion limitations, the contact time can be halved, keeping the same performances, thus determining the minimum amount of catalyst necessary to completely convert tars.

To perform activity tests in fluidized bed conditions, a pilot scale steam fluidized bed gasifier has been developed. Catalytic activity tests were carried out in the biomass fluidized bed gasifier using traditional primary catalysts: dolomite, olivine and a Ni/Al_2O_3 catalyst. Among these materials, the Ni/Al_2O_3 had the best tar conversion activity and the higher H_2/CO ratio.

The results obtained in the fluidized bed gasifier showed that the activity in biomass tar conversion of conventional catalysts followed the same trend in terms of activity in the fluidized bed gasifier and in the fixed bed screening plant.

The whole experimental results here above discussed allows to expect that the proposed catalyst is a good candidate to explore for its catalytic activity in the fluidized bed biomass gasifier.

The study of this catalyst in real conditions of biomass steam gasification in the pilot scale fluidized bed will be performed in future work. This will involve the use of a more mechanically resistant support (likely a harder γ-alumina), able to strengthen the catalyst and thus resist the high attrition rates occurring in fluidized beds. The scale up of the synthesis process to produce catalyst in the kilo-range will also be the object of particular attention.

Another feature of catalytic biomass gasification is the sensitivity of the catalyst to poisons like chlorine, sulfur or ammonia. The resistance of the novel catalyst to these elements could be the other crucial aspect to investigate in the future.

ANNEXES

In fluidized bed technology applied to biomass conversion, the physical segregation of biomass and volatiles, due to the difference of density between the fuel and the bed material and to the formation of endogenous volatiles bubbles is a critical feature. These segregation phenomena results in an inefficient contact of solid and gaseous fuel (product of devolatilization) with the catalytic bed material and consequent incomplete conversion of the fuel. In order to maximize the contact between formed species and the catalytic surface, different solutions have been studied. Two approaches can be used to solve this problem: modification of the bed inventory or modification of the reactor configuration.

The individuation of a support with a density as close as possible to that typical of the biomass (500-1000 $kg \cdot m^{-3}$) and its physical, chemical and mechanical characterization constituted a preliminary part of the experimental research activity. The relative results are reported in the Annex A.

The use of a conical distributor was able to increase the circulation of the materials inside the bed, thus, limiting the segregation phenomena. The visual observation of the mixing efficiency achieved in this reactor configuration has been performed in a Plexiglas reactor. The relative results are reported in the Annex B.

Annex A

A preliminary study was performed in order to find a low density material to be used as catalyst support to avoid biomass segregation which was able to resist to the operative conditions typical of biomass gasification in fluidized bed. Hollow cenospheres (Fillite 300A provided by Trelleborg Italia), generated from coal-fired thermal power plants and basically consisting in alumino-silicates, may limit the segregation phenomena due to the inner cavity which reduces the intrinsic material density to values close to that typical of biomass. For this reason, they were thought to be a good candidate as catalytic support for use in fluidized bed. The properties of this material, given by are reported in Table A1.

Table A1. Properties of cenospheres (Fillite 300A)	
Particles size distribution	5-355 microns
Average wall thickness	5-10 % of sphere diameter
Average particle density	700-900 $kg \cdot m^{-3}$
Average bulk density	400-480 $kg \cdot m^{-3}$
Packing factor	60-65 %
Melting temperature	1400°C
Shell hardness	Mohs scale 6
Crush strength	140-280 $kg \cdot cm^{-2}$
Filling gas	70% CO_2, 30 % N_2

In order to avoid cohesive comportment, we first sieved the former material to obtain a range of 125-212 microns. The morphology of the material was investigated with a Philips XL30 SEM equipped with a EDAX instrument. The pictures are reported in Figure A1.a and b.

The particles are quite spherical with bubbles inclusions in the shell. They are mainly constituted of Si and Al oxides with some traces elements as Fe, Na, Ti, Ca and K (Table A2). The Sauter diameter of the microspheres (particle size size range 125-212 μm) is 146.5 μm (Figure A1-c).

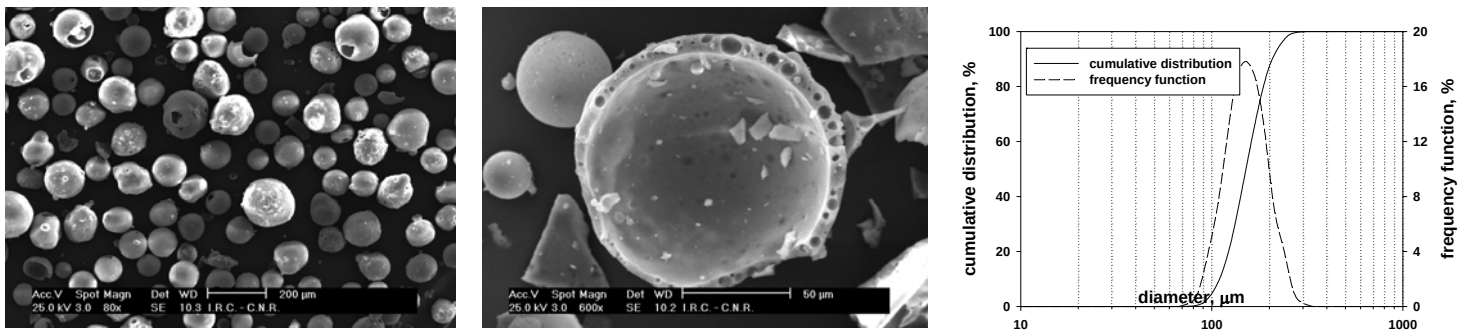

a) **b)** **c)**

Figure A1. a) SEM image of cenospheres (particle size 125-212 μm), **b)** SEM image of inner surface and shell of one sphere, **c)** Size distribution.

Table A2. EDX analysis of cenospheres on the external surface of a sphere.							
Elements	Na	Al	Si	K	Ca	Ti	Fe
weight percent	1.04	33.25	59.51	0.98	0.39	3.25	1.58

The X-Ray diffraction pattern of grinded cenospheres clearly shows the amorphous quartz and crystalline mullite parts of the material (Figure A2).

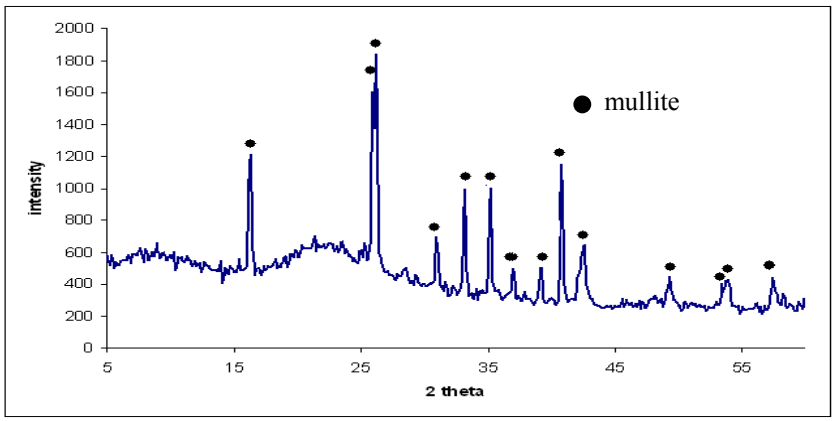

Figure A2. X-Ray pattern of the cenospheres.

As the use in fluidized bed for biomass gasification was the aim of the present research, a critical point was to determine the fluidization properties of the cenospheres. The material in the selected range is a "class A" material according to Geldart classification.

Fluidization tests were performed in the stainless steel cylindrical reactor (diameter = 1" and 400 mm high), described in § II.1.2.

A fluidization test at ambient temperature followed by another at 800°C confirmed the ability to fluidize of the micro spheres. Pressure drops versus superficial gas velocity have been measured in experiments carried out at 25°C and 800°C (Figure A3). Experimental data have been worked out to obtain the experimental values of the minimum fluidization velocities (U_{mf}) found to be 0.6 $cm \cdot s^{-1}$ at 800°C and 0.8 $cm \cdot s^{-1}$ at 25°C.

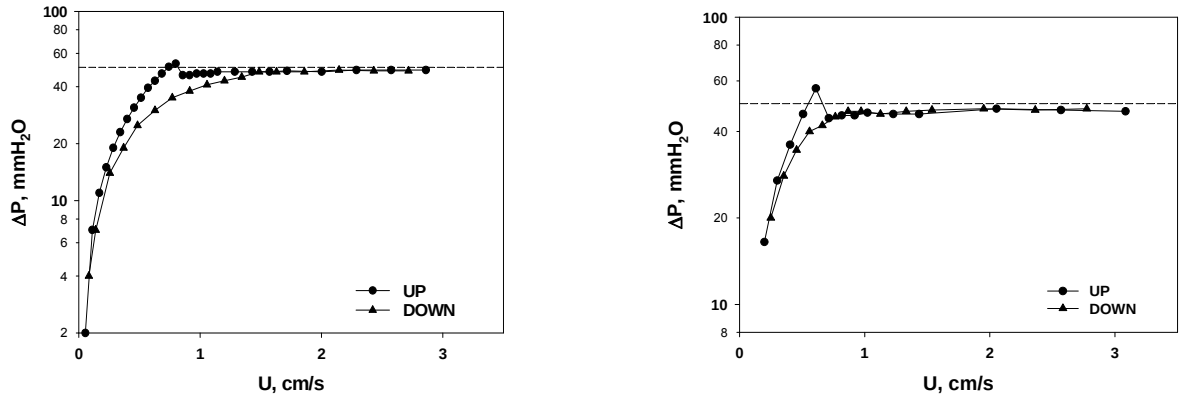

Figure A3. Fluidization curves of cenospheres material in the size range 125-212 µm. Right at 25°C, Left at 800°C. UP = increasing superficial velocity, DOWN = decreasing superficial velocity.

To verify the resistance of cenospheres to attrition in operating conditions, we performed an ad-hoc test at 800°C and U=10 cm·s^{-1} (more than ten times the U_{mf} at this temperature but far below the velocity at which the bed is carried away). Such a measurement was carried out in the reactor reported in § II.1.2.

Figure A4 shows the curve of attrited fines of cenospheres (125-212 μm) under non reactive conditions. It is possible to note that after the initial peeling off of the particle asperities, a steady state condition is approached with a relatively low value of E = 2 to 3 mg·min^{-1}. Granulometric analysis have also been performed on samples after fluidization tests at 25°C or 800°C and after attrition test.

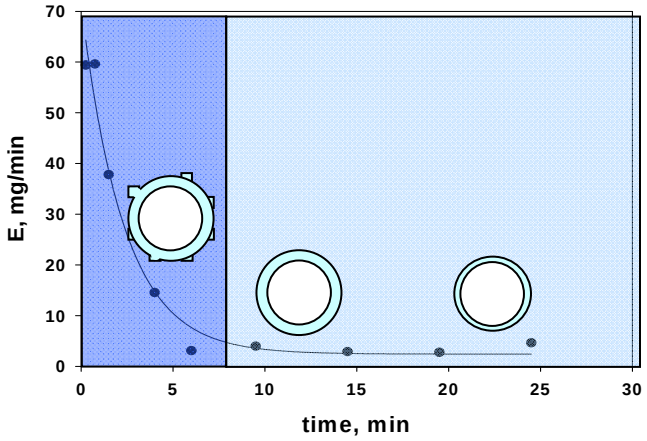

Figure A4. Abrasion curve of cenospheres (125-212 μm), 800°C, U=10 cm·s^{-1}

Under the experimental conditions tested, Sauter diameter of three distributions are practically the same (Table A3). However, according to a shrinking particle model with no collapses of the particle during its life-time inside the bed, assuming a reduction of the external size of the particle due to attrition, a relatively short life time is expected. This is of course a critical feature for an industrial applications (costs linked to bed replacement) of the support considered. In fact the mass loss due to attrition can drive both to material transport out of the bed as elutriable fines or collapsing of the particles into elutriable or relatively highly dense not elutriable fragments.

Table A3. Particles size distribution evolution after exposure to different conditions

	d_{Sauter} (μm)
Fresh cenospheres	146.5
Cenospheres after fluidization at 25°C	146.5
Cenospheres after fluidization at 800°C	147.2
Cenospheres after abrasion test at 800°C and 10 $cm \cdot s^{-1}$	151.6

Deposition of the active mixed oxide on the cenospheres is not a trivial task for two main reasons: i) cenospheres have a very low surface area and a small concentration of hydroxyl groups to graft the metal oxide, ii) cenospheres floats on water (generally used as solvent) leading to a poor contact between support and precursors salts. Different techniques have been used to deposit metals on this material, by surface modification (activation) or electroless process (Drozhzhin et al., 2002; Shukla et al, 2002). On the basis of preliminary investigations, ethanol is the most suitable solvent since it allows both a good cenospheres immersion and a complete precursors salts dissolution. Coating of cenospheres with a thin alumina layer prior to the active phase, providing both a higher surface area and a mechanical strengthening, has been carried out with no success.

Annex B

Another approach to limit the segregation phenomena is to modify the geometry of the reactor, using a conical distributor in order to realize a non uniform gas distribution and promoting a "gulf stream" circulation.

In order to verify the quality of the mixing between biomass and bed material in the fluidized bed gasifier, a Plexiglas reactor has been assembled to provide a direct view of the bed inventory during fluidization operation at ambient temperature (see Figure B1).

The vessel was set-up on the basis of the fluidized bed gasifier and has an internal diameter of 120 mm in the upper part and a conical distributor having the same angle as the one used in the fluidized bed gasifier at the bottom part. This distributor was fed by 32 tubes of 6 mm diameter, all connected in derivative way to a main feeding flexible in order to have an identical distribution of the flow as in the pilot scale fluidized bed.

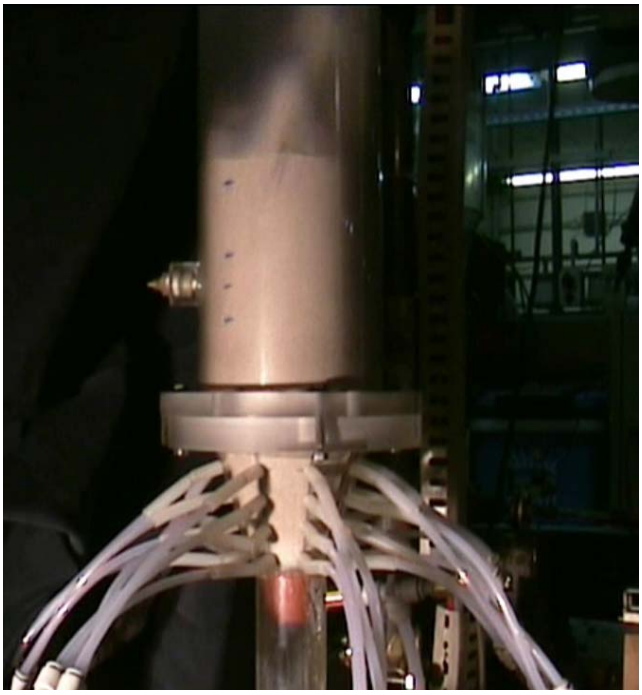

Figure B1. Plexiglas reactor for the study of mixing efficiency.

The gasification agent superficial velocity in gasification conditions at 800°C was 32 $cm \cdot s^{-1}$ in the 140 mm ID reactor (see § II-3.1). The same gas superficial velocity was used, at 25°C in the 120 mm ID Plexiglas tube. Air was used as the fluidizing gas, at superficial velocities of 17.2, 24.6 and 29.5 $cm \cdot s^{-1}$ to simulate the conditions used in real gasification conditions. During the experiments, the same H/D ratio as in the pilot scale fluidized bed was used, and char residues from the pilot scale fluidized bed gasifier was introduced in the same char/bed ratio as found in the proper gasifier. The chosen bed material was quartzite, in order to allow visualization of the char (even if more dense, olivine is black), but still having a bed material much more dense than the biomass and char, so that the conditions were in favour of segregation.

The visual observation of the bed inventory during the performed tests showed that the char was continuously recirculated in the reactor, thanks to the contribution of the conical reactor. This indicative result showed that the mixing of biomass and bed material was efficient during real gasification conditions in the fluidized bed gasifier.

BIBLIOGRAPHY

Abächerli A.: "Lignin types and sources" ILI newsletter (1996) 6-7

Abu-El-Rub Z., Bramer E. A., Brem G.: "Review of Catalysts for Tar Elimination in Biomass Gasification Processes" *Industrial and Engineering Chemistry Research* **43** (2004) 6911-6919

Ammendola P., Chirone R., Ruoppolo G., Russo G.: "Production of hydrogen from thermo-catalytic decomposition of methane in a fluidized bed reactor" *Chemical Engineering Journal*, in press. Doi 10.1016/J.CEI.2009.03.048

Antal M. J., Varhegyi G.: "Cellulose pyrolysis kinetics: The current state of knowledge" *Industrial and Engineering Chemistry Research* **34** (1995) 703-717

Antunes A. P., Ribeiro M. F., Silva J. M., Ribeiro F. R., Magnoux P., Guisnet M.: "Catalytic oxidation of toluene over CuNaHY zeolites - Coke formation and removal" *Applied Catalysis B: Environmental* **33** (2001) 149-164

Arvelakis S., Vourliotis P., Kakaras E., Koukios E. G.: "Effect of leaching on the ash behavior of olive residue during fluidized bed gasification" *Biomass & Bioenergy* **22** (2002) 55-69

Asadullah M., Ito S. I., Kunimori K., Yamada M., Tomishige K.: "Energy efficient production of hydrogen and syngas from biomass: Development of low-temperature catalytic process for cellulose gasification" *Environmental Science and Technology* **36** (2002) 4476-4481

Asadullah M., Fujimoto K., Tomishige K.: "Catalytic performance of Rh/CeO_2 in the gasification of cellulose to synthesis gas at low temperature" *Industrial and Engineering Chemistry Research* **40** (2001) 5894-5900

Bangala D. N., Abatzoglou N., Martin J. P., Chornet E.: "Catalytic gas conditioning: Application to biomass and waste gasification" *Industrial and Engineering Chemistry Research* **36** (1997) 4184-4192

Baker E. G., Mudge L. K., Brown M. D.: "Steam Gasification of Biomass with Nickel Secondary Catalysts" *Industrial and Engineering Chemistry Research* **26** (1987) 1335-1339

Bartels M., Lin W., Nijenhuis J., Kapteijn F., van Ommen J. R.: "Agglomeration in fluidized beds at high temperatures: Mechanisms, detection and prevention" *Progress in Energy and Combustion Science* **34** (2008) 633-666

Bassilakis R., Carangelo R. M., Wojtowicz M. A.: "TG-FTIR analysis of biomass pyrolysis" *Fuel* **80** (2001) 1765-1786

Biagini E., Pintus S., Tognotti L.: "Characterization of high heating-rate chars from alternative fuels using an electrodynamic balance" *Proceedings of the Combustion Institute* **30** (2005) 2205-2212

Bridgwater A. V.: "A techno-economic comparison of power production by biomass fast pyrolysis with gasification and combustion" *Renewable and Sustainable Energy Reviews* **6** (2002) 181-248

Bridgwater A. V.: "Renewable fuels and chemicals by thermal processing of biomass" *Chemical Engineering Journal* **91** (2003) 87-102

Bridgwater A. V.: "Biomass fast pyrolysis" *Thermal Science* **8** (2004) 21-49

Bruni G., Solimene R., Marzocchella A., Salatino P., Yates J. G., Lettieri P., Fiorentino M.: "Self-segregation of high-volatile fuel fuel particles during devolatilization in a fluidized bed reactor" *Powder Technology* **128** (2002) 11-21

Caglar A., Demirbas A.V.: "Hydrogen rich gas mixture from olive husk via pyrolysis" *Energy Conversion and Management* **43** (2002) 109-117

CEN/TS 15439 (2006) Technical Specification: Biomass gasification-Tar and particles in produced gas-Sampling and analysis

Chaudhari T., Bej S. K., Bakhshi N. N., Dalai K.: "Steam gasification of biomass-derived char for the production of carbon monoxide-rich synthesis gas" *Energy and Fuels* **15** (2001) 736-742

Chen G., Andries J., Spliethoff H.:"Catalytic pyrolysis of biomass for hydrogen rich fuel gas production" *Energy Conversion and Management* **44** (2003) 2289-2296

Cimino S., Landi G., Lisi L., Russo G.: "Rh–La(Mn,Co)O_3 monolithic catalysts for the combustion of methane under fuel-rich conditions" *Catalysis Today* **117** (2006) 454-461

Cimino S., Landi G., Lisi L., Russo G.: "Development of a dual functional structured catalyst for partial oxidation of methane to syngas" *Catalysis Today* **105** (2005) 718–723

Collot A.-G., Zhuo Y., Dugwell D. R., Kandiyoti R.: "Co-pyrolysis and co-gasification of coal and biomass in bench-scale fixed bed and fluidised bed reactors", *Fuel* **78** (1999) 667-679

Corella J., Aznar M. P., Gil J., Caballero M. A.: "Biomass gasification in fluidized bed: where to locate the dolomite to improve gasification?" *Energy and Fuels* **13** (1999) 1122-1127

Courson C., Makaga E., Petit C., Kiennemann A.: "Development of Ni catalysts for gas production from biomass gasification. Reactivity in steam- and dry-reforming" *Catalysis Today* **63** (2000) 427–437

Cui H., Grace J. R.: "Fluidization of biomass particles: A review experimental multiphase flow aspects" *Chemical Engineering Science* **62** (2007) 45-55

Darvell L. I., Heiskanen K., Jones J. M., Ross A. B., Simell P., Williams A.:"An investigation of alumina-supported catalysts for the selective catalytic oxidation of ammonia in biomass gasification" *Catalysis Today* **81** (2003) 681-692

Dayton D.: "A review of the literature on catalytic biomass tar destruction" Milestone completion report (2002) NREL/TP-510-32815.

Demirbas A.: "Biomass resource facilities and biomass conversion processing for fuels and chemicals" *Energy Conversion and Management* **42** (2001) 1357-1378.

Demirbas A.: "Gaseous products from biomass by pyrolysis and gasification: effects of catalyst on hydrogen yield" *Energy Conversion and Management* **43** (2002) 897–909.

Devi L., Ptasinski K. J., Janssen F. J. J. G.: "A review of the primary measures for tar elimination in biomass gasification processes" *Biomass and Bioenergy* **24** (2003) 125-140

Drozhzhin V. S., Danilin L. D., Pikulin I. V., Khovrin A. N., Maximova N. V., Regiushev S. A., Pimenov V. G.: "Functional materials on the basis of cenospheres" *Proceedings SWEMP Cagliari Italy* **118** (2002)

Essig M., Richards G. N., Schenck E.: "Cellulose and Wood-Chemistry and Technology" (Ed. Schuerch), Wiley New York (1989) 841-862

FAO corporate document depository "Integrated energy systems in china: the cold northern region experience.7-The research program of biomass pyrolysis processes" *http://www.fao.org* (1994)

Ferreira R. S. G., de Oliveira P. G. P., Noronha F. B.: "Characterization and catalytic activity of $Pd/V_2O_5/Al_2O_3$ catalysts on benzene total oxidation" *Applied Catalysis B: Environmental* **50** (2004) 243-249

Fino D., Russo N., Saracco G., Specchia V.: "Catalytic removal of NOx and diesel soot over nanostructured spinel-type oxides" *Journal of Catalysis* **242** (2006) 38-47

Fiorentino M., Marzocchella A., Salatino P.: "Segregation of fuel particles and volatile matter during devolatilization in a fluidized bed reactor -I. Model development" *Chemical Engineering Science* **52** (1997) 1893 a

Fiorentino M., Marzocchella A., Salatino P.: "Segregation of fuel particles and volatile matter during devolatilization in a fluidized bed reactor -II. Experimental" *Chemical Engineering Science* **52** (1997) 1909 b

Foscolo P. U., Germanà A., Jand N., Rapagnà S.: "Design and cold model testing of a biomass gasifier consisting of two interconnected fluidized beds" *Powder Technology* **173** (2007) 179-188

Ganesh, A. : “Studies on Characterisation of Biomass for Gasification” *Ph.D Thesis* (1990) *Indian Institute of Technology, New Delhi*

Garcia L., French R., Czernik S., Chornet E.: “Catalytic steam reforming of bio-oils for the production of hydrogen: effects of catalyst composition” *Applied Catalysis A: General* **201** (2000) 225-239

Gil J., Corella J., Aznar M.P., Caballero M.A.: “Biomass gasification in atmospheric and bubbling fluidized bed: effect of the type of gasifying agent on the product distribution” *Biomass and Bioenergy* **17** (1999) 389-403

Glarborg P.: “Hidden interactions – trace species governing combustion and emissions” *Proceedings of the combustion institute* **31** (2007) 77-98

Goring D. A. I.,.: “Thermal softening of lignin, hemicellulose and cellulose” *Pulp and Paper Magazine Canada* **64** (1971) 517-527

Goyal H. B., Seal D., Saxena R. C.: “Bio-fuels from thermochemical conversion of renewable resources: a review” *Renewable and Sustainable Energy Reviews* **12** (2008) 504-517

Gray M. R.: “The Effects of moisture and ash content on the pyrolysis of a wood-derived material” *PhD Thesis* (1984) *California Institute of Technology*

Haykiri-Acma H.: “The role of particle size in the non-isothermal pyrolysis of hazelnut shell” *Journal of Analytical and Applied Pyrolysis* **75** (2006) 211-216

Hepola J., Simell P.: “Sulphur poisoning of nickel-based hot gas cleaning catalysts in synthetic gasification gas: -I. Effect of different process parameters” *Applied Catalysis, B: Environmental* **14** (1997) 287-303 a

Hepola J., Simell P.: “Sulphur poisoning of nickel-based hot gas cleaning catalysts in synthetic gasification gas: -I. Chemisorption of hydrogen sulphide” *Applied Catalysis, B: Environmental* **14** (1997) 305-321 b

Hu G., Xu S., Li S., Xiao C., Liu X.: “Steam gasification of apricot stones with olivine and dolomite as downstream catalysts” *Fuel Processing Technology* **87** (2006) 375-382

Hwang C. P., Yeh C. T., Zhu Q.: “Rhodium-oxide species formed on progressive oxidation of rhodium clusters dispersed on alumina” *Catalysis Today* **51** (1999) 93

Juutilainen Sami J., Simell Pekka A., Krause A. Outi I.: “Zirconia: Selective oxidation catalyst for removal of tar and ammonia from biomass gasification gas” *Applied Catalysis B: Environmental* **62** (2006) 86-92

Kallioinen A., Vaari A., Rättö M., Konn J., Siika-aho M., Viikari L.:“Effects of bacterial treatments on wood extractives” *Journal of Biotechnology* **103** (2003) 67-76

Lei Q., Zhao T., Li F., Zhan L., Wang Y.:“Catalytic cracking of large molecules over hierarchical zeolites” *Chemical Communications* 1 (2006) 1769-1771

Le Minh C., Jones R.A., Craven I.E., Brown T.C.: "Temperature programmed oxidation of coke deposited on cracking catalysts: Combustion mechanism dependence" Energy & Fuels 11 (1997) 463-469

Li Chao'en, Brown T. C.: "Carbon oxidation kinetics from evolved carbon oxide analysis during temperature-programmed oxidation" *Carbon* **39** (2001) 725-732

Lisi L., Bagnasco G., Ciambelli P., De Rossi S., Porta P., Russo G., Turco M.: "Perovskite-type oxides II. Redox properties of $LaMn_{1-x}Cu_xO_3$ and $LaCo_{1-x}Cu_xO_3$ and methane catalytic combustion" *Journal of Solid State Chemistry* **146** (1999) 176-183

Matsumura Y., Minowa T.: "Fundamental design of a continuous biomass gasification process using a supercritical water fluidized bed" *International Journal of Hydrogen Energy* **29** (2004) 701-707

McKendry P.: "Energy production from biomass (part 3): gasification technologies" *Bioresource* **83** (2002) 55-63

Milne T. A., Evans R. J .: "Biomass gasifier "Tars": their nature, formation, and conversion" NREL (1998), *Golden, CO, USA, Report no.* NREL/TP-570-25357.

Morf P., Hasler P., Nussbaumer T.: "Mechanisms and kinetics of homogeneous secondary reactions of tar from continuous pyrolysis of wood chips" *Fuel 81* (2002) 843-853

Natarajan E., Ohman M., Gabra M., Nordin A., Liliedahl T., Rao A. N.: "Experimental determination of bed agglomeration tendencies of some common agricultural residues in fluidized bed combustion and gasification" *Biomass and Bioenergy* **15** (1998) 163-169

Ni M., Leung D. Y. C., Leung M. K. H., Sumathy K.: "An overview of hydrogen production from biomass" *Fuel Processing Technology* **87** (2006) 461-472

Nordgreen T., Liliedahl T., Sjostrom K.: "Metallic iron as a tar breakdown catalyst related to atmospheric, fluidised bed gasification of biomass" *Fuel* **85** (2006) 689–694

Obernberger I., Brunner T., Barnthaler G.. : "Chemical properties of solid biofuels-significance and impact" *Biomass and Bioenergy* **30** (2006) 973-982

Pengmei Lv, Chang J., Xiong Z., Huang H., Wu C., Chen Y., Zhu J.: "Biomass air-steam gasification in a fluidized bed to produce hydrogen-rich gas" *Energy and Fuels* **17** (2003) 677-682

Perry Handbook 5th ED., sect. 5, p. 54

Pfeifer C., Hofbauer H.: "Development of catalytic tar decomposition downstream from a dual fluidized bed biomass steam gasifier" *Powder Technology* **180** (2008) 9

Pfeifer C., Hofbauer H., Rauch R.: "In-bed catalytic tar reduction in a dual fluidized bed biomass steam gasifier" *Industrial and Engineering Chemistry Research* **43** (2004) 1634-1640

Prins Mark J., Ptasinski Krzysztof J., Janssen Frans J. J. G. : "Torrefaction of wood Part 1. Weight loss kinetics" *Journal of Analytical and Applied Pyrolysis* **77** (2006) 28-34

Rao T.R., Bheemarasetti J. V. R.: "Minimum fluidization velocities of mixtures of biomass and sands" *Energy* **26** (2001) 633-644

Rapagna S., Provendier H., Petit C., Kiennemann A., Foscolo P. U.: "Development of catalysts suitable for hydrogen or syn-gas production from biomass gasification" *Biomass and Bioenergy* **22** (2002) 377-388

Rapagnà S., Jand N., Kiennemann A., Foscolo P. U.: "Steam gasification of biomass in a fluidised-bed of olivine particles" *Biomass and Bioenergy* **19** (2000) 187-197

Rasul M. G.: "Fluidization characteristics of bagasse in a gas-fluidized bed" *Particle & Particle Systems Characterization* **15** (1998) 243-247

Raveendran K., Ganesh A., Khilar K. C.: "Pyrolysis characteristics of biomass and biomass components" *Fuel* **75** (1996) 987-998

Raveendran K.: "Influence of mineral matter on biomass pyrolysis characteristics" *Fuel* **74** (1995) 1812-1822

Russo N., Fino D., Saracco G., Specchia V.: "Studies on the redox properties of chromite perovskite catalysts for soot combustion" *Journal of Catalysis* **229** (2005) 459-469

Sales F. G.,. Abreu C. A. M, Pereira J. A. F. R..: "Catalytic wet-air oxidation of lignin in a three-phase reactor with aromatic aldehyde production" *Brazilian Journal of Chemical Engineering* **21** (2004) 211-218

Saxena R. C. , Seal D., Kumar S., Goyal H. B.: "Thermo-chemical routes for hydrogen rich gas from biomass: A review" *Renewable and Sustainable Energy Reviews* **12** (2008) 1909-1927

Scala. F: "A new technique for the measurement of the product CO/CO_2 ratio at the surface of char particles burning in a fluidized bed" *Proceedings of the combustion institute* **32** (2009) 2021-2027

Shafizadez F.: "Pyrolysis and combustion of cellulosic materials" *Advanced Carbohydrate Chemistry* **23** (1968) 419-474

Shan W., Luo M., Ying P., Shen W. and Li C.: "Reduction Property and Catalytic Activity of $Ce_{1-x}Ni_xO_2$ Mixed Oxide Catalysts for CH_4 Oxidation" *Applied Catalysis A: General* **246** (2003) 1-9

Shen L., Xiao J., Niklasson F., Johnsson F..: "Biomass mixing in a fluidized bed biomass gasifier for hydrogen production" *Chemical Engineering Science* **62** (2007) 636-643

Shukla S., Seal S., Rahaman Z., Scammon K.: "Electroless copper coating of cenospheres using silver nitrate activator" *Materials Letters* **57** (2002) 151-156

Simell P. A., Hirvensalo E. K., Smolander V. T., Krause A. Outi I.: "Steam reforming of gasification gas tar over dolomite with benzene as a model compound" Industrial Engineering Chemistry Research **38** (1999) 1250-1257

Simell P. A., Hepola J. O., Krause A. Outi I.: "Effects of gasification gas components on tar and ammonia decomposition over hot gas cleanup catalysts" *Fuel* **76** (1997) 1117-1127

Simell P. A., Leppalahti J. K., Kurkela E. A.: "Tar decomposing activity of carbonate rocks under high CO_2 partial pressure" *Fuel* **74** (1995) 938-945

Simell P. A., Leppalahti J. K., Son Bredenberg J. B.: " Catalytic purification of tarry fuel gas with carbonate rocks and ferrous materials" *Fuel* **71** (1992) 211-218

Stanmore B. R., Brilhac J. F., Gilot P.: "The oxidation of soot: a review of experiments, mechanisms and models" *Carbon* **39** (2001) 2247-2268

Strohm J. J., Zheng J., Song C.: "Low temperature steam reforming of jet fuel in the absence and presence of sulphur over Rh and Rh-Ni catalysts for fuel cells" *Journal of Catalysis* **238** (2006) 309-320

Sutton D., Kelleher B., Ross J. R. H.: "Review of literature on catalyst for biomass gasification" *Fuel Processing Technology* **73** (2001) 155-173

Tomishige K., Asadullah M., Kunimori K.: "Syngas production by biomass gasification using $Rh/CeO_2/SiO_2$ catalysts and fluidized bed reactor" *Catalysis Today* **89** (2004) 389-403

Truex T. J.: "Interaction of sulphur with automotive catalysts and the impact on vehicle emissions" *SAE paper 011243* (1999)

Uddin Azhar Md., Tsuda H., Wu S., Sasaoka E.: "Catalytic decomposition of biomass tars with iron oxide catalyst" *Fuel* **87** (2008) 451-459

Uner D., Demirkol M. K., Denairka B.: "A novel catalyst for diesel soot oxidation" *Applied Catalysis B: Environmental* **61** (2005) 334-345

Vamvuka D., Troulinos S., Kastanaki E.: "The effect of mineral matter on the physical and chemical activation of low rank coal and biomass materials" *Fuel* **85** (2006) 1763-1771

Yang H.: "Thermogravimetric Analysis-Fourier Transform Infrared Analysis of Palm Oil Waste Pyrolysis" *Energy & Fuels* **18** (2004) 1814-1821

Zhang X., liu J., Jing Y. and Xie Y.: "Support Effects on the Catalytic Behaviour of NiO/Al_2O_3 for Oxidative dehydrogenation of ethane to ethylene" *Applied catalysis A: General* **240** (2003) 143-150